

# The Noncanonical Roles of Two Primordial Molecules in Flagella

Xiaoyan Zhu  
*Marquette University*

---

## Recommended Citation

Zhu, Xiaoyan, "The Noncanonical Roles of Two Primordial Molecules in Flagella" (2017). *Dissertations (2009 -)*. 734.  
[http://epublications.marquette.edu/dissertations\\_mu/734](http://epublications.marquette.edu/dissertations_mu/734)

**THE NONCANONICAL ROLES OF TWO PRIMORDIAL MOLECULES IN  
FLAGELLA**

by

Xiaoyan Zhu, B.S.

A Dissertation Submitted to the Faculty of the Graduate School,

Marquette University,

in Partial Fulfillment of the Requirements for

the Degree of Doctor of Philosophy

Milwaukee, Wisconsin

August 2017

**ABSTRACT**  
**THE NONCANONICAL ROLES OF TWO PRIMORDIAL MOLECULES IN**  
**FLAGELLA**

**Xiaoyan Zhu, B.S.**

**Marquette University, 2017**

Motile cilia and flagella are ancient organelles that eukaryotic organisms today still rely on to thrive in their natural environment. Not surprisingly, accumulated evidence has shown that the intricate motility machinery, the microtubule-based axoneme, is evolutionarily conserved down to the molecular level. This notion is epitomized by the signature axonemal complex, the radial spoke (RS). The RS is part of a control center conferring the high frequency and tightly regulated movement. Key RS proteins discovered in biflagellate green alga, *Chlamydomonas reinhardtii*, are also generated by nearly all ciliated organisms, including *Homo sapiens*. Among them are two subunits from primordial protein families, nucleoside diphosphate kinase (NDK) and heat shock protein (HSP) 40, that are positioned at a critical juncture where two arms merge into a singular stalk in the Y-shaped complex. While it is well accepted that NDKs and HSP40s maintain nucleotide homeostasis and assist HSP70 chaperone in protein folding respectively, these actions fail to explain observations in myriads of vital cellular processes. Using the experimental approaches possible in the biflagellate green algae, genetics in particular, this dissertation discovers non-canonical applications of these two spoke proteins in the assembly and motility of the RS and entire flagellum. The versatility sheds light on the canonical mechanisms, the diverse processes adopting the non-canonical mechanisms, and their preservation since their conscription perhaps by the cell ancestral to all eukaryotes.

## ACKNOWLEDGEMENTS

### **Xiaoyan Zhu, B.S.**

My deepest gratitude goes to my mentor, Dr. Pinfen Yang, for her greatest patience in cultivating me to be a critical thinker and for her care and guidance of my growth in and outside of the laboratory. I feel blessed to work with a passionate scientist with fantastic mind and insight for the past six years. Her mentoring motivates me to be a better student, scientist and person every day.

I would like to thank all my committee members, Dr. Kathleen Karrer, Dr. Rosemary Stuart, Dr. Allison Abbott and Dr. Martin St. Maurice, for their insightful suggestions, feedback and guidance. I also would like to thank our collaborators for their great support and beautiful works.

I would like to thank the best lab member, Yi Liu, for all the help and critical evaluation of my work. I am also thankful to my best friends Pinqing Kan, Yan Li and Yulin Zhao, for their precious friendship and warm familial care.

Most importantly, I would like to thank my parents and grandparents. It is their invaluable love and support that made my dream of studying aboard come true. Especially, I am thankful to my dearest Mother, my best lifetime friend, who has always being there for me during the stressful times.

## TABLE OF CONTENTS

ACKNOWLEDGEMENTS.....	i
LIST OF TABLES.....	vi
LIST OF FIGURES.....	vii
LIST OF ABBREVIATIONS.....	ix
<b>CHAPTER 1: INTRODUCTION</b>	
1.1 Cilia and Flagella.....	1
1.2 <i>Chlamydomonas</i> as a Flagella Model Organism.....	3
1.3 Intraflagellar Transport – A Tale of Two Cities.....	4
1.4 The RS Complex.....	7
1.4.1 The Role of RS.....	8
1.4.2 The Composition of the RS.....	9
1.4.3 The Assembly of the RS.....	11
1.4.4 The Two Primordial Molecules in the Neck of the RS.....	13
1.4.4.1 HSP40.....	14
1.4.4.2 NDK.....	18
1.5 Objectives of This Dissertation.....	20
1.5.1 Elucidation of NDK5 in the RS .....	21
1.5.2. Elucidation of the Noncanonical Role of Spoke HSP40.....	21
<b>CHAPTER 2: MATERIALS AND METHODS</b>	
2.1 Materials.....	22
2.1.1 <i>Chlamydomonas</i> Strains.....	22
2.1.2 Culture Conditions.....	22

2.1.3 Antibodies.....	22
2.2 Molecular Biology.....	26
2.2.1 PCR-based Genotyping.....	26
2.2.1.1 Characterization of the Insertional Site in <i>ndk5</i> .....	26
2.2.1.2 Characterization of Mutation Site in <i>pf33</i> .....	26
2.2.2 Engineering of Genomic Constructs.....	26
2.2.2.1 Engineering of NDK5 Genomic DNA Constructs.....	26
2.2.2.2 Engineering of HSP40 Genomic DNA Constructs.....	27
2.3 <i>Chlamydomonas</i> Experiments.....	30
2.3.1 Backcross.....	30
2.3.2 Transformation.....	30
2.3.3 Flagellar Length Quantification.....	30
2.3.4 Dikaryon Rescue.....	31
2.4 Biochemistry.....	31
2.4.1 Flagella Preparation and Western Blot.....	32
2.4.2 Purification of Bacterial Recombinant Proteins.....	32
2.4.3 Pull-down Assay.....	32
2.4.4 Nucleotide Diphosphate Kinase Activity Assay.....	33
2.5 Microscopy.....	33
2.5.1 Light Microscopy.....	33
2.5.2 Electron Microscopy.....	34
2.6 Modeling.....	34

**CHAPTER 3: GENERAL AND SPECIFIC PROMOTIONS OF FLAGELLAR ASSEMBLY BY A FLAGELLAR NUCLEOSIDE DIPHOSPHATE KINASE**

3.1 Introduction.....	36
3.2 Results.....	39
3.2.1 NDK5 <sup>H121A</sup> Minigene Caused Paralyzed Short Flagella.....	39
3.2.2 RS Defects in Paralyzed Flagella of an <i>ndk5</i> Insertional Mutant....	42
3.2.3 RS Deficiencies of <i>ndk5</i> Flagella.....	43
3.2.4 Short Flagella of <i>ndk5</i> .....	44
3.2.5 3D Reconstruction of NDK5 Axoneme with Cryo-electron Tomography.....	47
3.2.6 Full Rescue of <i>ndk5</i> Phenotypes by NDK5 and NDK5 <sup>H121A</sup> .....	48
3.2.7 Rescue of the Short Flagella of a Spoke-less <i>pfl4</i> Allelic Mutant.....	52
3.2.8 Dominant Negative Effect of NDK5 <sup>H121A</sup> Genomic DNA.....	54
3.2.9 Hypophosphorylated NDK5 in the Cell Body.....	57
3.3 Discussion.....	59
3.3.1 NDK5 is a Structural Protein for Proper Assembly of the RS Head-Neck Region.....	60
3.3.2 NDK5 Promotes Phosphorylation-related Assembly.....	60

#### **CHAPTER 4: NON-CANONICAL ACTIONS OF HSP40 IN THE ASSEMBLY OF THE FLAGELLAR RS COMPLEX**

4.1 Introduction.....	65
4.2 Results.....	68
4.2.1 Discovery of a HSP40 Transposon Insertional Mutant.....	68
4.2.2. Cryo-electron Tomography of HSP40-minus RSs.....	74
4.2.3 Identical Assembly Polarity but Distinct Efficiencies in the Repair of HSP40 and RSs.....	76

4.2.4 Low Affinity of Recombinant HSP40 and NDK5.....	83
4.2.5 Structural Modeling of HSP40 and the RS Neck.....	85
4.3 Discussion.....	89
4.3.1 HSP40 is Needed for RS Structural Stability.....	89
4.3.2 Delayed Repair of Existing HSP40-minus RSs Sheds Light on HSP40 and Dikaryon Rescue.....	90
4.3.3 Modeling Predicts the Actions of HSP40.....	92
 <b>CHAPTER 5: DISCUSSION</b>	
5.1 New Spokeneck Model.....	95
5.2 Refined Structural Roles of NDK5.....	100
5.3 Inter-subunit Crosstalk of NDK.....	101
5.3.1 Inter-subunit Crosstalk for the Canonical Mechanism of NDK....	102
5.3.2 Implications of Inter-subunit Crosstalk.....	102
5.4 Structural Role of Spoke HSP40.....	104
5.5 Trafficking and Assembly of Spoke HSP40.....	105
5.6 Potential Mechanisms of DN Phenotypes .....	111
<b>BIBLIOGRAPHY</b> .....	114



## LIST OF TABLES

<b>Table 1-1.</b> RS subunits in <i>Chlamydomonas</i> .....	11
<b>Table 1-2.</b> Molecular domains in Group I and Group II human NDKs.....	20
<b>Table 2-1.</b> Strains generated in this dissertation.....	23
<b>Table 2-2.</b> Antibodies used in this dissertation.....	25
<b>Table 2-3.</b> Oligonucleotides used in this dissertation.....	28
<b>Table 3-1.</b> List of strains described in this study and their corresponding motility, flagellar generation and RS assembly phenotypes.....	52
<b>Table 4-1.</b> <i>Chlamydomonas</i> mutant strains deficient in the head or neck region of the RS.....	67

## LIST OF FIGURES

<b>Figure 1-1.</b> <i>Chlamydomonas</i> flagella.....	2
<b>Figure 1-2.</b> Model of intraflagellar transport (IFT) dependent RS assembly.....	6
<b>Figure 1-3.</b> Surface rendering of RS in <i>Chlamydomonas</i> .....	7
<b>Figure 1-4.</b> Generalized domain structures of HSP40 protein family.....	15
<b>Figure 1-5.</b> Canonical model of the core HSP70-HSP40 machinery's action in protein folding.....	17
<b>Figure 1-6.</b> Crystal structure of a Group I NDK.....	19
<b>Figure 3-1.</b> NDK5 <sub>H121A</sub> expressed from a minigene caused paralyzed short flagella in WT cells.....	41
<b>Figure 3-2.</b> Characterization of an <i>ndk5</i> insertional mutant.....	43
<b>Figure 3-3.</b> The <i>ndk5</i> mutant is defective in RSs and flagellar assembly.....	46
<b>Figure 3-4.</b> Structure of RSs from WT (A, B) and <i>ndk5</i> mutant (C, D) <i>Chlamydomonas</i> .....	48
<b>Figure 3-5.</b> Genomic DNA expressing NDK5 or NDK5 <sub>H121A</sub> rescued both the paralysis and length phenotypes of <i>ndk5</i> .....	51
<b>Figure 3-6.</b> Diminished RSs result in short flagella.....	53
<b>Figure 3-7.</b> NDK5 <sub>H121A</sub> expression from a genomic transgene in WT cells impaired flagellar motility, length, RS assembly and RS phosphorylation.....	56
<b>Figure 3-8.</b> Accumulated hypophosphorylated NDK5 polypeptides in the cell body of the DN strain.....	59
<b>Figure 4-1.</b> Phenotyping of a new HSP40 mutant, <i>pf33</i> .....	70
<b>Figure 4-2.</b> Genotyping of <i>pf33</i> .....	72
<b>Figure 4-3.</b> The <i>pf33</i> transformant cells expressing GFP-HSP40.....	74
<b>Figure 4-4.</b> The side view, top view and longitudinal view of averaged cryo-electron tomography of WT and <i>pf33</i> axonemes.....	76

<b>Figure 4-5.</b> Possible outcomes of dikaryon rescue experiments testing how HSP40 is transported and assembled.....	78
<b>Figure 4-6.</b> Distinct efficiencies in the repair of missing RSs and HSP40 in dikaryon rescues.....	82
<b>Figure 4-7.</b> Low co-purification of recombinant His-HSP40 and His-NDK5 <i>in vitro</i> despite the requirement of NDK5 for the assembly of HSP40 <i>in vivo</i> .....	85
<b>Figure 4-8.</b> Structural modeling of the RS neck region.....	88
<b>Figure 4-9.</b> A schematic picture depicting coupled trafficking and refolding of HSP40 and its RS client.....	91
<b>Figure 5-1.</b> New spokeneck model.....	98
<b>Figure 5-2.</b> New RS assembly model.....	107
<b>Figure 5-3.</b> Summary of the interactions and functions of HSP40, NDK and HSP70.....	110

**LIST OF ABBREVIATIONS**

EM	Electron Microscopy
Cryo-ET	Cryo-electron Tomography
ET	Electron Tomograph
RS	Radial Spoke
RSP	Radial Spoke Protein
CP	Central Pair
ODA	Outer Dynein Arm
IDA	Inner Dynein Arms
BB	Basal Body
IFT	Intraflagellar Transport
NDK	Nucleotide Exchange Factor
HSP	Heat Shock Protein
AH	Amphipathic Helix
G/F	Glycine/phenylalanine
ZnF	Zinc finger
UTR	Untranslated Region
WT	Wild Type
DN	Dominant Negative
GFP	Green Fluorescence Protein
mNG	Monomeric NeonGreen
HPD	His-Pro-Asp
PMM	Paromomycin

HYG	Hygromycin
PCR	Polymerase Chain Reaction
PCD	Primary Cilia Dyskinesia
PDB	Protein Data Bank
EMDB	Electron Microscopy Data Bank

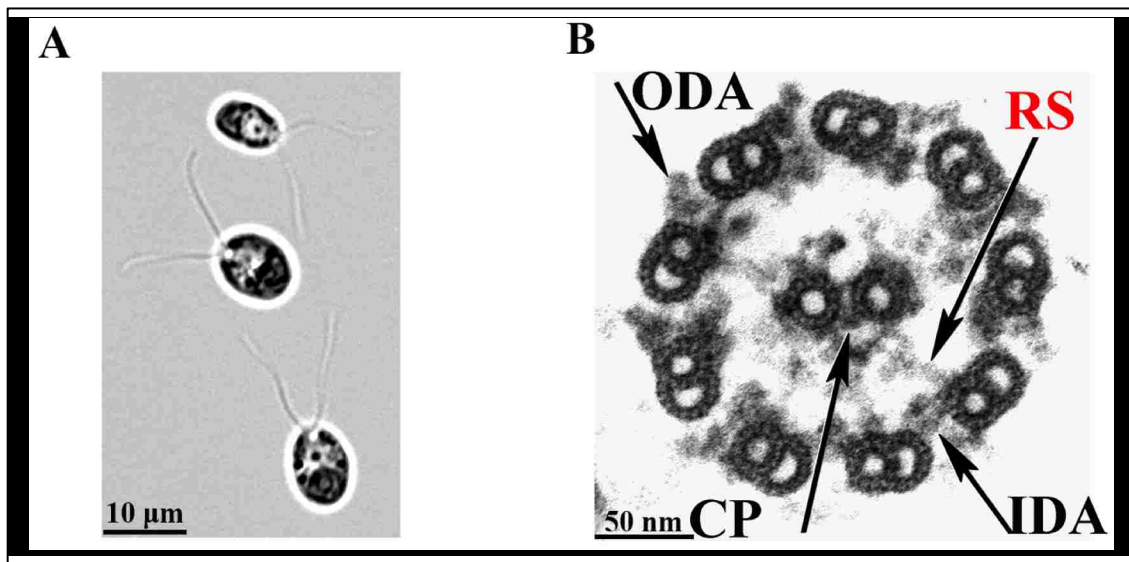
## CHAPTER 1: INTRODUCTION

### *1.1 Cilia and Flagella*

Cilia and flagella are synonymous lengthy organelles that are made by a wide variety of eukaryotic organisms ranging from protists (Figure 1-1A) to humans. Albeit differing in length and number, they are identical mechanistically. For more than 300 years, they have been recognized as a device for propelling fluid. The most recognized one is the flagellum of sperm. This motile device is the most common modality that male gametes use to reach oocytes in multi-cellular animals. The female reproductive track, respiratory track and the epithelium lining the cerebral ventricle grow tufts of cilia to sweep away the surrounding fluid for the respective physiology. However, the accumulated studies from the past 25 years have unequivocally demonstrated that cilia and flagella are also signaling centers that detect various stimuli through a host of receptors, channels and enzymes enriched in the membrane. The signaling not only regulates the motility but also signals a number of events and directs cellular homeostasis (reviewed by Pan and Snell, 2007). Both roles are crucial for organisms to thrive in their natural environment.

Studies of the motility of these slender organelles that perpetually whip through viscous fluid at high frequency have shed critical insight on physiology and pathology of ciliated organs as well as leading to many fundamental questions (reviewed by Zhu *et al.*, 2016). The beating is generated by the evolutionarily conserved 9+2 axoneme inside each cilium and flagellum. The format is named after 9 outer doublet microtubules that surround 2 singlet microtubules in the center (Figure 1-1B) revealed in the thin section

electron microscopy (EM). These microtubules further associate with a number of molecular complexes such as outer dynein arms (ODA), inner dynein arms (ODA) and radial spokes (RSs). The two singlet microtubules and their associated complexes are collectively referred to the central pair (CP) apparatus. These complexes are positioned at precise locations every 96-nm to generate motion and to stabilize the inherent instability of microtubules (Kubo *et al.*, 2015). The continuous advancement in cryo-electron tomography (ET) has revealed unprecedented details in this nanomachine that are not possible using traditional EM.



**Figure 1-1.** *Chlamydomonas* flagella. (A) Bright field microscopy of biflagellate green alga *Chlamydomonas reinhardtii*. (B) Cross section electron microscopy of an axoneme with 9 microtubule outer doublets surrounding 2 singlets in the central pair (CP) apparatus. Each outer doublet associated with outer dynein arms (ODA) and inner dynein arms (IDA) that power inter-doublet sliding and with radial spokes (RS, red) that contacts the CP apparatus intermittently to transduce mechanical feedback.

As dynein motors are distributed throughout every outer doublet, it is evident that only subsets of motors can be active at one time and different subsets take turns to become activated to generate back-and-forth movement. An early electron microscopy study concluded that the beating is founded on the inter-doublet sliding (Sale and Satir, 1977). The other axonemal complexes, albeit lacking motor activity, operate concertedly to generate motions. Studies of *Chlamydomonas reinhardtii* mutants defective in individual axonemal complexes revealed pathogenesis of primary cilia dyskinesia (PCD) in mammals (reviewed by Zhu *et al.*, 2016).

While PCD is not lethal, PCD patients have diminished quality of life. In addition to sterility, most patients suffer from severe chronic respiratory infections, which can eventually require lung transplantation. Patients have enlarged brain ventricles or complain of frequent headaches, likely due to poor circulation of cerebral spinal fluid and perhaps abnormal neuronal migration along ventricular epithelium during early development (Horani *et al.*, 2016). As with many congenital diseases, PCD used to be considered untreatable. The recurrent respiratory tract infections are primarily managed by antibiotics. However, given the maturation of gene editing technologies and the superficial location of cilia that is conducive for gene therapy, there is a ground swell of enthusiasm for curing PCD. Understanding the genetic defects and how possibly to repair the defects will provide a solid foundation to cure PCD in the foreseeable future.

### ***1.2 Chlamydomonas as a Flagella Model Organism***

Although a number of simple flagellated organisms are used for the investigation of flagella biology, the haploid genetics and presence of two flagella that are easy to



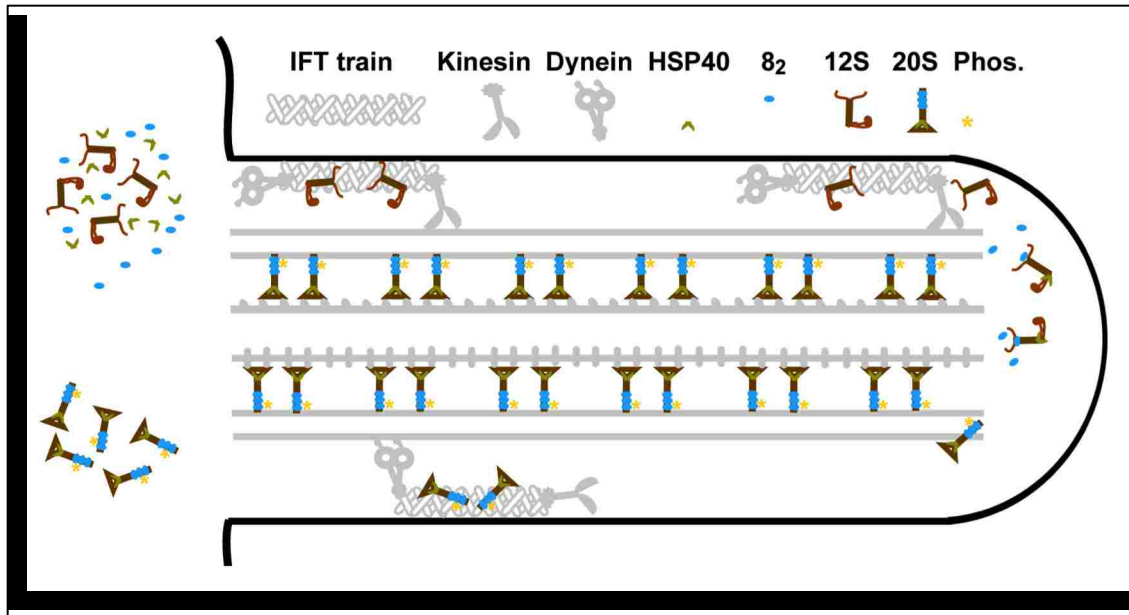
characterize distinguish *Chlamydomonas* from the others. As such, studies of *Chlamydomonas* flagella have revealed fundamental mechanisms that stoke further research in other organisms, which provide the context of tissue and development that the green algae cannot. The complexity of cilia and flagella is first revealed by *Chlamydomonas* flagellar proteome that contains more than 600 distinct polypeptides, among which more than 400 reside in the axoneme (Pazour *et al.*, 2005). Because of the conserved 9+2 format, most flagellar proteins are also evolutionarily conserved and primarily expressed in ciliated tissues in multicellular organisms (Figure 1-1B). With diverse experimental approaches, studies of *Chlamydomonas* revealed the molecular basis of flagellar beating, and calcium- and cAMP-dependent regulation (reviewed by Zhu *et al.*, 2016). Observations of this simple organism also inspired fundamental and important questions.

### ***1.3 Intraflagellar Transport – A Tale of Two Cities***

The long-standing questions in this field are how the whip-like structure protruding from the surface of the cells is generated, how it is resorbed before cell division, and how the length is determined. These phenomena are particularly intriguing given the slender organelle does not possess translation machinery, whereas the microtubule plus end where assembly occurs is at the tip of a flagellum, distal to the cell body (Rosenbaum and Child, 1967). Thus, all the flagella proteins must be synthesized in the cell body and then delivered to flagella tip for final assembly. This prediction is validated by the observation of bi-directional movement of particles along the length of paralyzed flagella with differential interference contrast (DIC) microscopy (Kozminski *et*

*al.*, 1993). The 2-4  $\mu\text{m}/\text{sec}$  velocity, directionality and processivity suggest that the movement is powered by molecular motors rather than by passive diffusion. In theory, it only takes intraflagellar transport (IFT) 3 seconds to deliver molecules from the cell body to the tip of a 12- $\mu\text{m}$  flagellum.

The seminal discovery of IFT is followed by a slew of significant findings. Moving particles of IFT complexes were extensively characterized and referred to trains for associating with motors and cargoes (Figure 1-2). The anterograde motor, kinesin, (Cole *et al.*, 1998) drives IFT trains to the tip, whereas the retrograde cytoplasmic dynein motor (Pazour *et al.*, 1998) powers IFT trains back to the cell body. Various cargoes, such as axonemal complexes (Qin *et al.*, 2004; Ahmed *et al.*, 2008; Hou *et al.*, 2007) and membrane-bound proteins (e.g. Lechtreck *et al.*, 2009) have been co-purified or co-localized with IFT trains. Cargoes are presumably loaded onto IFT trains near the basal body (BB) area and beneath the gated flagellar entrance (Deane *et al.*, 2001). IFT mutants grew stubby or short flagella, indicating that IFT is required for flagellar assembly (e.g. Pazour *et al.*, 1998). The arrival of the genomic era further accelerated the discoveries of the orthologous genes involved in IFT in all ciliated organisms. Collectively, these discoveries established that bi-directional IFT delivers various cargoes in and out of the flagellar compartments for flagellar assembly, disassembly and signaling. Defects in this process underlie a host of mysterious orphan congenital disorders that are now collectively referred to ciliopathies (Horani *et al.*, 2016).



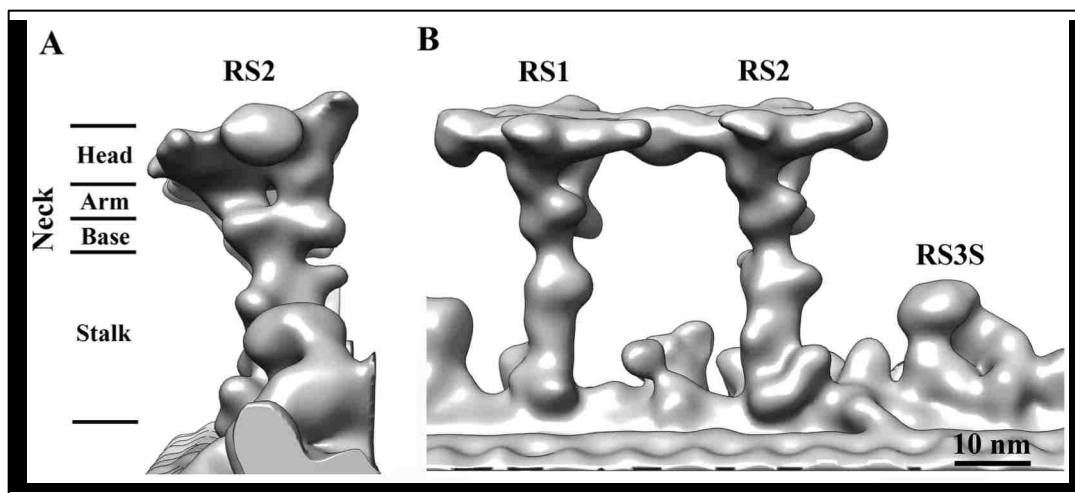
**Figure 1-2.** Model of intraflagellar transport (IFT)- dependent RS assembly. RS subunits are synthesized and preassembled into 12S precursors in the cell body. Anterograde IFT train driven by kinesin motor delivers RS precursors to flagella tip, where the precursors are refolded into 20S mature RS for final assembly. The assembly scheme of HSP40 and LC8 (8<sub>2</sub>) that are excluded from RS precursors are unclear. Flagella tip undergoes constant turnover. Retrograde IFT train driven by dynein motor delivers the turnover products including 20S mature RS back to the cell body.

Given the numerous axonemal proteins and the requirement of assembly at the tip, proteins in one axonemal complex are prepackaged into a precursor complex for coordinated trafficking (Fowkes and Mitchell, 1998; Qin *et al.*, 2004). Presumably upon passing through the gated flagellar entrance and reaching the tip, cargoes are unloaded and assembled, along with tubulins and other complexes, into the axoneme. The retrograde trains are then driven back to the BB area for subsequent deliveries. After flagella reach full-length, IFT continues for maintenance, albeit the transport frequency and the occupancy of cargoes are reduced (Craft *et al.*, 2015). However, studies of RSs

strongly suggest that much remains to be learned about the assembly processes that take place at two opposing ends of flagella and coupled by IFT.

#### 1.4 The RS Complex

RS is one of the signature complexes in the 9+2 axoneme. Cryo-ET revealed RSs as a Y-shaped complex with two bifurcated arms connecting two enlarged spokeheads to a singular stalk (Pigino *et al.*, 2011) (Figure 1-3). The stalk anchors to the A tubule of each outer doublet, adjacent to the base of IDAs, whereas the head projects toward the CP apparatus (Figure 1-1B). From the longitudinal view, typically there are three RSs every 96 nm in each outer doublet. The third RS in *Chlamydomonas* appears as a remnant and is referred to RS3S (Figure 1-3).



**Figure 1-3.** Surface rendering of RSs in *Chlamydomonas*. (A) The Y-shaped RS viewed from the tip. It could be further divided into the head, neck (including two arms and a base), and stalk region. (B) Side view of seemingly connected RS1 and RS2, and RS3S (Pigino *et al.*, 2011).

### ***1.4.1 The Role of RS***

Although it is clear that inter-doublet sliding of 9+2 axoneme is ultimately converted into rhythmic beating, it has taken diverse experimental approaches over a span of 4 decades to reveal the basis of this conversion. The spinning of the CP once per beat cycle (Omoto and Kung, 1979) inspired much imagination. The most interesting model is that the RS is the ATPase driving the CP rotation (Burton, 1973; Ogawa and Gibbons, 1976). It turns out that the spinning of the CP is not universal (reviewed by Omoto *et al.*, 1999) and instead is a consequence of inter-doublet sliding (Mitchell, 2003; Mitchell and Nakatsugawa, 2004). The RS ATPase theory was also debunked by the RS proteome that shows no RS subunits are ATPase or have ATPase domain (Yang *et al.*, 2006).

Without an ATPase, the mechanism of the RS and CP is still fascinating. The deviation of the CP from the center of a mutant lacking RSs (Mitchell and Sale, 1999), and the lengthening and tilt of RSs only at the bend of mussel gill cilia captured during beating indicate that RSs contact the CP transiently (Warner and Satir, 1974). It was proposed that the transient contact between RSs and the CP apparatus transduces mechanical feedback that directs alternate sliding of opposing subsets of outer doublet microtubules. Consistent with this, *Chlamydomonas* mutant flagella lacking RS and CP are paralyzed. In fact, flagella lacking the entire RS or only the spokehead are equally paralyzed (Huang *et al.*, 1981). Furthermore, CP deviates from the center in RS mutants (Mitchell, 2003; Mitchell and Nakatsugawa, 2004). Together, these observations indicate that the direct intermittent contact between CP and RS was central to flagellar motility. The requirement of direct physical interaction between the RSs and CP is recently

demonstrated by an elegant experiment: it was shown that simply tagging proteins to a spokehead subunit could rescue the paralysis of a mutant that misses part of the CP projection and thus the RS and CP periodical contact (Oda *et al.*, 2014).

Interestingly, in the presence of the original defects, paralysis of the RS and CP can be rescued when dynein motors or the nearby nexin-dynein regulatory complex (N-DRC) is mutated (Huang *et al.*, 1982). Based on the observations of suppressor mutations, it was proposed that the RS and CP constitute a control center governing dynein activation through N-DRC.

These independent lines of experimental evidence inspired the geometric clutch theory (Lindmann, 2004). When a power stroke is initiated via sliding within subset adjacent outer doublet microtubules, the force transverse to the flagella axis - T-force - develops at the curvature due to the accumulation of tension and compression on the outer doublet microtubules. As the flagella bend to the critical curvature for switching, T-force is large enough to disengage the dynein motors on the active microtubules and transferred to RSs and CP, which not only bear the transmitted forces but also restrain the distortion of the axoneme. This initiates a recovery stroke by engaging the dynein motors on the opposing outer doublet microtubules. This theory is proposed as the physical mechanism supports the rhythmic beating of motile cilia and flagella.

#### ***1.4.2 The Composition of the RS***

A central question is how a RS is built so that it can withstand distortions and transmit transverse force to ensure rhythmic beating. Analysis of RS mutants (Huang *et al.*, 1981), biochemical extractions (Yang *et al.*, 2001), mass spectrometry of isolated RSs

(Yang *et al.*, 2006) and perturbation experiments (Sivadas *et al.*, 2012; Gopal *et al.*, 2012; Gupta *et al.*, 2012; Oda *et al.*, 2014) identified 19 distinct RS proteins (RSPs) and predicted their respective locations (Table 1-1). Consistent with the nearly symmetric Y-shaped morphology of the RS, most RSPs are homodimers that contain a dimerization domain (Wirschell *et al.*, 2008), paralogues or paired subunits that share an identical domain (reviewed by Zhu *et al.*, 2016). Among the 19 polypeptides, 17 are exclusive subunits of the RS, whereas calmodulin and LC8 (Yang *et al.*, 2001) are present in a number of molecular complexes inside and outside of flagella. Given the importance of the RSs in flagellar motility that is used by numerous organisms in reproduction and other critical actions necessary to thrive in their natural environment, it is not surprising that the basic platform and composition of the RSs are remarkably conserved (Satouh *et al.*, 2005; Satouh and Inaba, 2009).

Each of the two spokehead modules is predicted to contain one copy of RSP1, 4, 6, 9 and 10 (Pigino *et al.*, 2011; Oda *et al.*, 2014). Among them, RSP1 and 10 are paralogues (Yang *et al.*, 2006), whereas RSP4 and 6 are encoded by duplicated genes located in tandem (Curry and Rosenbaum, 1992). The neck with the bifurcated arm is predicted to consist of HSP40, RSP2 and NDK5, each containing a Dpy30 domain (Yang *et al.*, 2004; Patel-King *et al.*, 2004), which is named after the protein vital for nematode development (Hsu *et al.*, 1995) and key to a number of molecular complexes, including Set1-like H3K4 histone methyltransferase (Jiang *et al.*, 2011). The stalk contains the rest of the RS subunits.

Location in RS	Name of the Subunit	Reference
<b>Scaffold</b>	<b>RSP3</b>	Yang <i>et al.</i> , 2006
<b>Head</b>	<b>RSP1</b>	
	RSP4	
	RSP6	
	RSP9	
	RSP10	
<b>Neck</b>	<b>RSP2</b>	
	<b>HSP40 (RSP16)</b>	
	<b>NDK5 (RSP23)</b>	
<b>Stalk</b>	RSP5	
	RSP7	
	RSP8	
	RSP11	
	RSP12	
	RSP13	
	RSP14	
	RSP17	
	RSP20 (Calmodulin)	
	RSP22 (LC8)	

**Table 1-1.** RS subunits in *Chlamydomonas*. \* Bolded, subunits relevant to this dissertation.

### 1.4.3 The Assembly of the RS

It is not immediately clear how the various RSPs assemble to form the particular Y-shaped complex that can transduce mechanical feedback. Much attention was centered on RSP3 that is essential for the assembly since RSs are diminished in the flagella of the RSP3 mutant, *pf14* (Diener *et al.*, 1993). As recombinant RSP3 N-terminal region binds to *pf14* axonemes but not tubulins, it was proposed that RSP3 forms the RS base anchoring the RS complex to the outer doublets (Diener *et al.*, 1993). Subsequently, it was demonstrated that RSP3 forms a homodimer (Wirschell *et al.*, 2008). By expressing



truncated RSP3, identifying the interacting domains (Sivadas *et al.*, 2012; Gopal *et al.*, 2012) and by tagging the opposing ends of RSP3 (Oda *et al.*, 2014), it was firmly established that RSP3 homodimer is a structural scaffold spanning the RS complex enabling the assembly of the rest of the RSPs and for anchoring RS to the outer doublets. A Y-shaped complex built on a backbone of one linear homodimer is conceivably more suitable to withstand and transmit forces than one built from a chain of subunits.

Surprisingly, RS precursors and mature RSs in the axoneme differ substantially, indicating that the prepackaging in the cell body is far from complete. Velocity sedimentation shows that precursors sediment as 12S particles, contrary to the 20S mature RSs isolated from flagella (Qin *et al.*, 2004). Furthermore, precursors appear like a  $\Gamma$ -shaped structure, distinct from the Y-shaped complex (Diener *et al.*, 2011). At least two RS components, HSP40 and LC8, are excluded from precursors (Yang *et al.*, 2005; Gupta *et al.*, 2012). Thus RS precursors packaged in the cell body are not ready to be assembled into the axoneme and must undergo substantial changes to become mature complexes.

Both HSP40 and LC8 are chaperones for protein folding and assembly for a wide variety of macromolecular complexes, although only HSP40 is considered to be a co-chaperone of a chaperone system. While spoke HSP40 is an isoform specific to the RS complex, LC8, a 10-kb small molecule (Jaffrey and Snyder, 1996; Liang *et al.*, 1999) is exceedingly conserved, abundant and ubiquitous. It is present in diverse molecular complexes, including dynein motor complexes and the RS (Pazour *et al.*, 1998; Yang *et al.*, 2001). As such it was proposed to serve as molecular glue using two grooves at the dimeric interphase to bring together two molecules in order to stabilize molecular

complexes (Williams *et al.*, 2007). A number of LC8 homologues are also present in dynein motors. Together they are grouped into a dynein light chain family (reviewed by King, 2016).

Differential impacts on dynein motors and the RS in an LC8 mutant indicate that this small dimer is not merely molecular glue (Yang *et al.*, 2009). It was found that RSP3, the backbone molecule, contains a multitude of LC8 binding sites. In vivo and in vitro experiments support a model where a stack of LC8 dimers bind to RSP3 to form the base of the stalk (Gupta *et al.*, 2012). This modality is analogous to the assembly of the scaffold of the nuclear pore complex (Stelter *et al.*, 2007; Nyarko *et al.*, 2013), and illustrates how the LC8 dimer, one or a multitude that are closely or loosely packed, could be used to build a variety of molecular complexes with differential physical properties. Binding of LC8 could change molecular interactions, triggering many downstream events (reviewed by Barbar and Nyarko, 2015). In the RS, it facilitates the assembly of the stalk base, accelerating its phosphorylation and docking to the axoneme.

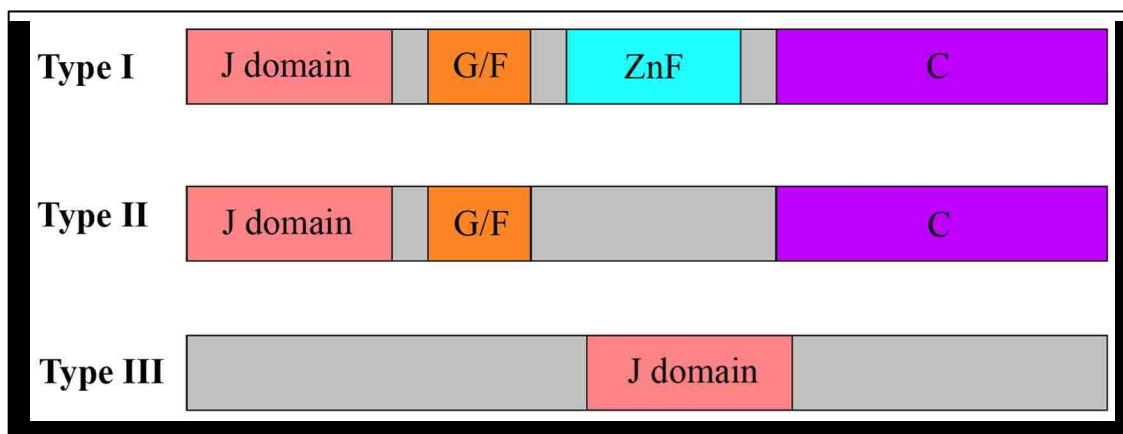
#### ***1.4.4 The Two Primordial Molecules in the Neck of the RS***

Similar to LC8, spoke HSP40 and NDK5 belong to large evolutionarily conserved families. Comparison of structural and compositional defects of the RS in mutants predicts that both proteins are co-localized with RSP2 to the neck of the RS (Yang *et al.*, 2006). Both RSP2 and NDK5 contain a Dpy3 domain for dimerization and docking, whereas RSP3 contains an amphipathic helix (AH) for anchoring the Dpy3 domain, indicating that these two molecules contribute to the assembly of the RS backbone. Consistent with this, orthologous RSP2 molecules also contain an  $\alpha$ -helix with a strong

propensity to form coiled coil, and RSP2 is required for the formation of the neck proteins and the spokehead. Therefore, it was proposed that RSP2 associates with the RSP3 scaffold to form the bifurcated arms connecting two head modules to the stalk (Gopal *et al.*, 2012; Sivadas *et al.*, 2012). In contrast, the roles of HSP40 and NDK5 in RS assembly are not obvious. Elucidation of the structural and functional roles of these two molecules in the context of RS will shed light on the fundamental mechanisms of these two important ancient protein families and their diversified usages in numerous cellular reactions and processes.

#### ***1.4.4.1 HSP40***

HSP40 was initially named based on the increased abundance of a 40-kDa protein induced by heat shock treatments. It was discovered subsequently that heat shock aggravates the needs of protein refolding which are mediated by various HSPs that constitute a number of chaperone systems. Since then a host of HSP40 genes have been discovered via diverse approaches. Despite sequence divergence, they all contain a signature J domain (Figure 1-4). Therefore, they are often referred to J proteins. For clarity, I will refer these proteins to HSP40s in this dissertation. Based on the common domains, HSP40s are separated into three categories.

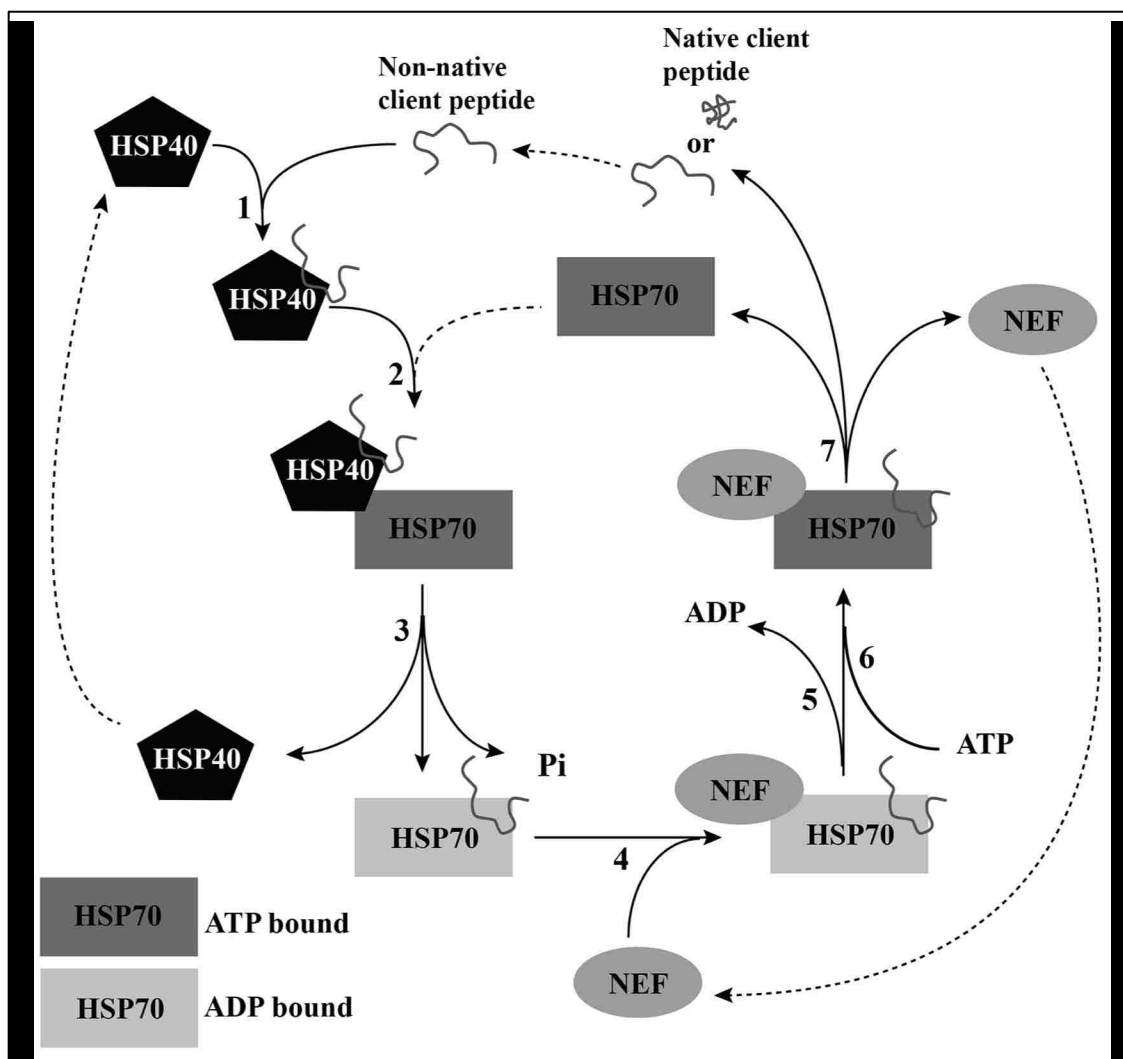


**Figure 1-4.** Generalized domain structures of HSP40 protein family. HSP40 proteins are classified into three types. Type I typically consists of a J domain, followed by a glycine/phenylalanine (G/F)-rich region, zinc finger (ZnF) domain and C domain. Type II is similar to Type I except lacking the ZnF domain. Spoke HSP40 is a Type II HSP40. The other HSP40s that don't have these features are designated as Type III and only harbor the signature J domain.

In spite of the sequence variations and divergent functions, HSP40s are still primarily known to act as co-chaperones of HSP70s to assist in a myriad of folding-related processes, such as folding of nascent polypeptides, refolding or degradation of misfolded polypeptides, and disassembly of folded multi-molecular complexes (Kampinga and Craig, 2010). In a well-accepted model, the HSP40 dimer binds and presents client peptides to HSP70, and, in the meantime, stimulates the ATPase activity of HSP70 (Figure 1-5). ATP hydrolysis stabilizes HSP70-client interaction. The client is released to allow refolding when nucleotide exchange factor (NEF) transforms HSP70 from ADP-bound high-client-affinity state to ATP-bound low-client-affinity state.

Released HSP40 recruit a new client, starting the cycle again. However, the exact molecular mechanisms remain elusive.

Accumulated evidence showed that a number of HSP40 paralogues, including spoke HSP40 (Yang *et al.*, 2005, 2008), don't require an HSP70 partner (Tamadaddi and Sahi, 2016), even though their J domain appears conserved. The seemingly normal RS morphology in the HSP40-null flagella (Yang *et al.*, 2008) and the absence of HSP40 in the 12S precursor (Yang *et al.*, 2005) indicate that spoke HSP40 is not required for the refolding of the  $\Gamma$ -shaped precursor into the Y-shaped complexes. Nonetheless, spoke HSP40 is indispensable. HSP40-null flagella jerk incessantly (Yang *et al.*, 2008). Elucidation of the application of HSP40 in the RS will shed light on a host of vital reactions mediated by HSP70-independent HSP40s (Tamadaddi and Sahi, 2016).



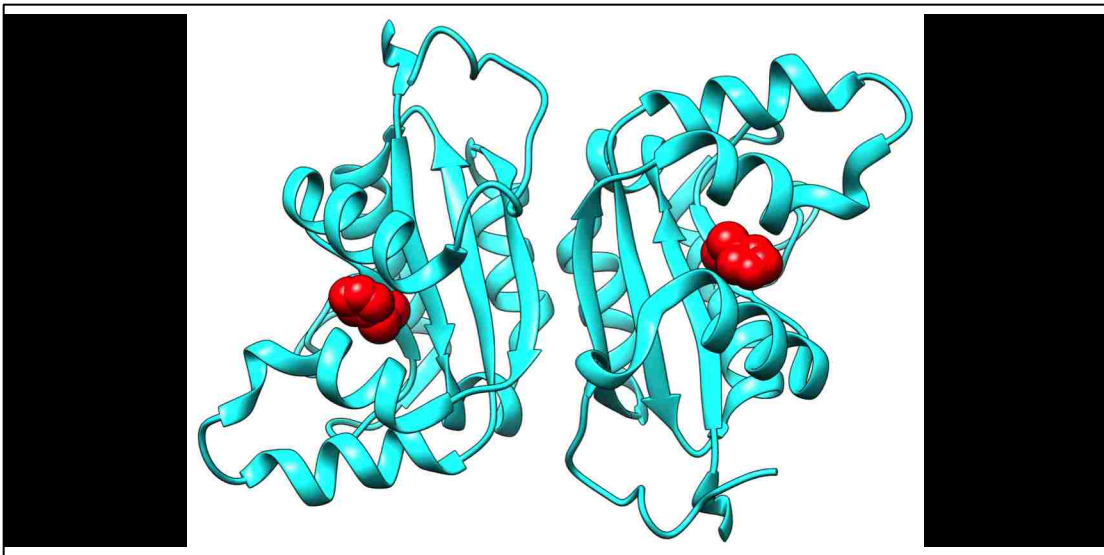
**Figure 1-5.** Canonical model of the core HSP70-HSP40 machinery's action in protein folding (adapted from Kampina and Craig, 2010). As a co-chaperone, HSP40 recruits client peptide (1), binds ATP-bound HSP70 and stimulates its ATPase activity (2). ATP hydrolysis increases HSP70 affinity for client peptide and releases HSP40 from the HSP70-client complex (3). Nucleotide exchange factor (NEF) binds HSP70 (4), replacing ADP with ATP (5, 6). The ATP-bound HSP70 with low affinity to client releases the client peptide that could undergo refolding (7). Those that remain a non-native conformation can rebind HSP40 via hydrophobic interaction, starting the chaperone cycle again. Dashed arrows represent the start of the next cycle.

#### **1.4.4.2 NDK**

NDKs were initially discovered in the 1950s as enzymes that balance the homeostasis of intracellular nucleoside triphosphate (NTP) via Ping-Pong mechanism (Cheng *et al.*, 1973). However, unlike typical protein kinases, their phosphotransfer is actually rather nonspecific. In general, the  $\gamma$ -phosphate from NTP is first transferred to a strictly conserved histidine residue to form a high-energy phosphohistidine intermediate. In theory, the phosphate is readily transferred and forms a covalent bond with nearby molecules, such as NDPs or proteins. For a long time, protein phosphorylation by NDKs was considered to be a side effect from the His-dependent spurious phosphate relay. Yet independent lines of evidence from the past two decades have unequivocally demonstrated that NDKs can also serve as protein histidine kinases via the same phosphotransfer pathway to regulate crucial cellular processes in eukaryotic cells (Attwood and Wieland, 2014). The phosphorylation sites are rather specific even though exactly how the catalytic active site binds the substrate remains elusive (Wagner and Vu, 1995; Muimo *et al.*, 2000; Cuello *et al.*, 2003; Srivastava *et al.*, 2006; Cai *et al.*, 2014). Importantly, the most interesting reactions mediated by NDKs, such as suppression of cancer metastasis (e.g. Steeg *et al.*, 1988; MacDonald *et al.*, 1993; 1996; Chang *et al.*, 1994; 1996; Wagner *et al.*, 1997; Carotenuto *et al.*, 2013) and transcription regulation of myc oncogene are independent to His-phosphorylation (e.g. Postel *et al.*, 1993; Thakur *et al.*, 2009). Exactly what molecular mechanisms these NDKs adopted to mediate the reactions remains unclear.





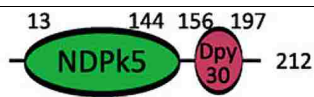

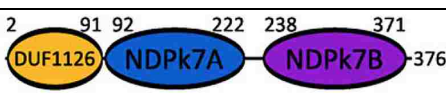
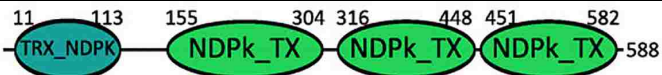

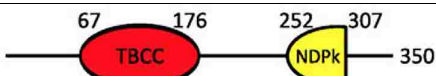
Studies of NDKs have been largely centered on Group I NDKs. Crystal structures of Group I NDK orthologs show their tertiary structure is conserved (Figure 1-6). Group

II NDKs have one or multiple NDK domains whose sequences diverge from Group I NDKs and additional domains that may specify locations or functions (Table 1-2) (Desvignes *et al.*, 2009). No crystal structure of Group II NDK has been acquired so far due to their precipitation propensity. Functional studies of these NDKs have found that they primarily operate in motile cilia, like NDK5, and mitochondria. Studies of mammalian mutants have revealed the functional significance of ciliary NDKs, but further studies remain limited. Investigation of NDK5 in the RS could reveal novel mechanisms in the RSs and NDKs.



**Figure 1-6.** Crystal structure of a NDK dimer in the hexameric human NDK1 (PDB accession number, 4ENO) (Kim *et al.*, 2013). The conserved histidine residue that is in the catalytic cleft and strictly required for the NDK activity is highlighted as red spheres.



	Name	Domain Structure	Significance
Group I	NDK1		Carcinogenesis
	NDK2		Oncogene transcription factor
	NDK3		Unclear
	NDK4		Myelodysplastic syndrome
Group II	NDK5		Primary cilia dyskinesia
	NDK6		Located in Mitochondria
	NDK7		Primary cilia dyskinesia
	NDK8		Primary cilia dyskinesia
	NDK9		Unknown
	NDK10		Unknown

**Table 1-2.** Molecular domains in Group I and Group II human NDKs. The NDK domains, synonymous to NDPK, have diverged. Those diverging substantially are depicted with a color other than green. NDK10 is the outgroup that contains a partial NDK domain. Inserted cartoon are modified after Desvignes *et al.*, 2009.

### 1.5 Objectives of This Dissertation

The well-characterized motility machinery of flagella, the extensive understanding of the RS complex and the model organism *Chlamydomonas* that is

amenable to many experimental approaches present an excellent opportunity to discover the roles and divergent molecular mechanisms of the primordial HSP40 and NDK families. This dissertation, made possible by new *Chlamydomonas* mutant strains, accomplishes two objectives.

### ***1.5.1. Elucidation of NDK5 in the RS***

A previous study has shown indirectly that NDK5 has NDK activity. This project aims to answer if the NDK activity is crucial for flagella or dispensable as proposed (Munier *et al.*, 2003), and how this Group II NDK committed specifically to the RS operates. The unexpected results shed light on long standing questions in the NDK field and reveal the broad contributions of the RS beyond motility control.

### ***1.5.2 Elucidation of the Non-canonical Role of Spoke HSP40***

This project investigates the role of HSP40 in RS assembly and determines how HSP40 that is separated from RS precursors during fractionations is assembled into the RSs. The results explain HSP70-dependent canonical mechanisms and similar non-canonical mechanisms in diverse cellular processes. In addition, it sheds light on how assembly of axonemal complexes occurring at opposite ends of flagella is integrated; and shows what future research portends.

## CHAPTER 2: MATERIALS AND METHODS

### ***2.1 Materials***

#### ***2.1.1 Chlamydomonas Strains***

Wild type (WT) (cc124 and cc125) and *pf14* allelic mutants - cc613, cc1032 and cc2496 - were acquired from the *Chlamydomonas* Resource Center. The *ndk5* insertional mutant (LMJ.SG0182.001362) and the parental strain, CMJ030, were provided by the Jonikas laboratory at the Carnegie Institute of Science (Li *et al.*, 2015). The *pf33* mutant was generated by UV mutagenesis (Kamiya, 1988). Strains related or used in this dissertation are listed in Table 2-1.

#### ***2.1.2 Culture Conditions***

Cells were grown in minimal M media (Sager and Granick, 1953) or Tris-acetate-phosphate media (TAP; Harris, 1989) as indicated.

#### ***2.1.3 Antibodies***

NDK5 western blots were probed with the rabbit polyclonal antibody raised against Ni-NTA purified His-tagged NDK5<sub>1-201</sub> unless indicated otherwise. 3G3 was a mouse monoclonal antibody raised against 120-kDa spoke proteins spot-purified from 2-D gels of axonemes (Williams *et al.*, 1989). This study showed that 3G3 recognized NDK5. Anti outer dynein arm subunit IC1 (formerly IC78 and IC80) was also a mouse monoclonal antibody (King *et al.*, 1991). The affinity-purified rabbit polyclonal antibodies for NDK5<sub>8-586</sub>, polyclonal antibodies for other RSPs, inner dynein arm subunit

p28 and IC140, and CP projection CPC1 used in this study are listed in Table 2-2.

<b>WT strains</b>				
<i>cc124</i>				
<i>cc125</i>				
<b>Mutant strains</b>	<b>Mutated gene</b>			
<i>pf14</i> ( <i>cc613</i> , <i>cc1032</i> and <i>cc2496</i> )	RSP3			
<i>ndk5</i>	NDK5/RSP23			
<i>pf33</i>	HSP40/RSP16			
<i>pf24</i>	RSP2			
<i>pf18</i>	Pf18			
<i>fla10</i>	Fla10			
<b>Transgenic strains</b>	<b>Parental strains</b>	<b>Plasmid</b>	<b>Antibiotic Selection marker</b>	<b>Tag</b>
<i>ndk5</i> ::NDK5-HYG	<i>ndk5</i> (LMJ.SG0182)	pNDK5-HYG	HYG	
<i>ndk5</i> ::NDK5 <sub>H121A</sub> -HYG	<i>ndk5</i> (LMJ.SG0182)	pNDK5 <sub>H121A</sub> -HYG	HYG	
WT::NDK5-HYG	cMJ030	pNDK5-HYG	HYG	
WT::NDK5 <sub>H121A</sub> -HYG	cMJ030	pNDK5 <sub>H121A</sub> -HYG	HYG	
<i>ndk5</i> ::NDK5-mNG-3HA-6His-HYG	<i>ndk5</i> (LMJ.SG0182)	pNDK5-mNG-3HA-6His-HYG	HYG	mNG; 3HA-6His
<i>ndk5</i> ::NDK5 <sub>H121A</sub> -mNG-3HA-6His-HYG	<i>ndk5</i> (LMJ.SG0182)	pNDK5 <sub>H121A</sub> -mNG-3HA-6His-HYG	HYG	mNG; 3HA-6His
<i>ndk5</i> ::NDK5 <sub>H121A/K12A</sub> -HYG	<i>ndk5</i> (LMJ.SG0182)	pNDK5 <sub>H121A/K12A</sub> -HYG	HYG	
<i>ndk5</i> ::NDK5 <sub>H121A/H55A</sub> -HYG	<i>ndk5</i> (LMJ.SG0182)	pNDK5 <sub>H121A/H55A</sub> -HYG	HYG	
<i>ndk5</i> ::NDK5 <sub>H121A/P104G</sub> -HYG	<i>ndk5</i> (LMJ.SG0182)	pNDK5 <sub>H121A/P104G</sub> -HYG	HYG	
<i>ndk5</i> ::NDK5 <sub>H121A/R108</sub>	<i>ndk5</i>	pNDK5 <sub>H121A/R108A</sub> -	HYG	

$\Delta$ -HYG	(LMJ.SG0182)	HYG		
<i>ndk5</i> ::NDK5 <sub>H121A/N118</sub>	<i>ndk5</i>	pNDK5 <sub>H121A/N118A</sub> <sup>-</sup>	HYG	
$\Delta$ -HYG	(LMJ.SG0182)	HYG		
<i>ndk5</i> ::NDK5 <sub>S123G</sub> -HYG	<i>ndk5</i>	pNDK5 <sub>S123G</sub> -HYG	HYG	
DN::RSP3-mNG-PMM	DN	pRSP3-mNG-PMM	PMM	mNG
<i>pf33</i> :: HSP40	<i>pf33</i> mt(-)	pHSP40	PMM	
<i>pf33</i> :: GFP-HSP40	<i>pf33</i> mt(-)	pGFP-HSP40	PMM	GFP
<b>Backcross strains</b>	Parental strains			
<i>ndk5</i> mt(+)/mt(-)	cc620 mt(+); cc125 mt(+); <i>ndk5</i> mt(-)		PMM	
<i>pf33</i> mt(+)	cc125 mt(+); <i>pf33</i> mt(-)			
<b>Double mutants</b>	Parental strains			
<i>pf14/pf33</i> mt(+)/mt(-)	<i>cc1032 pf14</i> mt(+); <i>pf33</i> mt(-)			
<i>pf18/pf33</i> mt(+)/mt(-)	<i>cc1036 pf18</i> mt(+); <i>pf33</i> mt(-)			
<i>fla10/pf33</i> mt(+)/mt(-)	<i>cc4180 fla10-2</i> mt(+); <i>pf33</i> mt(-)			

**Table 2-1.** Strains used or generated in this dissertation.

Antibody	Host	Reference
<b>Primary Antibody</b>		
Anti-RSP1	Rabbit	Yang <i>et al.</i> , 2006
Anti-RSP2	Rabbit	Yang <i>et al.</i> , 2006
Anti-RSP3	Rabbit	Yang <i>et al.</i> , 2006
Anti-RSP4	Rabbit	Yang <i>et al.</i> , 2006
Anti-RSP5	Rabbit	Yang <i>et al.</i> , 2006
Anti-RSP6	Rabbit	Yang <i>et al.</i> , 2006
Anti-RSP9	Rabbit	Yang <i>et al.</i> , 2006
Anti-RSP10	Rabbit	Yang <i>et al.</i> , 2006
Anti-HSP40	Rabbit	Yang <i>et al.</i> , 2005
Anti-NDK5 <sub>1-201</sub>	Rabbit	Zhu <i>et al.</i> , submitted
Anti-NDK5 <sub>5-586</sub>	Rabbit	Patel-King <i>et al.</i> , 2004
p28	Rabbit	LeDizet and Piperno, 1995
CPC1	Rabbit	Patel-King <i>et al.</i> , 2004
IC140	Rabbit	Yang and Sale, 1998
IC1	Mouse	King <i>et al.</i> , 1991
3G3	Mouse	Williams <i>et al.</i> , 1989
<b>Secondary Antibody</b>		
Anti-rabbit IgG-peroxidase	Goat	Sigma
Anti-mouse IgG-peroxidase	Goat	Sigma

**Table 2-2.** Antibodies used in this dissertation.

## ***2.2 Molecular Biology***

### ***2.2.1 PCR-based Genotyping***

Standard PCR reactions typically underwent 35 cycle with an anneal temperature near the melting temperatures of primer pairs. Reactions underwent only 20 cycles for site-directed mutagenesis. All primer sequences are listed in Table 2-3.

#### ***2.2.1.1 Characterization of the Insertional Site in ndk5***

PCR was conducted to amplify the PMM-resistance cassette-genome junctions, the upstream *SPL4* gene and across *NDK5*. Templates were genomic DNA freshly prepared from *ndk5* cells and its parental strain CMJ030. Briefly, approximately 1µl cells from TAP plates were re-suspended in 20 µl 10 mM EDTA and boiled for 5 minutes. Following a 30-second vortex and 3-min centrifugation, the supernatant containing genomic DNA was used immediately as template in PCR. The primer pairs designed for PCR are N-P1S and N-P1As, N-P2S and N-P2As, N-P3S and N-P3As.

#### ***2.2.1.2 Characterization of Mutation Site in pf33***

Genomic DNA template preparation is the same as described above. Four pair of primers, H-P1S and N-P1As, H-P2S and H-P2As, H-P3S and H-P3As, H-P4S and H-P4As, were used to amplify the entire genomic DNA of HSP40 from *pf33*, including 5' and 3' UTR, and the flanking sequences.

### ***2.2.2 Engineering of Genomic Constructs***

#### ***2.2.2.1 Engineering of NDK5 Genomic DNA Constructs***

An NdeI-NdeI fragment containing the *NDK5* gene was released from the 21I22 BAC clone (Clemson University Genome Institute) and ligated into the pGEM-T easy vector. The plasmid was further digested with EcoRV and SmaI, and blunt end-ligated to eliminate most of the neighboring *SLP4* gene. The resulting WT pNDK5 plasmid was converted into pNDK5<sub>H121A</sub> using site-directed mutagenesis and a pair of partial overlapped primers, NDK5MutS and NDK5MutAs, that both contain the mutation site.

A hygromycin (HYG) resistant cassette, PCR-amplified using pHyg3 as a template (Berthold, 2002) and primer pair NdeHygS/NdeHygAs containing an NdeI site, inserted into the NdeI site in both genomic constructs. The final constructs were 11.3-kb.

To express fluorescent RSPs in *Chlamydomonas*, mNeonGreen (NG) (Shaner *et al.*, 2013) codons modified in accordance with the *Chlamydomonas* codon bias (Harris *et al.*, 2015) were PCR-amplified using primer pair NeoS/NeoAs containing an XhoI site and cloned into the XhoI site inserted before the stop codons of the *NDK5* gene and *RSP3* gene (Sivadas *et al.*, 2012). The XhoI site in *NDK5* gene was inserted by site-directed mutagenesis using primer pair 5'XhoS/5'XhoAs.

#### **2.2.2.2 Engineering of HSP40 Genomic DNA Constructs**

The genomic DNA from WT cells was prepared the same way as described above. The entire genomic *HSP40* gene was recovered by two rounds of PCRs (Zhu *et al.*, 2013). In the first round, two primer pairs (GenS and P2As, P3S and GenAs; Table 2-3) were used to amplify two overlapping genomic DNA fragments that includes 5' and 3' UTR and the flanking sequences. The second round of PCR include equal amounts of the two fragments and the primer pair GenS and GenAs. The resulting full-length genomic DNA



was inserted into pGEM-T Easy vector. A KpnI-SpeI fragment purified from this plasmid was ligated into a plasmid containing the paromomycin (PMM) resistant cassette (Sivadas *et al.*, 2012) for single plasmid transformation.

To engineer the GFP-HSP40 genomic plasmid, GFP DNA (Rasala *et al.*, 2013) that was PCR-amplified using primers pair GFPS/GFPAs containing a NheI site (underlined) was cloned into the complementary XbaI site inserted downstream to the start codon of the *HSP40* gene. The primers for the XbaI restriction site insertion are 16XXS and 16XXAs, 16XBS and 16XBAs.

The RSP3-GFP construct was derived by replacing the tag sequence in the RSP3-3HA12His construct (Gupta *et al.*, 2012) with the GFP DNA flanked by XhoI restriction sites.

Name	Sequence
N-P1S	GCTCGTGGAGCTCTGAATCT
N-P1As	GATACACGAACTCCTGCGC
N-P2S	GCTGCATGTAGGAGGCGCCACCTACC
N-2As	GGTGGCATTCTGGGTGCCGTCGGTTCC
N-P3S	GGCAAATGGAGCTGTTTGGA
N-P3As	CCTTAAAGCGTGCTCCTGAC
H-P1S	GCAGTAAGTTACTTGGGTCTCAATGCG
H-P1As	GCAATTCAACTTACGATCGCAGAGC
H-P2S	CGTGAGTTTGGGAGACTGTAGGGTCCG
H-P2As	CGTGGAAGATCTCCTCCAGCGTAAGC
H-P3S	GCTGTCCAACCAGTTCGAGTCCATGACC
H-P3As	CCTGTCTCATGTAAACGCTCCAATCC
H-P4S	GGTAACTTGGTCATTGAGATCGACCTGC
H-P4As	GCGGTAGTGCTCTTGGACATTTTGTGC

NDK5MutS	CCCAGAATGCCACCGCGGGCAGCGACTCGCCTATCAGC
NDK5MutAs	GCTGCCCGCGGTGGCATTCTGGGTGCCGTCGGTTCC
NdeHygS	GCATATGGATTACGAATTCGATATCAAGCTTCTTTCTTGC
NdeHygAs	GCATATGCGCTTCAAATACGCCCAGC
NeoS	CTCGAGATGGTGTCCAAGG
NeoAS	CTCGAGCTTGTACAGCTCGTCC
5'XhoS	GGAGGCCGCTGAGCTCGAGTAAGGGCACAGAGCATGGGGT TGC
5'XhoAs	CCTTACTCGAGCTCAGCGGCCTCCGGCTCCGGCTCG
GenS	TGCCGTGTAAGGCCATGAGGCACACGC
GenAs	TCCCTTCTGCGCACCGTGTGCGGTACC
GFPS	GGCTAGCGATCCCCCAAGGGCGAGG
GFPAAs	GGCTAGCCTTGTACAGCTCGTCCATGCCGTGG
16XXS	GAAGCCAGCCCCGCCAATATGTCC
16XXAs	GGTCTAGAGCCCCGCGTCATTTTGCTGATAGC
16XBS	GGTCTAGATTGGACTATTACGAGGTCATGGGCCTTAC
16XBAs	CTGAACAGAAGCACCTTGCCTTTGTGC

**Table 2-3.** Oligonucleotides used in this dissertation.

## **2.3 *Chlamydomonas* Experiments**

### **2.3.1 Backcross**

*ndk5* mt(-) (Li *et al.*, 2015) was crossed with cc620 or cc125 mt(+) as indicated, using the synchronous gametogenesis method (Snell, 1976) followed by tetra dissection (Jiang and Stern, 2009). *pf33* mt(-) was crossed with cc125 mt(+) to generate *pf33* mt(+). Backcross strains and double mutant strains generated for the experiments not shown are listed in Table 2-1.

### **2.3.2 Transformation**

All transformations were conducted using the glass bead method as described (Yang *et al.*, 2006) with minor modifications. In *Chlamydomonas* transformation, transgene is integrated into the chromosome by non-homologous recombination. Minigene experiment was described in the dissertation of Dr. Radhika Gopal (2011). *NDK5* genomic constructs at a concentration of 1-2 µg were transformed into *ndk5* or its parental strain CMJ030 and the transformants were selected on TAP plates containing 10 µg/ml HYG. Similarly, RSP3 genomic constructs were transformed into *pf14* cells and HSP40 genomic constructs were transformed into *pf33* cells but the transformants were selected for PMM resistance (10 µg/ml). Fractions of single colonies resuspended in 200 µl double distilled water were placed in 96-well plates for motility analysis under a Leica MZ16 stereomicroscope.

### **2.3.3 Flagellar Length Quantification**

Cells fixed with 2.5% glutaraldehyde were placed on poly-L-lysine-coated slides for imaging. The lengths of 50 randomly selected flagella were measured using ImageJ software. For flagellar regeneration experiments, pH shock with acetate was used to excise flagella of log phase cells from TAP medium cultures. For NDK5 strains, after confirmation of deflagellation microscopically, an aliquot of the cells was fixed with 2.5% glutaraldehyde every 15 min for subsequent imaging. The lengths of 20 randomly chosen flagella were measured at each time point. For HSP40 strains, an aliquot of cells taken at indicated time was placed on polyethylenimine-coated slides instead for imaging.

#### ***2.3.4 Dikaryon Rescue***

Plate gametogenesis method (Martin and Goodenough, 1975) was used to produce gametes. Briefly, cells resuspended in H<sub>2</sub>O were plated on TAP plates. After 5 days under constant light, cells were hatched first in H<sub>2</sub>O and then supplemented with nitrogen-free TAP media. After shaking under light for 4-5 hours, equal amount of gametes of opposite mating types were mixed and then placed under light without agitation. An aliquot of cells taken periodically as indicated was placed on polyethylenimine-coated slides for imaging. For creating dikaryons with two growing flagella and two full-length flagella, recipient cells were triggered to shed flagella by pH shock in the presence of cycloheximide as described (Johnson and Rosenbaum, 1992). After confirmation of deflagellation microscopically, cells were allow to regrow flagella to about half or two thirds lengths and then mixed with donor cells.

#### ***2.4 Biochemistry***

#### **2.4.1 Flagella Preparation and Western Blot**

The light/dark cycle, flagella preparation and western blot analysis were as described previously (Yang *et al.*, 2001), except for the addition of protease inhibitor cocktail tablets (cOmplete Mini, EDTA-free, Roche, Basel, Switzerland) as indicated.

#### **2.4.2 Purification of Bacterial Recombinant Proteins**

To produce His-Luciferase, the firefly luciferase gene was amplified from pTRE2-Luc (Clontech, Mountainview, CA) and cloned into the pET28a vector. The plasmids for His-Luciferase and His-HSP40 (Yang *et al.*, 2005) were transformed into BL21 (DE3) for protein expression. MBP-His-NDK5<sub>1-201</sub> was expressed as described (Donnelly *et al.*, 2006). Each bacteria grew in 10 ml LB media shaking at 37 degree till reached OD 5.0~6.0. To induce recombinant protein expression, cultures were added with 50 ul, 200 mM IPTG and incubated at 18 degree overnight. All His-tagged recombinant proteins were purified with Ni-NTA matrix following the manufacturer's instruction (Qiagen, Hilden, Germany).

#### **2.4.3 Pull-down Assay**

His-HSP40 expression was described previously (Yang *et al.*, 2005). For NDK5<sub>1-201</sub>, the DNA was cloned into the pMCSG19 vector for the expression of MBP-TVMV site - 6His-TEV site-NDK5<sub>1-201</sub> in BL21 bacteria expressing TVMV protease (Donnelly *et al.*, 2006; Zhu *et al.*, submitted). His-tagged proteins in bacterial extract were purified with Ni-NTA matrix as described (Sivadas *et al.*, 2012). For pull down assay, 6His-TEV

site-NDK5<sub>1-201</sub> was treated with purified His-TEV protease overnight at 4°C in the presence or absence of His-HSP40 prior to incubation with Ni-NTA.

#### ***2.4.4 Nucleotide Diphosphate Kinase Activity Assay***

The assay measured luminescence emitted from luciferin and was catalyzed by luciferase using ATP generated by NDKs that transferred the  $\gamma$ -phosphate from GTP to ADP (Karamohamed *et al.*, 1999). An aliquot of 60 ng purified recombinant proteins or 1  $\mu$ g axonemes was added to the 0.2 ml assay buffer (0.1 M Tris-acetate pH 7.8, 10 mM MgSO<sub>4</sub>, 2 mM EDTA, 1 mM dithiothreitol, 1 mg/ml bovine serum albumin, 0.1 mg/ml D-luciferin, 10 ng/ml Ni-NTA-purified His-firefly luciferase, 0.5 mM ADP and 0.5 mM GTP in a cuvette placed in a Monolight 2010 luminometer (Analytical Luminescence Laboratory, Ann Arbor, MI). The change in light emission was measured for 10 seconds and expressed as relative light units (RLU, light emission/second) as recommended by the manufacturer. Each sample was analyzed in triplicate. The RLU of axonemes for each experimental group was then normalized to that of the WT control and denoted in as relative kinase activity (%).

### ***2.5 Microscopy***

#### ***2.5.1 Light Microscopy***

Bright field and fluorescent images were acquired at a 400 X magnification using a Nikon Eclipse E600W compound microscope equipped with a CoolSNAP-ES CCD camera (Photometrics, Tucson, AZ) and MetaMorph imaging system (Molecular Devices, Sunnyvale, CA). The MetaMorph program was also used for pseudocolor with a standard

rainbow color palette. ImageJ 1.50i was used to subtract background and the line tool was used to draw across the brightest region near the flagellar tip to obtain plot profiles. The peak value from each profile was used to calculate intensity ratios.

### **2.5.2 Electron Microscopy**

Thin section electron microscopy (EM) of axonemes was performed by Dr. Ritsu Kamiya (1988). Cryo-ET was performed by Drs. Emiliya Poghosyan and Takashi Ishikawa (Paul Scherrer Institute, Switzerland). Briefly, isolated axonemes were quick plunge frozen in liquid ethane at liquid nitrogen temperatures with the help of a vitrification device (Cryo-plunge, Gatan, Pleasanton, CA). Holey carbon grids (200 mesh, R3.5/1, Quantifoil Micro Tools GmbH, Großlobichau, Germany) were used. Gold colloid particles (10 nm) were applied to the sample, prior to freezing, as fiducial markers for tomographic reconstruction. Data collection was performed using a JEM2200FS transmission electron microscope (JEOL, Tokyo, Japan) equipped with an in-column energy filter, and a field emission gun. Micrographs were recorded with a 4k x 4k CMOS camera (F416 from TVIPS, Gauting, Germany). Tomographic image series were collected using a previously described procedure (Pigino *et al.*, 2011), except for the use of SerialEM software (Mastronarde, D.N. 2005 JSB 152, 36-51). Image analysis was performed as described previously (Pigino *et al.*, 2011).

### **2.6 Modeling**

Crystal structures retrieved from Protein Data Bank (PDB) were manually fit into cryo-ET taken from Electron Microscopy Data Bank (EMDB) using *Chimera UCSF* (Pettersen *et al.*, 2004).



## CHAPTER 3: GENERAL AND SPECIFIC PROMOTIONS OF FLAGELLAR ASSEMBLY BY A FLAGELLAR NUCLEOSIDE DIPHOSPHATE KINASE

### 3.1 Introduction

It is well established that nucleoside diphosphate kinases (NDKs) transfer a phosphate from NTPs to NDPs (Berg and Joklik, 1953) via a Ping-Pong mechanism. The  $\gamma$ -phosphate of an NTP first forms a high-energy intermediate with a conserved histidine (designated as H121 in this dissertation) located in a narrow catalytic cleft. Following the departure of the resulting NDP, the phosphate is transferred to the recipient NDP containing the same or a different base (reviewed by Lascu and Gonin, 2000). These reactions enable the levels of nucleotide species to be appropriately balanced in diverse cellular compartments. Consistent with the fundamental importance in nucleotide metabolism, NDKs are ubiquitous, expressed in both prokaryotes and eukaryotes, often by multiple NDK genes. Based on sequence similarities, NDKs have been divided into Group I (NDK1-4) and Group II (NDK5-10) (reviewed by Desvignes *et al.*, 2009).

However, accumulating evidence indicates that NDKs are not merely interconverting NDPs and NTPs. They interact with many molecules (reviewed by Steeg *et al.*, 2011). Direct interactions allow NDKs to stimulate GTP loading of their dynamin GTPase partners that drive constant fission and fusion of diverse membranous compartments (Boissan *et al.*, 2014). Furthermore, NDK2 modulates G-proteins and cation channels as a histidine protein kinase (Srivastava *et al.*, 2006; Di *et al.*, 2010; Cai *et al.*, 2014). It is thought that the phosphate transiently linked to H121 in NDKs can be preferentially transferred to specific residues in target proteins instead of to NDPs (reviewed by Attwood and Wieland, 2015). Although histidine phosphorylation is a

common prokaryotic regulatory mechanism, NDK2-mediated histidine phosphorylation is a *bona fide* eukaryotic strategy for regulating critical processes, such as lymphocyte activation. A number of NDK-mediated reactions - such as metastasis suppression of cancer cells (e.g. Steeg *et al.*, 1988; MacDonald *et al.*, 1993; 1996; Chang *et al.*, 1994; 1996; Wagner *et al.*, 1997; Carotenuto *et al.*, 2013) and transcriptional regulation of c-myc oncogene (e.g. Postel *et al.*, 1993; Thakur *et al.*, 2009) - do not correlate with the NDK activity or require H121. Similarly, a heterozygous NDK mutation (*killer-of-prune* or *kpn*) is lethal to a seemingly healthy *Drosophila* strain with purple eyes (*prune*) (Sturtevant, 1956; Rosengard *et al.*, 1989; D'Angelo *et al.*, 2004; Carotenuto *et al.*, 2013; Zhang *et al.*, 2015; reviewed by Takacs-Vellai, 2015), although the mutation itself does not affect the NDK activity (Lascu *et al.*, 1992). While metastasis suppression and dominant negative (DN) lethality naturally have attracted much interest for decades, the molecular underpinnings remain uncertain (Steeg *et al.*, 2011).

Group II NDKs diverged from Group I before chordate radiation (Desvignes *et al.*, 2009) and perhaps even before the divergence from the last common eukaryotic ancestor. Most Group II NDKs have acquired additional molecular modules, and primarily reside in motile cilia and flagella which likely exist in the eukaryotic ancestor (Mitchell, 2007). Flagellar NDKs are built into the microtubule-based axonemal superstructure in motile cilia and flagella (Ogawa *et al.*, 1996; Padma *et al.*, 2001; Munier *et al.*, 2003; Sadek *et al.*, 2003; Patel-King *et al.*, 2004; Duriez *et al.*, 2007). In humans and other mammals, defects in these NDKs results in Primary cilia dyskinesia (PCD), demonstrating their importance in cilia biology (Duriez *et al.*, 2007; Vogel *et al.*, 2012). However, surprisingly the H121 residue that is required for phosphate transfer between NDPs and

NTPs and conserved in Group I NDKs is not strictly conserved in Group II NDKs (Munier *et al.*, 2003; Patel-King *et al.*, 2004). Furthermore, respiratory cilia of NDK8 PCD patients lacked the NDK8-containing outer dynein complex (Duriez *et al.*, 2007).

These observations lead to a prediction that flagellar NDKs are structural proteins, and the H121 in some NDK domains and thus the NDK activity are merely an evolutionary relic (Munier *et al.*, 2003). However, other lines of evidence argue that the NDK activity is important. For example, NDK7 co-purifies with the  $\gamma$ -tubulin ring complex from the centrosome that supports ciliogenesis at the interphase and only recombinant NDK7 with H121 could promote microtubule polymerization from the centrosome *in vitro* (Liu *et al.*, 2014). NDK5 (alias NME5, NDPK5, NM23-5 and RSP23) is a constitutive subunit of the radial spoke (RS), a molecular complex that exhibits NDK activity (Patel-King *et al.*, 2004) and controls flagellar motility. Mouse NDK5 mutation affects the motility of sperm flagella and of both airway and ependymal cilia but does not disturb left-right asymmetry, a process requires nodal cilia that lack radial spokes (Vogel *et al.* 2012). Although cilia and flagella dyskinesia is the only known phenotype from RS deficiencies in diverse organisms (e.g. Huang *et al.*, 1981; Jeanson *et al.*, 2015), *ndk5* knockout mice are sterile and have sperm that are apoptotic, with short flagella or completely aflagellate (Vogel *et al.*, 2012), similar to mutant mice defective in adenylate kinase 7 that is supposed to produce NTP (Fernandez-Gonzales *et al.*, 2009). These observations raised the possibility that flagellar NDKs are part of a redundant energy metabolic circuitry built-into the microtubule-based scaffold to supply NTP for reactions occurring throughout these lengthy organelles (Mitchell *et al.*, 2005; Takei *et al.*, 2014). To elucidate the role of NDK5 in cilia and flagella, we took advantage of *in vivo*

approaches that are uniquely possible in *Chlamydomonas* (Merchant *et al.*, 2007). The results revealed unexpected actions of NDK5 that shed light on NDKs and flagellar biology.

## **3.2 Results**

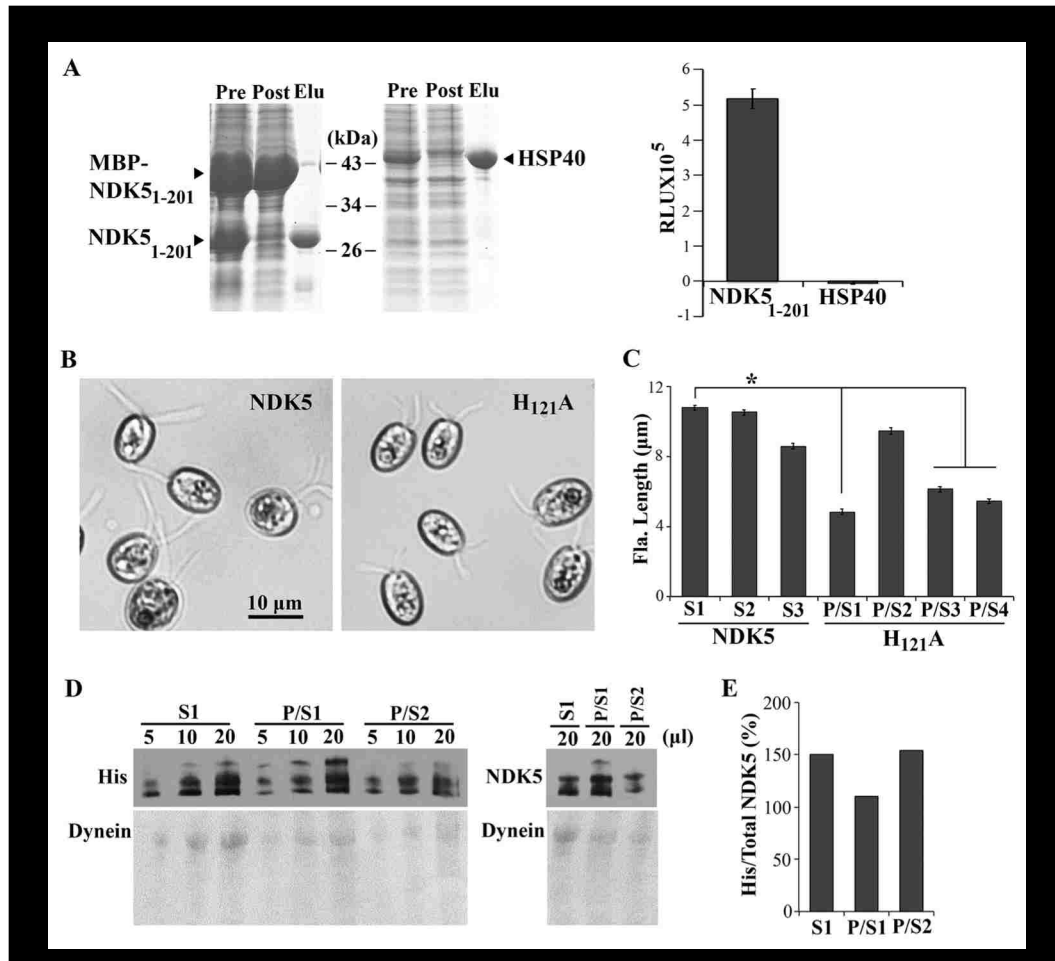
### **3.2.1 NDK5<sub>H121A</sub> Minigene Caused Paralyzed Short Flagella**

Previous studies demonstrate that isolated RS complexes exhibit NDK activity and that spoke-less mutant axonemes have one half of the NDK activity of wild WT axonemes (Patel-King *et al.*, 2004). To directly test the NDK activity of NDK5 and to overcome the propensity of NDK5 to precipitate (Munier *et al.*, 1998), we expressed in bacteria maltose-binding protein (MBP)-His-NDK5<sub>1-201</sub> (Donnelly *et al.*, 2006) that contains the conserved NDK domain and the Dpy30 domain but lacks the extended C-terminal tail unique to algal NDK5. After cleavage of the MBP moiety in bacteria (Donnelly *et al.*, 2006), soluble His-NDK5<sub>1-201</sub> in the extracts was purified by Ni<sup>2+</sup> affinity chromatography (Figure 3-1A, left panel). The NDK activity was measured using a luciferase-based bioluminometric assay (Karamohamed *et al.*, 1999). As expected, addition of purified His-NDK5<sub>1-201</sub> to the reaction mixture elicited  $5 \times 10^5$  relative light units (RLU), compared to  $-0.004 \times 10^5$  RLU for the His-HSP40 control (Figure 3-1A, right panel).

To elucidate the role of NDK5, we perturbed *NDK5* genetically. Although mutations of flagellar genes are mostly recessive (Luck *et al.*, 1977), based on NDK5's Dpy30 dimerization domain (Sivadas *et al.*, 2012) and the dominant negative (DN) effect observed for *Drosophila* NDK<sub>kpn</sub> and heteromeric oligomers (Wilkie *et al.*, 1994), we

predicted that expression of inactive NDK5 might also elicit DN effects. Therefore, we first engineered an NDK5-6His minigene, the NDK5 cDNA, with the regulatory elements of the LC8 gene, which encodes an abundant 10-kDa protein present in many molecular complexes, including RSs (Yang *et al.*, 2009). We also built into the plasmid a paromomycin (PMM)-resistance cassette for selecting transformants. To abolish the NDK activity, the codon for H121, which acts as the transient recipient of the NTP  $\gamma$ -phosphate, was mutated to an alanine codon. The *NDK5* and *NDK5<sub>H121A</sub>* minigenes were transformed into WT cells. All of the screened 300 PMM-resistant colonies in the NDK5 control group were indistinguishable from WT cells, indicating that the minigene itself was not harmful. In contrast, 4 of 300 clones in the *NDK5<sub>H121A</sub>* group (P/S1-4) contained Paralyzed cells and Swimmers. In three of the four P/S strains, the flagella were about half of the expected 10-12 micrometers. In 3-1B-C,  $p < 0.01$ ). Western blots of flagella did not reveal obvious anomalies, but confirmed the presence of His-tagged NDK5 and *NDK5<sub>H121A</sub>* in the flagella of the randomly selected S strain and two representative P/S strains (Figure 3-1D). Quantitative analysis showed a similar, if not higher, His-tagged NDK5 /Total NDK5 ratios in the S strain flagella (Figure 1E). Thus *NDK5<sub>H121A</sub>*, rather than the abundance of His tag NDK5 proteins, likely accounted for the motility and length phenotype. While these results were consistent with those in the sperm of *ndk5* mice, flagella lengths in *Chlamydomonas* varied among the strains; in contrast, none of existing RS mutants was known to exhibit such prominent length phenotype, except for the LC8 mutant (*fla14*) whose short flagella were attributed to pleiotropic deficiencies in multiple flagellar complexes (Pazour *et al.*, 1998; Yang *et al.*, 2009). We further

investigated an *ndk5* recessive mutant and generated genomic constructs to elucidate the role of NDK5 and to test the DN effect of NDK5<sub>H121A</sub> independently.



**Figure 3-1.** NDK5<sub>H121A</sub> expressed from a minigene caused paralyzed short flagella in WT cells. (A) Recombinant His-NDK5<sub>1-201</sub> exhibited NDK activity. Coomassie blue-stained SDS-PAGE showed Ni-NTA purification of His-tagged recombinant proteins (left panel). Pre, extract from bacteria expressing both MBP-His-NDK5<sub>1-201</sub> and the TVMV protease that could cleave off MBP. Post, the flow through. Elu, the eluate. Identical amounts of proteins were analyzed in triplicate for NDK activity using the luciferase-based bioluminescence assay (right panel). RLU: Relative Light Unit. (B) Representative transgenic strains from WT cells transformed with the minigene expressing full-length His-tagged NDK5 (left) or NDK5<sub>H121A</sub> (right). NDK5<sub>H121A</sub> transformants had short paralyzed flagella. The cells were fixed prior to light microscopy

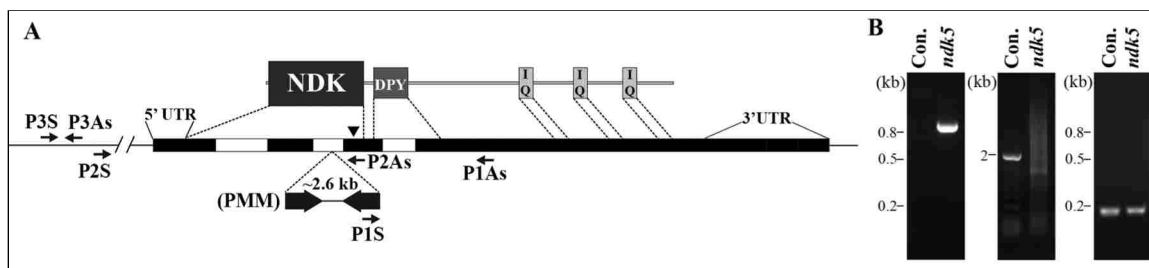
for length measurement. (C) Average flagellar length of transgenic strains expressing NDK5 or NDK5<sub>H121A</sub>. All strains from the NDK5 group, represented by randomly selected S1, S2 and S3 strains, contained only swimmers (S) like the parental strain. Four strains from the NDK5<sub>H121A</sub> groups contained mostly paralyzed cells but with a fraction of swimmers (P/S). Flagella of three of the four P/S strains had shorter flagella than those of the control strains. Asterisks, statistically significant differences (Student's t-test,  $p < 0.01$ ,  $n = 50$ ). (D) An anti-His western blot revealed His-tagged NDK5 polypeptides in the flagellar samples from randomly selected S strains and representative P/S strains (left, top panel). Different protein loads indicated the signals were not over-saturated. Both His-tagged and untagged-NDK5 proteins were revealed by NDK5 polyclonal antibody (right, upper panel). Total proteins were revealed by Ponceau red (bottom panels). Dynein, dynein heavy chains. (E) Plot Lanes analysis in the ImageJ software showed the ratio of His-tagged NDK5 versus total NDK5 in the 20- $\mu$ l flagellar samples in the western blots in (D).

### 3.2.2 RS Defects in Paralyzed Flagella of an *ndk5* Insertional Mutant

An *ndk5* mutant was isolated from a large-scale indexed insertional mutagenesis project (Li *et al.*, 2015). A 21-bp flanking sequence from high-throughput screening suggested that a PMM-resistance DNA fragment was inserted in the 2<sup>nd</sup> intron of the *NDK5* gene (Figure 3-2A) in this strain. The strain was paralyzed as expected of RS mutants. The insertion was confirmed by two PCR amplifications of predicted fragments from the genomic DNA using primer pairs that are conducive for either *ndk5* or its parental strain control (Con. in Figure 3-2B, left and middle panel). A nearby region amplified using a primer pair annealing to the middle of the neighboring gene, *SPL4*, which encodes a putative RNA splicing factor (Figure 3-2A and Figure 3-2B, right panel) showed that this region was intact in both strains. The trace amount of full-length NDK5 (Figure 3-3A and see discussion below) suggests there is no large deletion at 5' end of the *NDK5* gene in the mutant.

To segregate potential additional mutations that might have been present in *ndk5*, we backcrossed *ndk5* with WT cells. Although *ndk5* mated poorly, we managed to restore

mating ability by crosses with a high mating strain. The strict co-segregation of PMM resistance and paralyzed progeny confirm that NDK5 is required for flagellar motility but is not required for mating.



**Figure 3-2.** Characterization of an *ndk5* insertional mutant. **(A)** Schematic illustrating NDK5 protein and gene organization. NDK5 has an NDK domain followed by a Dpy-30 domain and an extended C-terminal tail containing three calmodulin-binding IQ motifs. The *ndk5* mutant has an insertion of a 2.6-kb PMM-resistance cassette in the 2<sup>nd</sup> intron. Black box, exon; white box, intron; black line, flanking sequence; arrowhead, the H121 codon; arrows, PCR primers. **(B)** PCR diagnosis of the insertion mutagenesis using templates prepared from *ndk5* and the parental strain (Con.). A 0.8-kb fragment at the 3' junction was amplified with the P1S and P1As primer pair from the mutant but not from Con. (left panel). A nearly 2-kb fragment at the 5' region including the 2<sup>nd</sup> intron was amplified with the P2S and P2As primer pair from the control but not from *ndk5* (middle panel). A ~0.2-kb fragment from the neighboring *SPL4* gene, about 5-kb upstream to the NDK5 gene, was amplified with the P3S and P3As primer pair from both templates (right panel).

### 3.2.3 RS Deficiencies of *ndk5* Flagella

Western blots probed with NDK5 polyclonal antibody detected two major ~120-kDa NDK5 bands in control axonemes. They were greatly diminished in both *ndk5* and *pf14* that lack most RSs (Diener *et al.*, 1993) (Figure 3-3A). Also diminished were RSP1 located in the spokehead and HSP40 (alias RSP16) that co-assembles with NDK5 and RSP2 in the neck region in WT cells. In contrast, RSP2 and the other representative



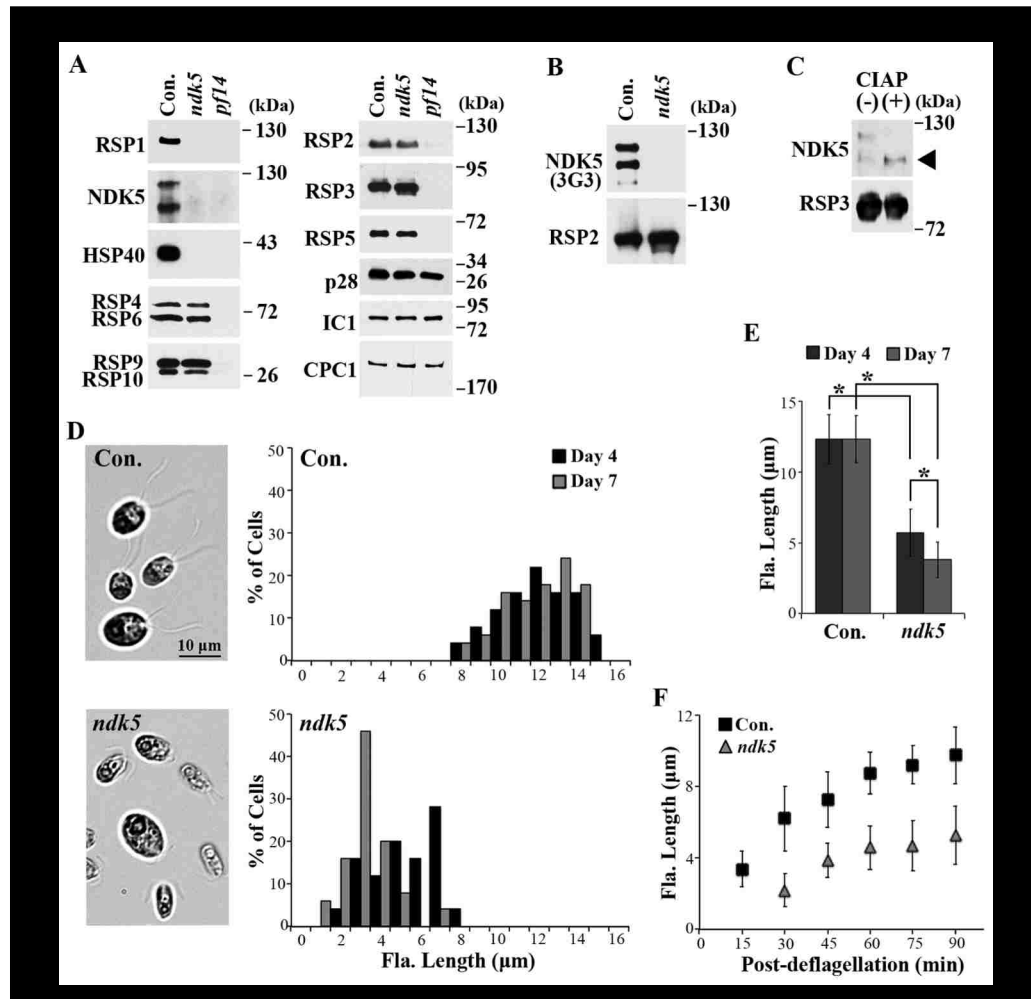
proteins were not significantly affected, including the other four spokehead proteins (RSP4, 6, 9 and 10). Although RSP3, a phosphorylated RS scaffold protein, appeared normal in abundance, a fraction consistently migrated faster. Proteins assayed as additional controls - inner dynein arms p28, outer dynein arms IC1 and CPC1 from the central pair - were present in normal amounts.

The 120-kDa NDK5 doublet bands revealed by the polyclonal antibody and the NDK activity resembled the 120-kDa doublet spoke protein bands revealed by the monoclonal antibody 3G3 and in-gel kinase assays (Yang *et al.*, 2004; William *et al.*, 1989). The absence of 3G3-reactive bands in *ndk5* axonemes that contained 120-kDa RSP2 (Figure 3-3B) indicated that NDK5, and not RSP2, is the 3G3 antigen, and that it can phosphorylate proteins, at least *in vitro*, as expected for NDKs. To determine whether the double bands were due to phosphorylation, control axonemes were treated with calf intestine alkaline phosphatase (CIAP). NDK5 in CIAP-treated axonemes co-migrated with the lower band of the NDK5 doublet in the sham-treated control (Figure 3-3C, top panel), indicating that the upper band was phosphorylated form. In contrast, CIAP treatment did not change RSP3 migration (bottom panel).

#### **3.2.4 Short Flagella of *ndk5***

We noticed that *ndk5* and paralyzed backcross progeny assembled shorter flagella than controls at log phase (Day 3) in Tris-acetate-phosphate (TAP) liquid media; at stationary phase, most cells lack flagella. In minimal media that is commonly used in phenotyping flagellar lengths of mutants (Kubo *et al.*, 2015), most *ndk5* cells had flagella suitable for quantitative analysis. Regardless of distribution or averages, *ndk5* flagella at

steady state were consistently shorter than the controls (Figure 3-3D-E). The difference became exacerbated as cultures progressed toward late log phase when nutrients were becoming depleted (compare Day 4 and Day 7). To evaluate flagella generation rate, flagella were first excised from log phase cells by pH shock. An aliquot of cells was fixed periodically afterwards to assess regenerated flagella. Compared to the control, *ndk5* cells re-grew flagella more slowly, and new flagella remained shorter even after 90 mins (Figure 3-3F,  $p < 0.01$ ).



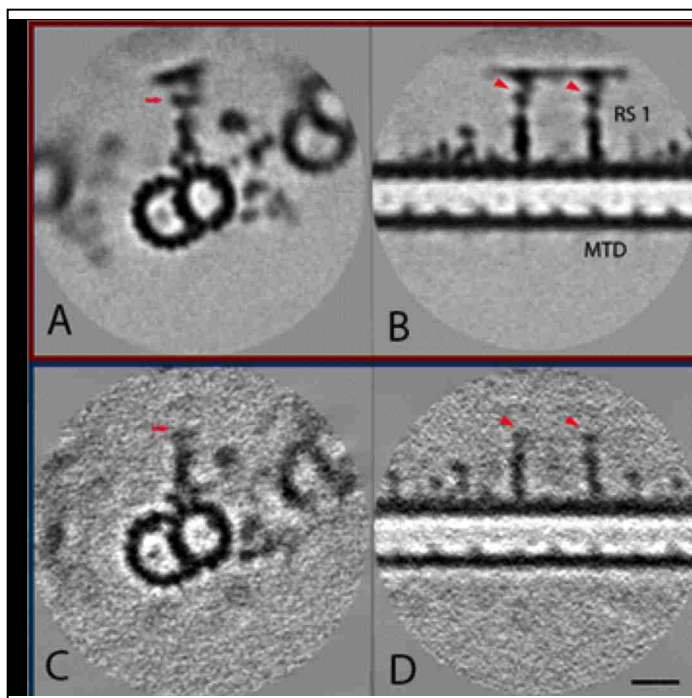
**Figure 3-3.** The *ndk5* mutant is defective in RSs and flagellar assembly. (A) Western blot analysis of axonemes revealed the absence of RSP1, NDK5 and HSP40 in the paralyzed *ndk5* flagella. A fraction of the spoke scaffold protein RSP3 migrated slightly faster than that in WT cells (control). The other spoke proteins in the head (RSP4/6 and RSP9/10) and neck (RSP2 and RSP5) appeared normal. The axonemal proteins p28, IC1 and CPC1 - subunits of inner dynein arms, outer dynein arms and the central pair, respectively - were used as controls. The spoke-less *pfl14* was a negative control. (B) The antigen of monoclonal antibody 3G3 is NDK5, and not RSP2 that is present in *ndk5* axonemes. (C) NDK5 is a phosphoprotein. NDK5 in axonemes receiving the sham CIAP treatment migrated as double bands. In CIAP treated axonemes, all NDK5 migrate with the lower band (arrowhead). CIAP treatment did not change the migration of the spoke scaffold protein RSP3. (D) Microscopy (left) and histogram (right) revealed short flagella on *ndk5* cells cultured in minimal media, in contrast to the full-length flagella of the parental strain (Con.). The length phenotype was more pronounced in late log phase (compare Day 4 and Day 7, n=50). (E) Average flagellar length corresponding to Figure 3-3D. Asterisks, statistically significant differences (p<0.01, n=50). (F) *ndk5* cells are deficient

in flagellar regeneration. Flagella were excised from log-phase cells by pH shock and allowed to regenerate. Aliquots of cells were fixed periodically and imaged. Compared to the control, *ndk5* cells regenerated flagella more slowly and the final lengths were shorter ( $p < 0.01$ ,  $n = 20$ ).

### ***3.2.5 3D Reconstruction of NDK5 Axoneme with Cryo-electron Tomography***

In order to characterize the structural components of RS complex with NDK5 protein missing, our collaborators Dr. Poghosyan Emiliya and Dr. Ishikawa Takashi from Paul Scherrer Institute performed cryo-ET and subsequent sub-tomogram averaging of the *ndk5* axoneme, based on the 96-nm periodic unit.

To visualize spoke lesions caused by diminished NDK5, HSP40 and RSP1, compared sub-tomogram averages of RSs from *Chlamydomonas* WT and *ndk5* flagella (Figure 3-4). The length of RSs in *ndk5* axoneme is considerably shorter (29 nm) than WT RSs (43 nm). Curiously, despite the seemingly normal abundance of RSP2 and the other four spokehead proteins in SDS-PAGE (Figure 3-3), sub-tomogram averages showed that RSs from *ndk5* (Figure 3-4C and 3-4D) are headless, resembling the RSs of the RSP2 mutant *pf24* (Pigino *et al.*, 2011), unlike the intact RSs from WT (Figure 3-4A and 3-4B). Density corresponding to the RS head is either missing or highly blurred. This is consistent with structural results on headless RS in respiratory cilia of PCD patients with a defective RSP1 gene (Lin *et al.*, 2014); and may explain why *ndk5* flagella are as paralyzed as the headless RS mutant flagella, rather than the jerky flagella that lack only HSP40 (Yang *et al.*, 2008). Alternatively, the spoke head may also be unaltered, but not fixed in position relative to the stalk and therefore not seen by the averaging method. Taken together, the results indicate NDK5 and RSP1 are necessary for the structural stability of the entire spokehead.



**Figure 3-4.** Structure of RSs from WT (A, B) and *ndk5* mutant (C, D) *Chlamydomonas*. Density maps were obtained by averaging sub-tomograms involving the 96 nm periodic unit from cryo-ET and shown as transverse (A, C) and longitudinal (B, D) sections. Corresponding positions on the RS neck are indicated by red arrows. The density at the position of spokehead components, RSP1, 4, 6, 9 and 10, are missing in averaged cryo-electron tomograms from the *ndk5* strain (C and D). Scale bar, 20 nm.

### 3.2.6 Full Rescue of *ndk5* Phenotypes by *NDK5* and *NDK5<sub>H121A</sub>*

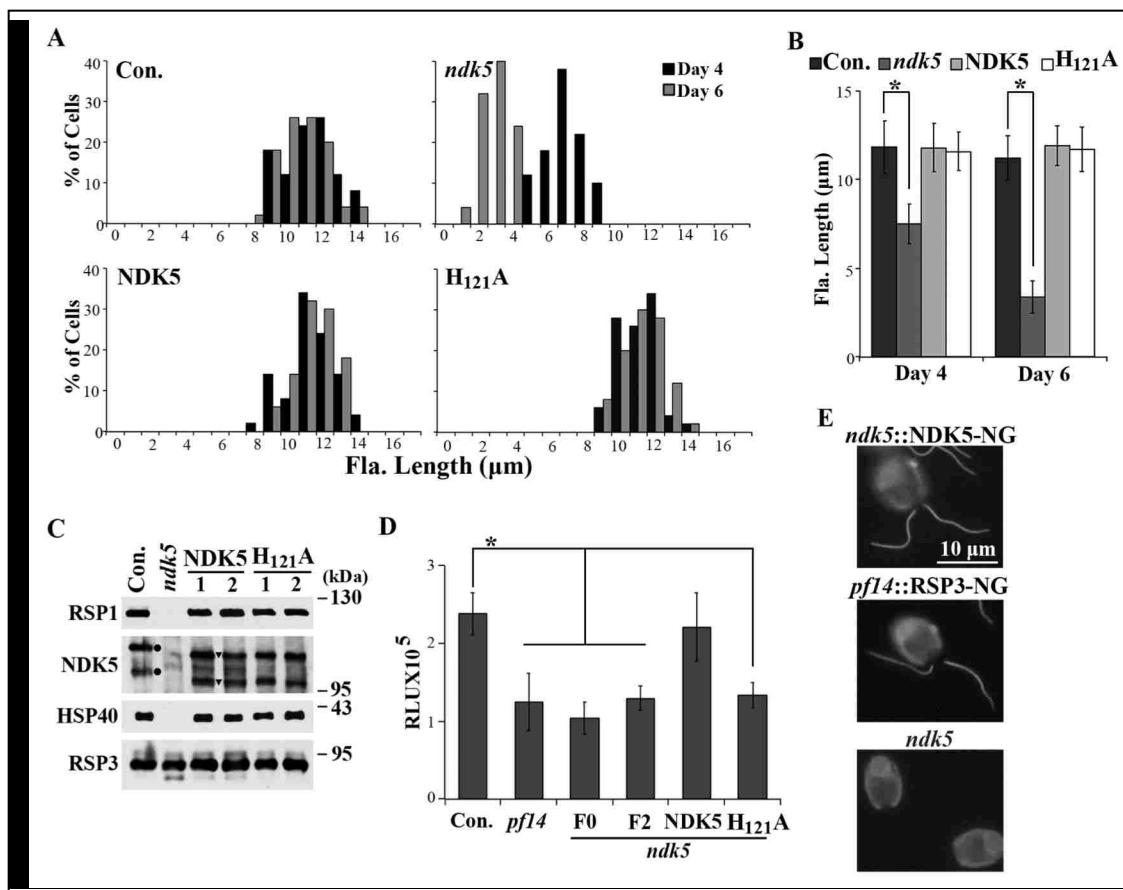
To determine whether the disrupted *NDK5* gene caused both paralysis and short flagella, we created plasmid pNDK5 that contained the *NDK5* genomic DNA and conferred hygromycin (HYG)-resistance. To test whether NDK activity is required for *NDK5* function, we further mutated this genomic construct to pNDK5<sub>H121A</sub>. The two constructs were transformed into *ndk5* cells. Surprisingly, both plasmids fully rescued *ndk5* with efficiencies expected for single plasmid transformations. In one experiment, the rescue rate was 50% for the pNDK5 group (22 swimmer clones out of 44 PMM-

resistant transformants) and 33% for the pNDK5<sub>H121A</sub> group (17 out of 51 screened). The rates varied in replica experiments but were not statistically different between the two groups. The rescued strains from both groups were indistinguishable from the *ndk5* parental strain (Con.) in both motility and flagellar length (Figure 3-5A and 5B). Western blot analysis showed that NDK5 polypeptides, HSP40 and RSP1 in the axonemes of rescued strains were restored (Figure 3-5C). Similar migration of both NDK5 and NDK5<sub>H121A</sub> expressed from the transgene indicates that H121A mutation did not affect NDK5 migration or phosphorylation. Therefore, H<sub>121</sub> is not required for the function or phosphorylation of NDK5 polypeptides. Note that the NDK5 from transgenes (triangle) migrated faster than the endogenous NDK5 in the control. The distance varied in each electrophoresis perhaps due to slightly different acrylamide concentration. The variation was also observed in other strains (Yang *et al.*, 2008) and may be due to differences at the evolutionarily divergent C-terminal sequence that interacts with calmodulin. Usefully, this feature allowed us to distinguish exogenous and endogenous NDK5 polypeptides. The NDK5 minigene also rescued *ndk5* but none of the rescue clones contained 100% swimmers, suggesting that the minigene was less efficient than the genomic construct.

We then compared NDK activities of various axonemes of equal weights. The spoke-less *pf14*, F<sub>0</sub> *ndk5*, F<sub>2</sub> *ndk5*, and, importantly, *ndk5* rescued with NDK5<sub>H121A</sub> exhibited similar NDK activities that were roughly one half lower than the positive control and the transgenic *ndk5* rescued with NDK5 (Figure 3-5D). Therefore H<sub>121A</sub> mutation indeed abolished the NDK activity of NDK5. Thus, the deficiencies in RS composition, motility and flagellar lengths of the *ndk5* strain are caused by diminished NDK5; although the NDK activity of NDK5 requires H121 as do other NDKs, this

enzymatic activity is dispensable for its function and phosphorylation in *Chlamydomonas* axoneme. The phenotypes of strains generated in this project are summarized in Table 3-1. We further performed site-directed mutagenesis on pNDK5<sub>H121A</sub> to replace residues predicted to bind NTP or catalyze phosphotransfer - including K12A, N118A, R108A and H55A (Tepper *et al.*, 1994; Tiwari *et al.*, 2004). The four constructs with double mutations still fully rescued *ndk5*, indicating that the mechanisms of NDK5 action has diverged substantially from the primordial NDK catalytic mechanism.

We also engineered the genomic construct to express fluorescent NDK5 with a tag containing NeonGreen (NG), a monomeric fluorescent protein with spectral properties similar to EGFP but 2.7-fold brighter (Shaner *et al.*, 2013). Fluorescent NDK5 expressed in *ndk5* transgenic cells decorated the entire flagella as did NG-tagged RSP3 expressed in *pfl4* transgenic cells (Figure 3-5E). The similar location and intensity of NDK5 and RSP3 suggest that each RS contains two NDK5 molecules as was found for RSP3 and some other RSPs (Sivadas *et al.*, 2012, Oda *et al.*, 2014; Kohno *et al.*, 2011); and suggests that NDK5 in the RS promotes full-length flagella.



**Figure 3-5.** Genomic DNA expressing NDK5 or NDK5<sub>H121A</sub> rescued both the paralysis and length phenotypes of *ndk5*. (A) Flagellar length distribution showed that the flagella of *ndk5* transgenic strains expressing NDK5 or NDK5<sub>H121A</sub> were longer than that of *ndk5* but similar to that of the *ndk5* parental strain. Cells cultured in minimal media were fixed at two indicated time points and the lengths measured from micrographs; n=50. (B) Average flagellar length of corresponding data from Figure 3-5A. Asterisks, statistically significant differences (p<0.01). (C) Western blot analysis of axonemes from representative transformants. RSP1, HSP40 and NDK5 polypeptides were restored. Note, NDK5 and NDK5<sub>H121A</sub> expressed by the BAC-derived transgene (triangle) migrated identically but faster than endogenous NDK5 (dot). (D) H121A mutation abolished NDK activity. The NDK activity of axonemes from *ndk5* transformants expressing NDK5 was restored to WT levels (Con.), whereas the activity of axonemes from NDK5<sub>H121A</sub> transformants, spokeless mutant *pf14* and *ndk5* strains (either F<sub>0</sub> or F<sub>2</sub> from backcross), was ~50% lower. The relative NDK activity was the RLU value normalized to the control. Quadruple aliquots from each sample were measured. Asterisks, statistically significant differences (Tukey HSD test, p<0.01). (E) Live cell imaging of transgenic *ndk5* expressing fluorescent NDK5 (top panel) and *pf14* expressing fluorescent RSP3 (middle



panel). *ndk5* (bottom panel) was a negative control. Neongreen-tagged NDK5 and RSP3 appeared identical in distribution and intensity throughout flagella.

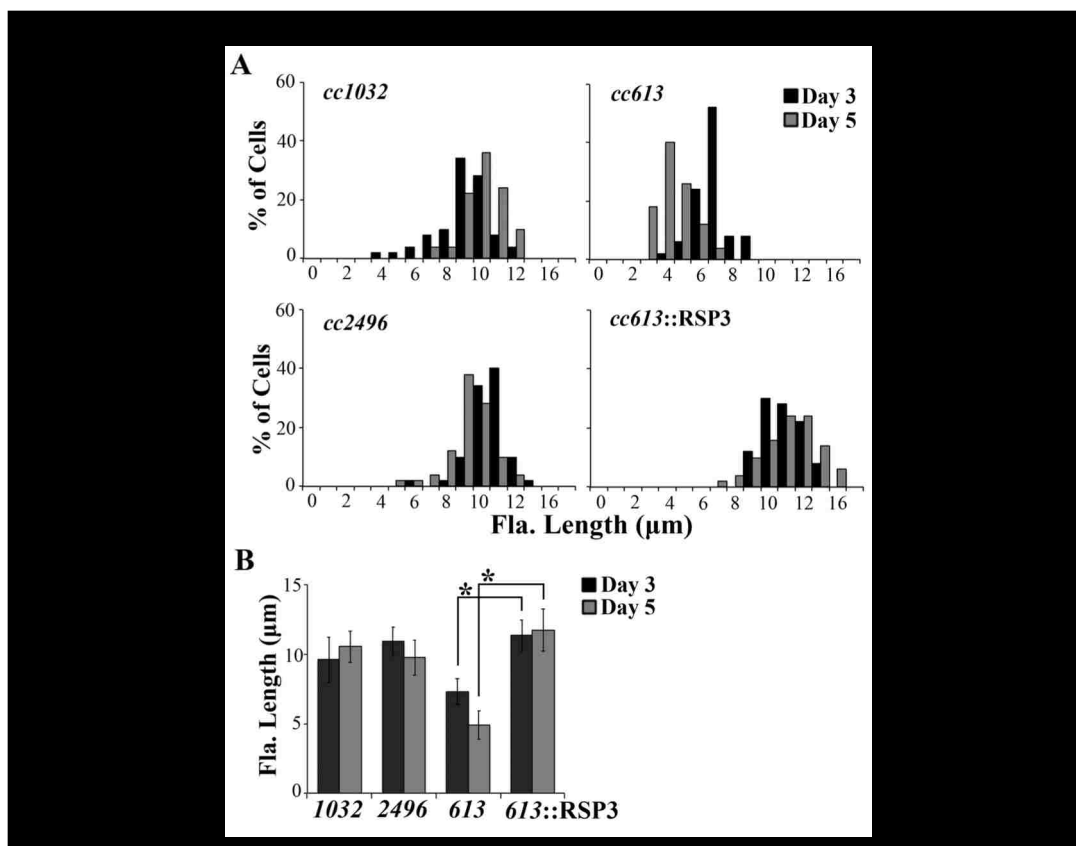
	WT	<i>ndk5</i>	<i>ndk5</i> :: <i>NDK5</i>	<i>ndk5</i> :: H <sub>121</sub> A	WT:: H <sub>121</sub> A(P/S)	WT:: H <sub>121</sub> A(P)
Motility	S	P	S	S	P/S	P
Fla. generation	++	+	++	++	++	+
HSP40; RSP1	++	-	++	++	++	+
NDK5	++	-	++	++	++	+
NDK5 Pho.	++	N/A	++	++	++	+
RSP3	++	++	++	++	++	+
RSP3 Pho.	++	++	++	++	++	+

**Table 3-1.** List of strains described in this study and their corresponding motility, flagellar generation and RS assembly phenotypes. S, Swimmers; P, Paralyzed cells. ++, Similar to the WT strain. +, Reduction in flagellar lengths, protein abundance or phosphorylation. -, Absence of proteins. N/A, Not applicable

### 3.2.7 Rescue of the Short Flagella of a Spoke-less *pf14* Allelic Mutant

We have noticed that flagella lengths of *pf14* allelic mutants that are mutant in RSP3 (Luck *et al.*, 1977) and lack most RSs vary considerably with growth conditions and from strain to strain. We hypothesized that the putative short flagella phenotype of *pf14* might be obscured by growth conditions and by backcrosses that led to preferential selection of paralyzed *pf14* progeny with long flagella conferred by other genes. To test this, we cultured three *pf14* strains - cc1032, cc2496 and cc613 - in minimal media. The latter two strains were derived from a single *pf14* isolate, whereas cc1032 was derived independently (Luck *et al.*, 1977; Diener *et al.*, 1993, see annotation in *Chlamydomonas* Resource Center). As expected, all three strains were paralyzed; and flagella lengths of the cc1032 and cc2496 strains were within the normal range, around 10-11 mm

throughout the culture. However, like *ndk5*, flagella of cc613 were short,  $7.32 \pm 0.95$   $\mu\text{m}$  on day 3 and barely 5  $\mu\text{m}$  on day 5 (Figure 3-6). Transformation of a RSP3 genomic construct into cc613 cells rescued paralysis. Importantly, flagellar lengths (as shown in a representative rescued strain cc613::RSP3) nearly doubled and were no longer sensitive to culture durations. Therefore, like *ndk5*, spoke-less mutants are deficient in flagellar generation, but this prominent phenotype has been overlooked due to variations in the genetic background.



**Figure 3-6.** Diminished RSs result in short flagella. (A) Flagellar length distribution of three *pfl4* strains cultured in minimal media. The defect in the *RSP3* gene of cc613 and cc2496 that were derived from one common isolate was identical. Only flagella of cc613 were particularly short and this was exacerbated at late log phase (Day 5). The length

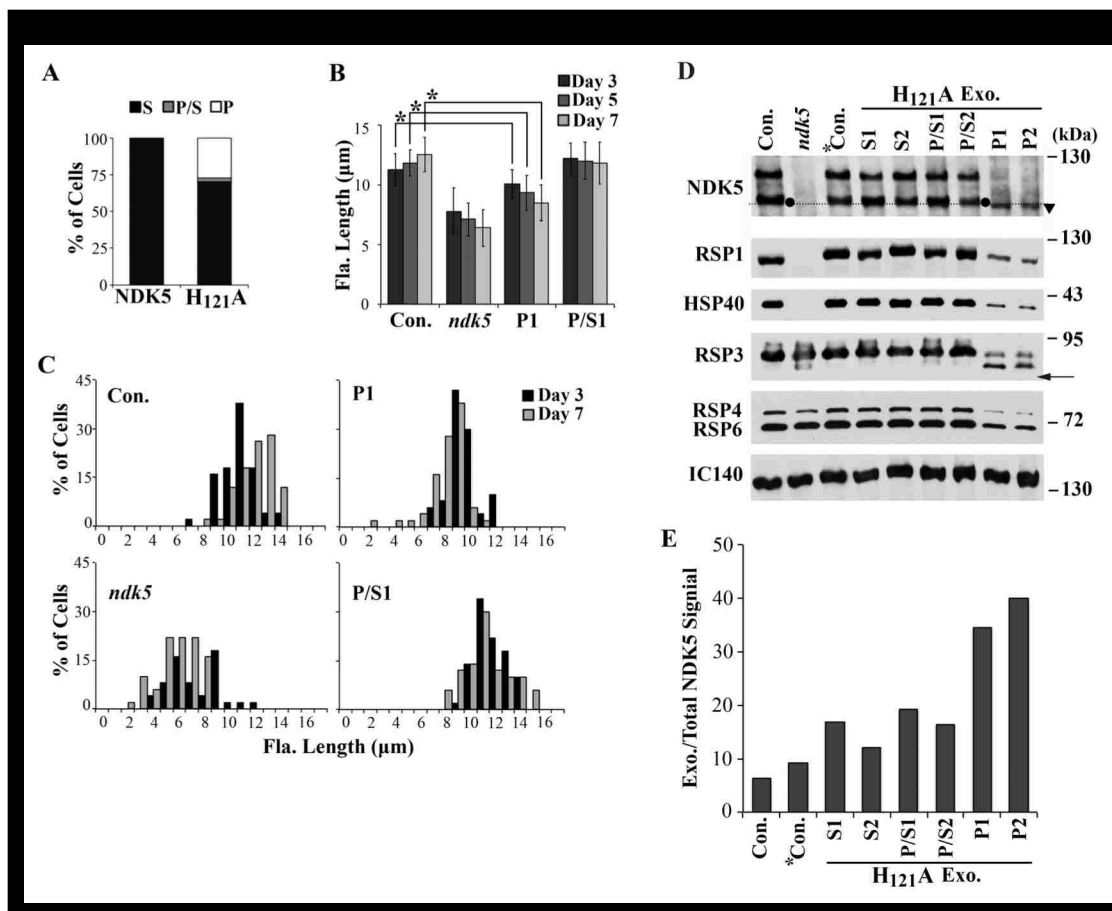
phenotype and paralysis were rescued by a RSP3 transgene. **(B)** Average flagellar lengths of *pf14* cells. Asterisks, statistically significant differences ( $p < 0.01$ ;  $n = 50$ ).

### 3.2.8 Dominant Negative Effect of *NDK5*<sub>H121A</sub> Genomic DNA

Figure 3-1 shows that *NDK5*<sub>H121A</sub> expressed from a minigene in *Chlamydomonas* had a dominant negative (DN) effect as *Drosophila* *NDK*<sub>kpn</sub>. To test this independently, we transformed WT cells with the p*NDK5*<sub>H121A</sub> genomic construct. All transgenic clones in the p*NDK5* control group were swimmers (S), whereas some clones for the p*NDK5*<sub>H121A</sub> group contained paralyzed cells. The percentages of clones with motility phenotypes varied among repeated transformations. In one experiment, 12 out of 44 PMM-resistant clones (27%) contained entirely Paralyzed (P) cells whereas 1 clone (2%) had both Paralyzed cells and Swimmers (P/S) (Figure 3-7A). The flagella of P strains were also short, albeit not as short as *ndk5* flagella, and the length phenotype was exacerbated as the cells approach stationary phase (Figure 3-7B-C, compare Day 3 and Day 7). Therefore, *NDK5*<sub>H121A</sub> – although rescued all the phenotypes when expressed in *ndk5* - has a DN effect in the presence of *NDK5*, regardless of whether the mutant protein is expressed from the minigene or genomic DNA.

Unexpectedly, western blots of randomly selected strains showed that unlike *ndk5* axonemes, DN axonemes from the two P strains (P1 and P2) actually contained all RSPs tested, including RSP1, HSP40 and fast-migrating *NDK5*<sub>H121A</sub> from the transgene (arrowhead in Figure 3-7D). However, all RSPs were less abundant than in controls, while *NDK5* and RSP3 appeared less phosphorylated. The loading control was IC140 of the inner dynein I1. To compare the abundance of endogenous and exogenous *NDK5*, we analyzed the western blot with the Plot Lanes program after several attempts that failed to

fully separate the two populations. The fast-migrating NDK5<sub>H121A</sub> (below the dash line in Figure 3-7D) constituted 34 and 40% of total NDK5 in the flagella samples from the two P strains (Figure 3-7E). This fraction was substantially lower for the other strains - respectively 17%, 12%, 19% and 16 % for S1, S2, P/S1 and P/S2 strains; and 6% and 9% for the control strains. The similar ratios in S strain and P/S strain samples suggest that a threshold level of NDK5<sub>H121A</sub> is needed to cause paralysis; whereas the level is higher to cause paralysis in all cells. The pNDK5<sub>H121A</sub>-NG that should have been useful to distinguish the two populations cannot elicit dominant negative effects perhaps due to the NG moiety.



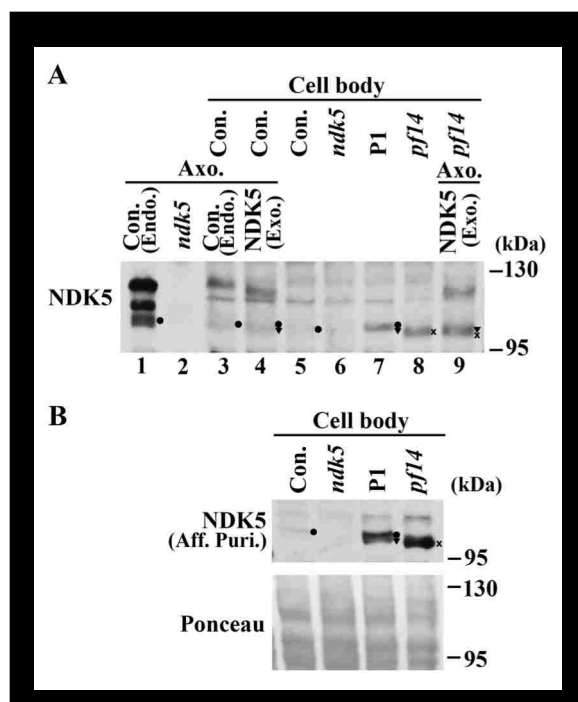
**Figure 3-7.** NDK5<sub>H121A</sub> expression from a genomic transgene in WT cells impaired flagellar motility, length, RS assembly and RS phosphorylation. **(A)** The percentages of clones with swimmers (S), paralyzed cells (P) or a mixture (P/S) expressing NDK5 (first bar) or NDK5<sub>H121A</sub> (second bar) from one experiment. Average flagellar length **(B)** and flagellar length distribution **(C)** of representative strains cultured in minimal media showed that flagella lengths of P strains (P1) was between the control and *ndk5*, whereas P/S strains (P/S1) had normal length flagella. Asterisks, statistically significant differences ( $p < 0.01$ ,  $n = 50$ ). **(D)** Western blot analysis of axonemes from transformants with different motility levels. RSPs in the flagella of P/S strains (P/S1 and P/S2) appeared normal but reduced in P strains (P1 and P2) (top panel). In addition, NDK5 and the scaffold protein RSP3 were hypophosphorylated (arrow), especially NDK5<sub>H121A</sub> (triangle). IC140, a subunit of inner dynein arm, was the loading control. \*Con., a WT strain transformed with pNDK5. **(E)** The ratio of fast migrating NDK5 from the transgenes relatively to total NDK5 in **(D)**. Dash line, the arbitrary line to distinguish exogenous proteins expressed from the transgenes. Ratio of exogenous protein in Con. strain represents the background.

### 3.2.9 Hypophosphorylated NDK5 in the Cell Body

RSP3 is hypophosphorylated in preassembled RSs in extracts from WT cell bodies (Qin *et al.*, 2004), and in mutant flagella with reduced amounts of RSs (Gupta *et al.*, 2012). To elucidate the underpinning of the DN effects, we analyzed NDK5 in cell body extracts from various strains by western blot analysis (Figure 3-8). Axonemes (lanes 1, 2) and cell body extracts (lanes 5, 6) of *ndk5* and its parental strain were controls. The lanes loaded with both axonemes and cell body extracts (lanes 3, 4, 9) tested whether sample preparations affected polypeptide migration. Given reduced RSs in the DN flagella, we also included a *pfl4* cell body extract (lane 8) as a control for impaired RS assembly. As cell bodies typically harbor enough axonemal proteins for the regeneration of two half-length flagella (Rosenbaum and Child, 1967), we reasoned that RSs that failed to assemble in flagella may accumulate in the cell body (Diener *et al.*, 2011). Anti-NDK5<sub>1-201</sub> polyclonal antibody revealed a faint putative NDK5 band in the parental control cell body extracts which largely co-migrated with the hypophosphorylated NDK5 band in control axonemes (Figure 3-8A, compare dots in lanes 1, 3, 5). Similar bands were more prominent in cell body extracts of the P1 DN strain that contained both endogenous (dot in lane 7) and exogenous NDK5 (triangle) or of *pfl4* that migrated slightly faster (asterisk in lane 8). These bands in the cell body of all strains except *ndk5* were confirmed by probing the duplicated blot with affinity-purified polyclonal anti-NDK5<sub>8-586</sub> (Patel-King *et al.*, 2004) (dot, triangle and asterisk in Figure 3-8B, top panel). Protein loads are shown in the Ponceau S stained blot (bottom panel). The 3G3 monoclonal antibody was too weak to reveal NDK5 in cell body samples. Duplicated

control blots probed for other RSPs contained multiple background bands and were not informative.

NDK5 is primarily hypophosphorylated in the cell body extracts, suggesting that it becomes phosphorylated to exit cell body or after entering flagella. The P1 cell body extract contained more NDK5 polypeptides than the control but was similar to *pf14* (compare lane 5, 7 and 8), indicating that NDK5<sub>H121A</sub>, which causes DN effects, is not excessively over expressed, and is not degraded either, unlike the presumptive effect caused by the *Drosophila kpn* mutation (Biggs *et al.*, 1988). The varied abundance of NDK5<sub>H121A</sub> expressed by minigene or genomic constructs in individual transformants may account for variations in phenotype severity, a scenario similar to *kpn* mutants (Biggs *et al.*, 1988).



**Figure 3-8.** Accumulated hypophosphorylated NDK5 polypeptides in the cell body of the DN strain. **(A)** A representative western blot of cell body extracts probed with anti-NDK5<sub>1-201</sub> serum. NDK5 in the DN strain P1 (lane 7) was more abundant than that in the control (lane 5) but similar to that in *pf14* (lane 8), a control for reduced RS abundance in flagella. Negative control was *ndk5* (lane 6). NDK5 bands in axonemes, by themselves or added to cell body extracts (lanes 1-4, and 9), served as markers for phosphorylated NDK5 and hypophosphorylated NDK5 that are endogenous (dot), compared to that from the transgene (triangle), or in *pf14* (x). The axoneme sample loaded in lane 3 was one sixth of the sample loaded in lane 1. **(B)** A western blot probed with affinity-purified anti-NDK5<sub>8-586</sub> polyclonal antibody independently confirmed the hypophosphorylated state of endogenous NDK5 (dot) in the control. The band was undetectable in *ndk5*. The protein load was shown by Ponceau S stain (bottom panel).

### 3.3 Discussion

NDK plays an important role in multiple biological processes. Some of these involve the nucleoside phosphorylase activity for which the proteins were named.

However, it has become increasingly clear that some others do not. More uncertain are



mechanisms in the events where the NDK activity is dispensable. The ability to manipulate the gene in transgenic strains of *Chlamydomonas* provides a unique opportunity to investigate the NDK activity-independent mechanism and the dominant negative effects of NDK.

### **3.3.1 NDK5 is a Structural Protein for Proper Assembly of the RS Head-Neck Region**

Diminished RSP1 and HSP40 in *ndk5* flagella (Figure 3-3) support the prediction that flagellar NDKs are structural proteins (Munier *et al.*, 2003); and are consistent with the distinctive assembly of RSP1 in comparison with the other four head proteins (Luck *et al.*, 1977). This also provides *in vivo* relevance to the chemical crosslinking of NDK5 and RSP1 (Kohno *et al.*, 2011). Since RSs in mutant flagella missing HSP40 or RSP1 still have NDK5 (Yang *et al.*, 2008; Patel-King *et al.*, 2004; Yang *et al.*, 2005; 2008), it is NDK5 that tethers RSP1 and HSP40 to the RS scaffold (Sivadas *et al.*, 2012), rather than *vice versa*. In addition, as seen from sub-tomogram average of *ndk5* axonemes (Figure 3-4), NDK5 has an important role in structural stability of the RS head/neck regions. Without NDK5, perhaps along with HSP40 and RSP1, the rest of the proteins in this region cannot form a singular stable structural unit. An assembly model involving molecular interplays among the neck proteins is proposed in the study of HSP40 (Figure 4-8).

### **3.3.2 NDK5 Promotes Phosphorylation-related Assembly**

NDK5 has two additional roles outside the head/neck region of RSs. First, phosphorylation of NDK5 and RSP3 is linked to RS assembly, since a major fraction of

NDK5 and RSP3 in axonemes is phosphorylated (Figure 3-3B; Piperno *et al.*, 1981; Gupta *et al.*, 2012), whereas both are hypophosphorylated in the cell body (Figure 3-7B; Qin *et al.*, 2004; Gupta *et al.*, 2012). Phosphorylation of RSP3 has been implicated in the docking of RSs to axonemes (Gupta *et al.*, 2012). Hypophosphorylation of both molecules in DN flagella shows that NDK5 perturbation results in RSP3 hypophosphorylation and reduces RS assembly (Figure 3-7D). Therefore, NDK5 promotes RSP3 phosphorylation and RS assembly. This role differs from its structural role for RSP1 and HSP40, since they are present at the spoke head-neck region of the DN flagella, while RS assembly involves docking of RSP3 docking domain at the spoke base (Diener *et al.*, 1993). We are currently investigating which step in the RS assembly process - including preassembly in the cell body, trafficking into the flagellum and final assembly at the flagellar tip (Gupta *et al.*, 2012) - is perturbed in the DN strain.

Second, *Chlamydomonas ndk5* (Figure 3-3D) and *ndk5* mouse sperm (Vogel *et al.*, 2012) have short flagella, and the phenotype can be rescued by the *NDK5* gene (Figure 3-5), indicating that NDK5 also promotes full-length flagella. Flagellar length is a multigenic trait ultimately determined by the balance between the rates of assembly and disassembly (Wallace and Rosenbaum, 2001; Kubo *et al.*, 2015). Defects in individual axonemal complexes, including absence of the spokehead, might shorten flagella slightly due to decreased microtubule stability. However, *ndk5* flagella are deficient in only three subunits at a similar region and are far shorter than the flagella lacking spokeheads. This strongly suggests that NDK5 participates in a distinct length promotion mechanism. This role appears to be played by the NDK5 in RSs since NDK5 and RSP3 had identical distributions (Figure 3-4E; Munier *et al.*, 2003); an allelic spoke-less strain *pfl4* also

exhibits a length phenotype of similar severity, and the length phenotype is rescued when RSs are restored (Figure 3-6). The significantly different flagellar lengths of two spokeless strains due to the same defective RSP3 gene further support the conclusion that the length phenotype caused by axonemal defects can be drastically influenced by different genetic backgrounds that differentially impact microtubule stability (Kubo *et al.*, 2015).

One possibility is that NDK5 promotes axoneme stability or axonemal cargo affinity to IFT trains via protein phosphorylation. Genetic studies have revealed a number of length-regulating protein kinases and phosphatases (Tam *et al.*, 2013; reviewed by Wilson *et al.*, 2008; Cao *et al.*, 2009). NDK5 and RSP3 as well as many other proteins near the RS base are phosphorylated (Lin *et al.*, 2011). We propose that NDK5 promotes phosphorylation of a multitude of axonemal proteins during the flagella assembly process, which in turn increases inter-molecular affinity, leading to greater axoneme stability and a faster assembly rate, thereby accounting for full-length flagella and a rapid flagella generation rate (Figure 3-3D-3F). The exacerbation of length phenotypes in stationary phase (Figure 3-3, 6, 7) may reflect declining assembly rates as nutrients become limiting, while NDK5 is used to maintain full-length flagella regardless of nutrient availability for algae or sperm.

It is not clear how NDK5 might promote protein phosphorylation. Unexpectedly, this ability does not require the canonical phosphotransfer pathway of NDK, since *ndk5* is fully rescued by NDK5<sub>H121A</sub> incapable of the His-dependent phosphotransfer (Figure 3-5) or by NDK5<sub>H121A</sub> lacking one of the additional four residues commonly involved in NTP catalysis. One possible explanation is that NDK5 or perhaps Group II NDKs evolved a distinctive phosphotransfer mechanism while maintaining the canonical one. This is

supported by the autophosphorylation of the mutated NDK whose conserved His is replaced (MacDonald *et al.*, 1993), the distinct residues critical for phosphotransfer in diverse NDKs (Tiwari *et al.*, 2004), and the sequence divergence of Group I and Group II NDKs (Desvignes *et al.*, 2009). Alternatively, NDK5 may recruit or activate a protein kinase. In either case, in *ndk5* that lacks most NDK a surrogate kinase may phosphorylate RSP3 molecules albeit less efficiently than NDK5 (Figure 3-3A, 5C and 7D). The presence of heterodimeric NDK5 in the DN flagella may hinder the surrogacy, leading to largely hypophosphorylated RSP3. This possibility is consistent with the known association of a MAP kinase with the N-terminal extension unique to mammalian RSP3 (Jivan *et al.*, 2009).

The most intriguing observation here is that although NDK5<sub>H121A</sub> rescued all the phenotypes of *ndk5* cells, it elicits DN effect in WT cells, perturbing phosphorylation of NDK5 and RSP3, and assembly of RSs and flagella. Likewise, NDK<sub>kpn</sub> that has DN effects in *Drosophila* is functional. The similar abundance of hypophosphorylated NDK5 polypeptides in the cell body of DN strains and *pfl4* (Figure 3-8) rules out protein degradation as attributed to the DN effect of NDK<sub>kpn</sub> (Biggs *et al.*, 1988; Lascu *et al.*, 1992; Karlsson *et al.*, 1996). Other common DN mechanisms (reviewed by Wilkie *et al.*, 1994), such as over-expression of inactive molecules, are also unlikely. Rather, we propose that the molecular movements for His-dependent and His-independent reactions of NDKs are different, but the two protomers must act in concert; and thus, heterodimers with two functional but incompatible variants exhibit impaired activity. Uncoordinated heterodimers – not limited to phosphorylation - are consistent with NDK mutations in cancer cells (e.g. Chang *et al.*, 1996), and NDK degradation in *Drosophila* embryos. It is

likely that NDK5 heterodimers are unable or less efficient in promoting phosphorylation-related trafficking and assembly. Consistent with this, only a small fraction of NDK5<sub>H121A</sub> is present in S/P flagella (Figure 3-7D-E). Varied rates of P strains among repeated transformations suggest that homo- and hetero-dimerization of NDK5 is not random.

In fact, inter-subunit crosstalk between NDK monomers has been clearly demonstrated (Tepper *et al.*, 1994; Dar *et al.*, 2010), and is consistent with classic enzymology studies that estimate only half of protomers in one NDK oligomer bind to phosphate at one time (reviews by Parks and Agarwal, 1973). However this notion has not yet gained deserved attention even though it is not contradictory to the well-established Ping-Pong mechanism that depicts phosphotransfer occurring within individual monomers. It is time to re-consider inter-subunit crosstalk of NDKs in a number of vital actions that remain to be resolved.

In conclusion, NDK5 is crucial for the assembly of functional motile cilia and flagella, aside from the redundant canonical roles in nucleotide homeostasis. It promotes proper assembly of the RS and full-length flagella as a structural protein and via phosphorylation-related mechanisms. These findings expand the versatility of this ancient molecular platform and provide new clues as to how NDK isoforms are involved in a wide array of cellular processes and how they become impaired.

## CHAPTER 4: NON-CANONICAL ACTIONS OF HSP40 IN THE ASSEMBLY OF THE FLAGELLAR RS COMPLEX

### *4.1 Introduction*

HSP40s (J proteins) and HSP70s constitute a vital chaperone system that perpetually refolds diverse polypeptides in both prokaryotes and eukaryotes. Together they promote formation of functional proteins, assist degradation of damaged proteins, prevent harmful aggregation of misfolded polypeptides and modulate protein-protein interactions (reviewed by Kampinga and Craig, 2010; Ajit Tamadaddi and Sahi, 2016). Interestingly, *HSP40* genes in each eukaryotic organism far outnumber HSP70 genes. Although one HSP70 could partner with several HSP40s, it is becoming clear that this ancestral paradigm is not obligatory. A few HSP40s - such as the HSP40 for cilia and flagella motility (Yang *et al.*, 2008), spliceosome disassembly (Pandit *et al.*, 2009) and polyglutamine aggregation prevention (Hageman *et al.*, 2010; Ito *et al.*, 2016) - operate in an HSP70-independent manner. The question is how HSP40s that are equipped to deliver diverse polypeptides and to activate HSP70s' ATPase activity are deployed for monogamous HSP70-independent functions. Elucidation of these "off-labeled" usages will shed light on the fundamental mechanisms of HSP40s and disparate reactions.

*Chlamydomonas* is an ideal model system for addressing this question. The green alga is amenable to various experimental approaches and has well characterized flagella (Merchant *et al.*, 2007). Eukaryotic cells use motile cilia and flagella to sweep the surrounding fluid for a myriad of processes that are crucial for their fitness in the natural environment. The rhythmic movement is typically generated by the 9+2 axoneme that has

9 microtubule outer doublets surrounding the central pair (CP) apparatus with 2 microtubule singlets. A number of molecular complexes, most notably dynein motors, radial spoke (RS) and CP projections, associate with microtubules at precise positions every 96 nm throughout the length of axoneme (reviewed by Zhu *et al.*, 2016). A HSP40 and HSP70A are located respectively in RSs and CP that contact intermittently to transduce mechanical feedback that governs the rhythmic beating (Satouh *et al.*, 2005; Yang *et al.*, 2005; 2008; Mitchell *et al.*, 2005; Oda *et al.*, 2014). HSP70A is also enriched at the tip of flagella (Bloch and Johnson, 1995).

Spoke HSP40 is the only HSP40 in *Chlamydomonas* flagella (Pazour *et al.*, 2005). Defects of RS mutants (Table 4-1) suggest that it is positioned at the neck region of the Y-shaped complex where the singular stalk splits into two bifurcated arms (Yang *et al.*, 2006; Pigino *et al.*, 2011). It is a typical type II DnaJ that contains a J domain, known for activation of HSP70's ATPase activity, followed by a Glycine/phenylalanine (G/F)-rich disordered region and a C domain for dimerization. The latter two domains also interact with various specific polypeptides, primarily via hydrophobic interactions (Perales-Calvo *et al.*, 2010; Kampinga and Craig, 2010). Spoke HSP40 is crucial for rhythmic beating. RNAi-mediated depletion results in jerky flagella missing only HSP40. Yet most RSs appear normal in thin-section electron microscopy (EM) except for a small subset of deformed RSs (Yang *et al.*, 2008). It is unclear if this minor anomaly is relevant to HSP40 deficiency. Independent lines of evidence indicate that HSP40 acts in an HSP70-independent manner. The jerky flagella of RNAi cells could be rescued immediately by electroporation of recombinant HSP40 with or without the J domain. In the same vein, although the J domain sequence appears highly conserved among spoke HSP40

orthologues, the His-Pro-Asp (HPD) tripeptide required for HSP70 activation is diverged (Yang *et al.*, 2008). Furthermore, the *Chlamydomonas* HSP70A mutant still generates motile, full-length flagella (Silflow *et al.*, 2011).

	Strain	Causative Gene	Deficient Subunits	References
Head mutants	<i>pf1</i>	<i>RSP4</i>	RSP1, 4, 6, 9 and 10	McVittie A, 1972 Huang <i>et al.</i> , 1981 Curry <i>et al.</i> , 1992
	<i>pf26</i>	<i>RSP6</i>	RSP1, 4, 6, 9 and 10	Curry <i>et al.</i> , 1992 Wei <i>et al.</i> , 2011
	<i>pf17</i>	<i>RSP9</i>	RSP1, 4, 6, 9 and 10	Huang <i>et al.</i> , 1981
Neck mutants	<i>pf24</i>	<i>RSP2</i>	RSP1, 4, 6, 9 and 10; RSP2, NDK5, HSP40	Huang <i>et al.</i> , 1981 Patel-King <i>et al.</i> , 2004 Yang <i>et al.</i> , 2004
	<i>ndk5</i>	<i>NDK5</i>	RSP1; NDK5, HSP40	Zhu <i>et al.</i> , submitted
	<i>pf33</i>	<i>HSP40</i>	HSP40	Yang <i>et al.</i> , 2005 Yang <i>et al.</i> , 2008

**Table 4-1.** *Chlamydomonas* mutant strains deficient in the head or neck region of the RS.

Spoke HSP40 is not a typical RS protein (RSP) in terms of trafficking. As cilia and flagella are devoid of protein synthesis machineries, all axonemal components are synthesized in the cell body. New components are added to the microtubule plus ends of the axoneme at the tip of growing flagella, distal from the cell body (Rosenbaum and



Child, 1967; Johnson and Rosenbaum, 1992). In general, components in an axonemal complex are synthesized and preassembled into a precursor complex in the cell body (Fowkes and Mitchell, 1998; Qin *et al.*, 2004), which is then delivered by anterograde intraflagellar transport (IFT) trains to the tip for the final assembly (reviewed by Rosenbaum and Witman, 2002). Notably, mature and precursor RSs appear rather different in size, shape and contents. Mature RSs sediment as 20S Y-shaped particles, whereas precursors sediment as 12S  $\Gamma$ -shaped particles (Yang *et al.*, 2001; Qin *et al.*, 2004; Diener *et al.*, 2011) containing most RSPs except HSP40 (Yang *et al.*, 2005) and chaperone-like LC8 (Gupta *et al.*, 2012).

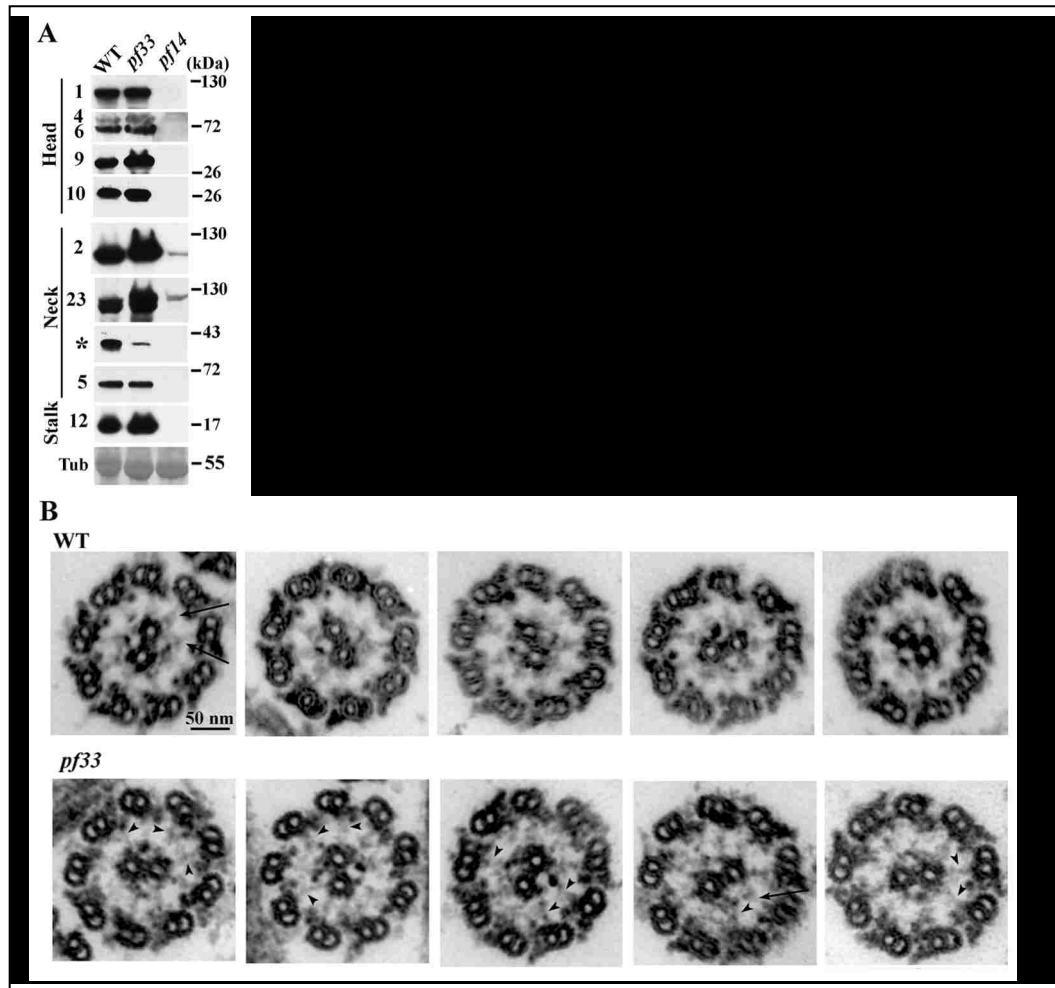
We took advantage of two new *Chlamydomonas* mutants, NDK5 mutant *ndk5* (Zhu *et al.*, submitted) and HSP40 mutant *pf33*, to elucidate this unusual HSP40. The results support a model predicting how a co-chaperone is conscribed in RS assembly processes that occurs at the opposite ends of flagella.

## **4.2 Results**

### **4.2.1 Discovery of a HSP40 Transposon Insertional Mutant**

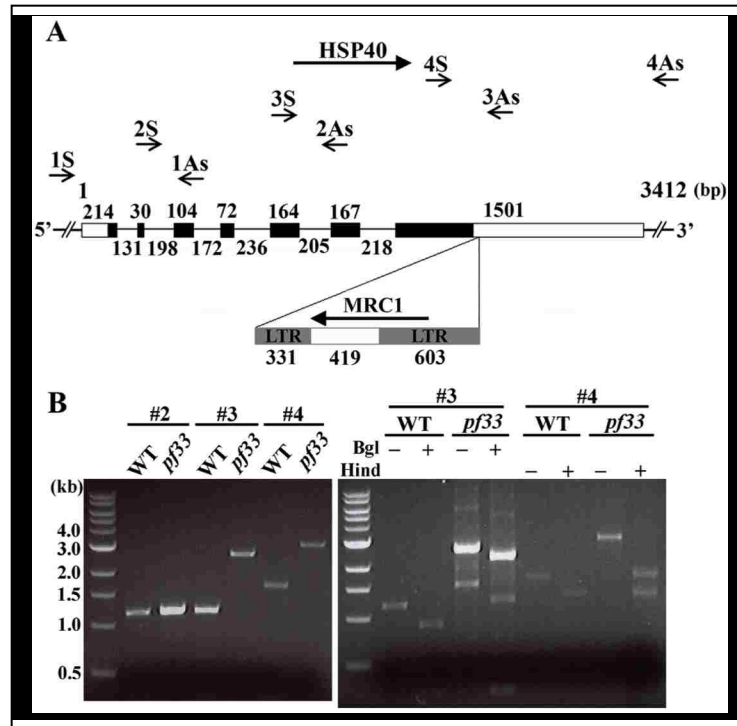
We attempted to use imaging to reveal the assembly of HSP40 in space and time. However, the HSP40 antibody is not compatible for immunolocalization, whereas the HSP40 RNAi strain is not conducive for expression of GFP-tagged HSP40. Our strategy was to identify a recessive HSP40 mutant. PCR-based restriction fragment length polymorphism (RFLP) analysis of mutants recovered from UV mutagenesis mapped the genetic defect in one strain near the *HSP40* gene (Kamiya, 1988). Like the RNAi strain, most cells of this strain designated as *pf33* had jerky flagella, although a few cells swam

like wild-type (WT) cells. Swimmers were still present in isolated single clones and backcrossed strains. Western blot analysis showed that, compared to WT, HSP40 was indeed drastically reduced in *pf33* axonemes whereas the representative proteins in the head, neck and stalk region of the RS complex appeared normal (Figure 4-1A). The positive and negative controls were from the WT strain and spokeless *pf14* mutant. Protein stain of a duplicated membrane demonstrated similar protein loads (bottom panel). Cross section EM, generated by our collaborator Dr. Ritsu Kamiya from the University of Tokyo, showed that, contrary to the Y-shaped RSs (arrows in Figure 4-1B) typical in WT axonemes (top panel), many RSs in *pf33* axonemes (bottom panel) appeared deformed. Although the split and/or tilted RSs (arrowhead) were similar to those in the EM of flagella sections of the RNAi strain (Yang *et al.*, 2008), the severity in axoneme sections was far more conspicuous.



**Figure 4-1.** Phenotyping of a new HSP40 mutant, *pf33*. **(A)** Western blots show a specific HSP40 deficiency (asterisk) in *pf33* axonemes. The other proteins located at three major areas of the RS appear normal. Tubulin (Tub) bands revealed by Ponceau S-stained membrane (bottom panel) show the protein loads. The WT strain serves as a positive control. The spokeless strain *pf14* serves as a negative control. **(B)** EM of axoneme cross sections. Nearly all 45 RSs in all 5 collected WT axoneme sections (top panel) appear like a typical Y-shaped complex (arrows), rendering an ordered appearance of axonemes. In contrast, the RSs in 5 images representing 12 focused *pf33* axoneme sections appear disordered (bottom panel). The head/neck region of some RSs appears split or tilted (arrowhead). Only one seems normal (arrow).

To test if *pf33*'s *HSP40* gene was mutated, we first PCR-amplified the *HSP40* gene with primer pairs positioned across the entire gene (Figure 4-2A). While N-terminal fragments amplified from the genomic DNA of *pf33* and WT cells were identical (represented by fragment 2), fragment 3 and fragment 4 amplified from *pf33* were 1.3-kB longer (Figure 4-2B, left panel). Restriction enzyme digestion (right panel) predicted additional sequences in the overlapping region near the stop codon. Sequencing of fragment 3 and 4 using primer 3AS and 4S respectively revealed the MRC1 transposon inserted 37 base-pair downstream to the stop codon in a reverse orientation. The 3' long terminal repeat (LTR) was 272-bp shorter, perhaps lost during insertion or due to decay afterwards (Kim *et al.*, 2006; Gallaher *et al.*, 2015). Curiously, the insertion site does not have the 5-bp target-site sequence identified previously, indicating that recognition for MRC1 insertion is not absolute. It is likely that UV radiation used in mutagenesis triggered MRC1 translocation (Kim *et al.*, 2006) into the *HSP40* gene in *pf33*.

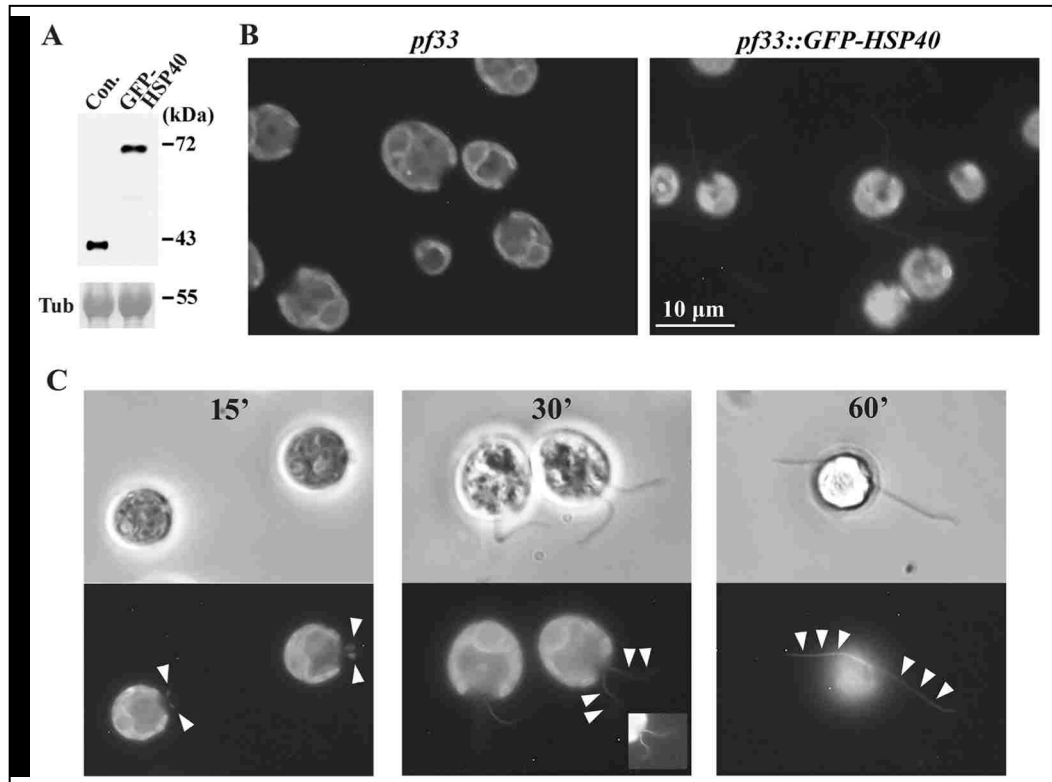


**Figure 4-2.** Genotyping of *pf33*. (A) A schematic depicting the *HSP40* gene, the PCR genotyping strategy and a partial MRC1 transposon inserted downstream to the stop codon in the reverse direction in *pf33*'s *HSP40* gene. The primer pairs for PCR are depicted in arrows. The base pair number of each segment is indicated above or below. (B) DNA gels of PCR products from WT and *pf33* cells (left panel) and restriction digest (right panel). PCR fragments of the N-terminal region from both strains are identical (eg. the #2 fragment amplified by the primer pair 2S and 2AS). But fragment #3 and #4 from *pf33* are 1.3-kb larger than those from the WT. The two fragments overlapped at the region around the stop codon. BglIII and HindIII digests demonstrate specific PCR amplification. Sequencing of fragment #3 and #4 showed that the additional sequence is a partial 1.3-kb MRC1 fragment. The 3' Long-terminal repeat (LTR) is truncated.

Using PCR and cloning, we recovered the entire *HSP40* genomic DNA from WT cells, and engineered it into two plasmids, pHSP40 and pGFP-*HSP40*. Both constructs fully rescued the jerky flagella of *pf33*. Western blots probed for *HSP40* showed that GFP-*HSP40* in the axoneme of motile *pf33* transformants was equally abundant as *HSP40* in the WT control (Figure 4-3A). Therefore, the phenotypes of *pf33* are due to the

mutation of the *HSP40* gene. The natural MRC1 re-translocation (Gallaher *et al.*, 2015; Mayfield *et al.*, 1987) could account for occasional observations of swimmers in independent *pf33* isolates. The residual HSP40 proteins in *pf33* axonemes (Figure 4-1A) may come from the few swimming revertants or incomplete block of gene expression by the transposon at the 3'UTR. Live cell fluorescence microscopy showed that, contrary to the dark flagella of *pf33* cells (Figure 4-3B, left panel), the entire flagella of rescued *pf33* transformants glowed uniformly (right panel). The intensity was dim compared to the autofluorescence of the cell body. The identical distributions of GFP-HSP40 throughout flagella and similar stoichiometry of HSP40 and the major RSPs that exist as a homodimer (Piperno *et al.*, 1981; Sivadas *et al.*, 2012; Oda *et al.*, 2014) suggest that HSP40 operates as a homodimer as most HSP40s (Kampinga and Craig, 2010) and is present in every RSs.

To reveal the timing of HSP40 assembly during flagellar generation, we used pH shock to trigger *pf33::GFP-HSP40* cells to shed flagella, and then imaged periodically as cells were growing back flagella. Once nascent flagella were visible in bright field microscopy (Figure 4-3C, top panel), they emitted fluorescence. Consistent with HSP40's role in motility, newly generated short flagella were already motile but immobilized poorly to the slide, leading to blurry fluorescent images following long exposures (first two time points). Therefore the assembly of GFP-HSP40, flagellar generation and motility are coupled.



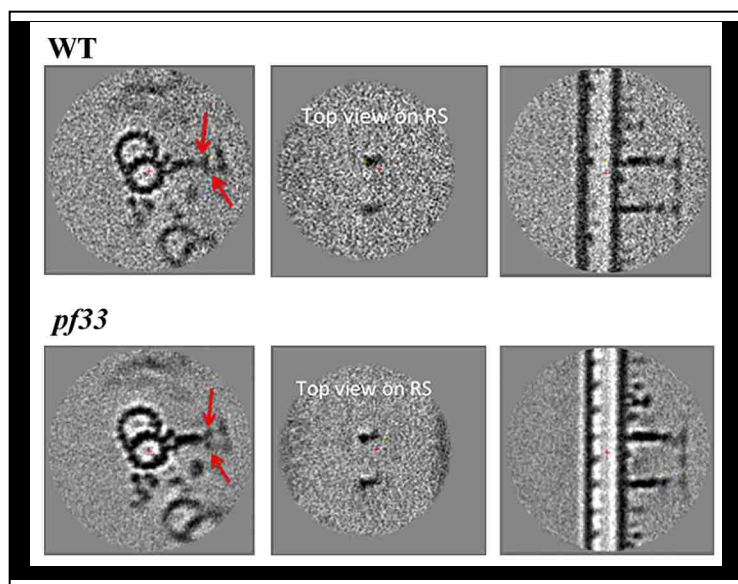
**Figure 4-3.** The *pf33* transformant cells expressing GFP-HSP40. **(A)** A western blot of axonemes probed with anti-HSP40 antibody shows similar abundance of HSP40 from WT control cells and GFP-HSP40 from motile transformants. **(B)** Fluorescence microscopy of *pf33* and GFP-HSP40 transformants. As expected for RSPs, GFP-HSP40 distributes evenly throughout the length of flagella in all cells from a motile transformant strain. Without fluorescing flagella for focusing, *pf33* cells were imaged at a slightly different focal plane. **(C)** Fluorescence microscopy of live *pf33* cells showed synchronized assembly of GFP-HSP40 and flagella (arrowhead). Inset, a brightened image with a lower magnification to reveal fluorescence at the tip of waving flagella. The experiment was performed three times.

#### 4.2.2 Cryo-electron Tomography of HSP40-minus RSs

To clarify different severities of deformed RSs in thin-section EM of *pf33* axonemes (Figure 4-1B) and RNAi strain flagella (Yang *et al.*, 2008), our collaborators Dr. Poghosyan Emiliya and Dr. Ishikawa Takashi performed cryo-ET that can minimize

distortions that are prone to occur in traditional EM (Nicastro, 2009). The subsequent sub-tomogram averaging showed that RSs in the two strains appeared identical (Figure 4-4). Therefore, rampant RS deformation in axoneme thin sections is aggravated by EM procedures. No electron density attributable to the dimer of nearly 40-kDa HSP40 at this resolution suggests that HSP40 is not required for the Y-shaped morphology of the RS or does not merely occupy one prominent structural module. Interestingly, in the side view digitally sectioned at a particular position, the once singular neck underneath the bifurcated arms appeared composed of two closely positioned lobules (between arrows in the bottom panel). This is consistent with the prediction that this region harbors two similar molecular modules, each containing an amphipathic helix (AH) from RSP3 anchoring a Dpy30 domain homodimer from RSP2 or NDK5 (Gopal *et al.*, 2012; Sivadas *et al.*, 2012).



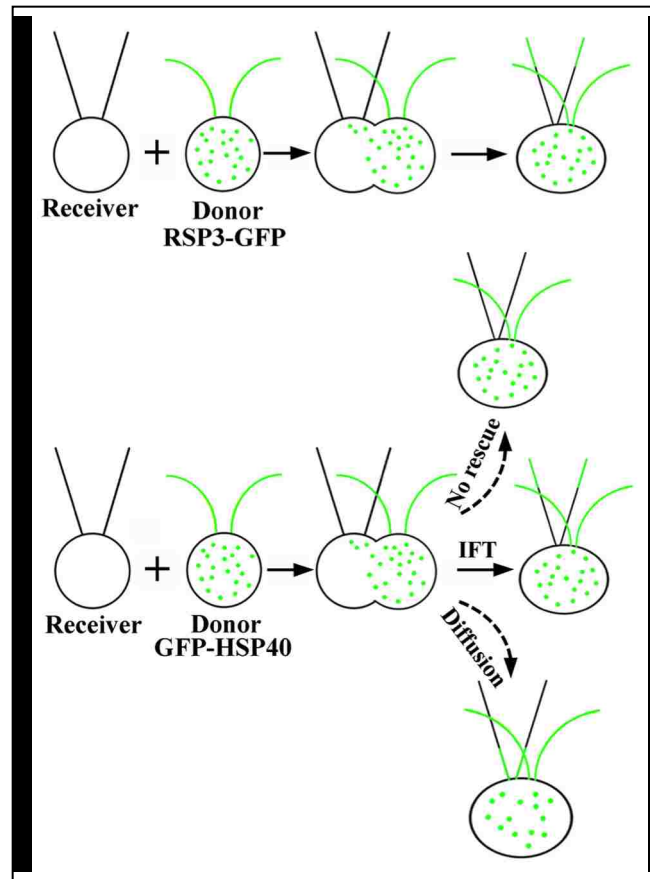


**Figure 4-4.** The side view, top view and longitudinal view of averaged cryo-ET of WT and *pf33* axonemes. The RSs with or without HSP40 appear identical. Note, the knot underneath the bifurcated arm appeared split in certain digital side view sections (see red arrows in *pf33*).

#### ***4.2.3 Identical Assembly Polarity but Distinct Efficiencies in the Repair of HSP40 and RSs***

To elucidate how HSP40 that sediments separately from RS precursors becomes a constitutive subunit of the mature RS, we performed dikaryon rescue (reviewed by Dutcher, 2014). *Chlamydomonas* gametes identify mates by flagella. Upon signaling through direct flagellar contact, gametes of opposite mating types fuse into a dikaryon with two nuclei and four flagella. This stage lasts for ~ 2.5 hours before flagella resorb. The cytosol contains components from both cells, allowing defects in one gamete to be complemented by normal proteins produced by its partner. Using this tool, it was demonstrated that a *pf14* gamete that cannot assemble RSs due to the defective RSP3 gene was rescued by its partner's RSP3 (Johnson and Rosenbaum, 1992). Notably, RSs

appeared first at the tip of paralyzed *pf14* flagella and the restoration progressed toward the base as observed by immunofluorescence (Figure 4-5, top panel). This and other evidence support the model that prepackaged axonemal complexes are delivered to the flagellar tip to be assembled to the microtubule plus ends for the growth of new flagella and the turnover of full-length flagella (Rosenbaum and Witman, 2002). We reasoned that if HSP40 was delivered in a similar manner as RS precursors, GFP-HSP40 would be restored to the tip of *pf33* flagella first as well (Figure 4-5, bottom panel). Alternatively, if HSP40 diffused into flagella, then the fluorescence might appear at the base first. If HSP40 by itself could not enter flagella, there would be no rescue.



**Figure 4-5.** Possible outcomes of dikaryon rescue experiments testing how HSP40 is transported and assembled. Immunofluorescence showed that RSs were restored to the RS-free flagella in the RSP3 mutant, *pf14* when a *pf14* cell is fused to a WT cell. Same results are expected in the control group using motile *pf14::RSP-GFP* as donor cells. There are three possible outcomes for dikaryons of *pf33* by the donor cell, *pf33::GFP-HSP40*. If HSP40 is delivered by IFT, the rescue pattern will be similar to that as the rescue of RSP3. If HSP40 cannot enter flagella, there will be no rescue. On the other hand, if HSP40 diffuse into flagella, the fluorescence will appear in a base-to-tip direction.

For the positive control of live imaging, we mixed the gametes of *pf14(-)* and *pf14(+)::RSP3-GFP* transformants. Afterwards, the cell mixture was imaged about every 15 mins with bright field and fluorescence microscopy. Due to the time constraints and faint fluorescence, we only captured focused flagellar images of a few dikaryons at each time point. In two repeated experiments, more than 5 dikaryons for each time point were imaged. Since all dikaryons did not form simultaneously, the one with the most extensive signal in the receiver flagella was presented. As in the previous study (Johnson and Rosenbaum, 1992), dikaryons with four flagella were observed readily within 15 mins after mixing. Donor flagella emitted fluorescence uniformly. Faint fluorescence was detectable at the tip of flagella of receiver cells (Figure 4-6A, arrowheads). At subsequent time points, signals brightened and extended toward the base of receiver flagella. By 90 mins, fluorescence was visible throughout flagella. Thus RSP3-GFP could replicate RSP3 immunofluorescence in dikaryons.

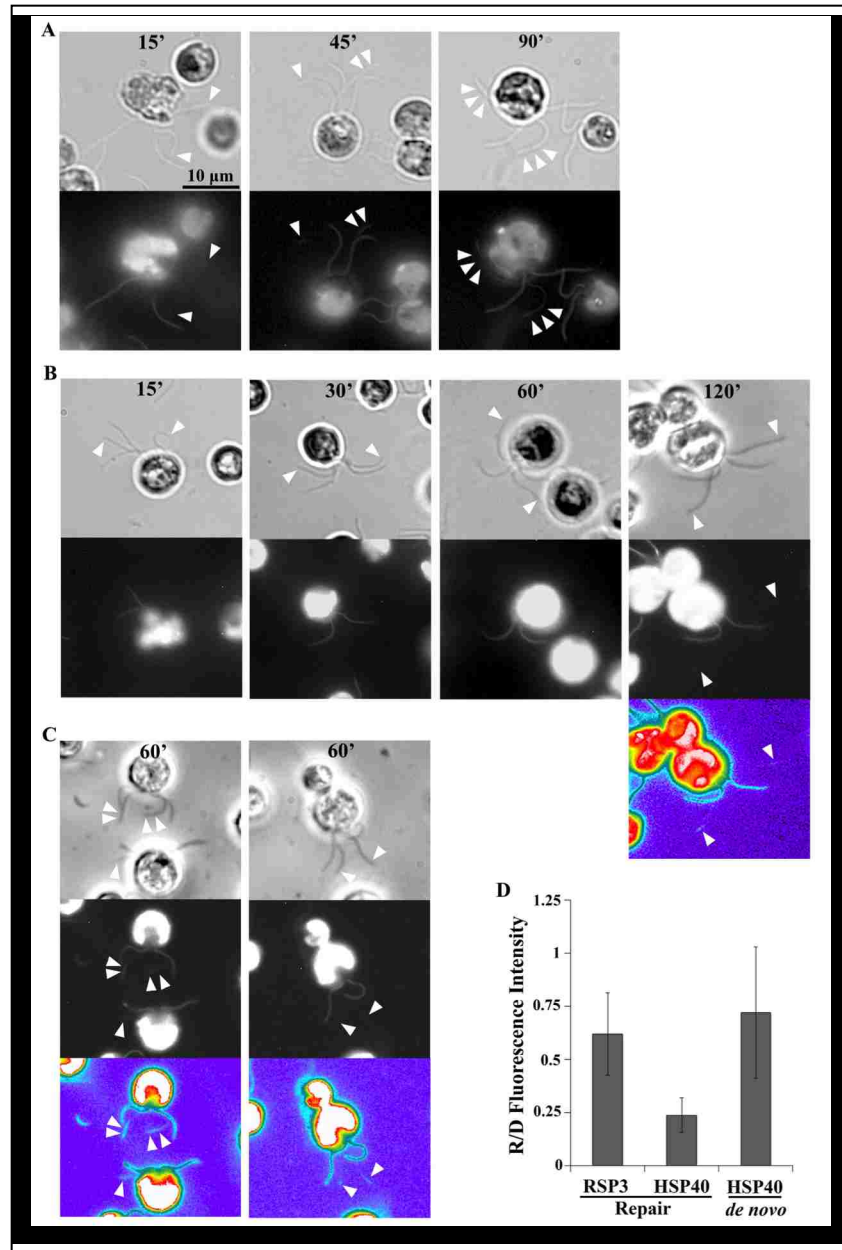
As for the group of *pf33(+)* by *pf33(-)::GFP-HSP40*, dikaryons also formed within 15 mins (Figure 4-6B, top panel), but GFP-HSP40 was not detectable in receiver HSP40-minus flagella in any dikaryon for more than 90 mins (bottom panel). After extensive search of three experiments we finally found 6 dikaryons with GFP-HSP40 at the tip of receiver flagella at 120 mins (bottom panel, arrowheads). Soon afterwards flagella absorbed. The tip-first recovery of GFP-HSP40 was identical to that of whole RSs (Figure 4-6A) and contrary to the polarity predicted by the diffusion model. However, compared to the nearby flagella from donor cells (Figure 4-6B) and to RSP3-GFP signal representing restored whole RSs at the 30-min time point (Figure 4-6A), the

rescue with GFP-HSP40 was delayed and the signal was weak. The pseudocolored panel was used to brighten the signal.

We then tested whether rescue efficiency of GFP-HSP40 would improve if receiver *pf33* cells were still growing back flagella and RS assembled *de novo* (Johnson and Rosenbaum, 1992). Following deflagellation and regeneration of flagella to about half-length or two thirds, *pf33* cells were mixed with donor cells that had full-length flagella. The entire experiment was conducted in the presence of cycloheximide to inhibit protein synthesis triggered by deflagellation. Generation of the proximal half of new flagella would largely deplete the axonemal components stowed in the *pf33* cytosol, while the distal part generated after fusion would mostly come from proteins produced by the donor cell. As cells with short flagella mated less efficiently, the cell mixture was imaged 60 mins after mixing, allowing gametes with short flagella to find mates and to finish regeneration. We successfully imaged 6 randomly selected dikaryons with donor and receiver flagella in focus. As expected, fluorescence distributed throughout two flagella of donor cells, and only at the new, distal part of the flagella of receiver cells (Figure 4-6C, arrowheads). The fluorescence in the receiver flagella varied in intensity - some nearly as intense as donor's flagella (the top cells in the left panel), whereas some others dimmer (right panel) perhaps due to incomplete inhibition of protein synthesis. Nonetheless, the rescue of GFP-HSP40 with *de novo* RS assembly was evident without (middle panels) or with pseudocolor (bottom panels).

To compare the intensity quantitatively, fluorescence intensity at the brightest spot near the tips of adjacent receiver (R) and donor (D) flagella in dikaryons from the three mating schemes was measured. The intensity ratio (R/D in Figure 4-6D) showed

that restoration of GFP-HSP40 to full-length flagella with HSP40-minus RSs after 120 mins (middle bar) was significantly lower than the restoration of whole RS to existing flagella (left bar,  $p < 0.001$ ) or *de novo* assembly of GFP-HSP40 with RSs in growing flagella (right bar,  $p < 0.001$ ) that were imaged at least 1 hour earlier.



**Figure 4-6.** Distinct efficiencies in the repair of missing RSs and HSP40 in dikaryon rescues. Cells were imaged by bright field (top) and fluorescence (bottom) microscopy approximately every 15 mins after mixing cells of opposite mating types. Each image represents at least 5 dikaryons. **(A)** Dikaryons of *pf14(-)* by *pf14(+)::RSP3-GFP*. Fluorescence, already detectable at the tips of receiver *pf14(+)* flagella after 15 mins (arrowheads), extended toward the base and became stronger as time progressed. The experiment was performed twice. **(B)** Delayed restoration of GFP-HSP40 to receiver *pf33(+)* flagella from *pf33(-)::GFP-HSP40*. Fluorescence was not detectable in receiver *pf33* flagella until 120 min after mixing. Fluorescence also appeared at the flagellar tip

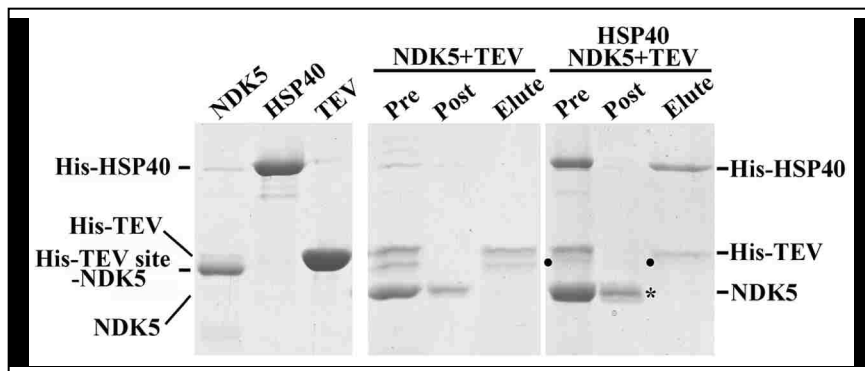
(arrowheads) of 6 dikaryons among many observed at the 120 min time point from total 3 experiments, but the intensity was exceedingly dim. Pseudocolor was used to highlight the restoration. Flagella were shed soon afterwards. The experiment was performed three times. **(C)** Efficient restoration of GFP-HSP40 requires *de novo* assembly of RSs in newly generated flagella. 30 mins after flagella excision, *pf33(+)* with half-length regenerating flagella was mixed with *pf33(-)::GFP-HSP40* with full-length flagella. GFP-HSP40 was restored to the distal part of growing HSP40-minus flagella of *pf33(+)* in all dikaryons 60 min after mixing. Fluorescence intensity in regenerating receiver flagella varies. All dikaryon rescue experiments were performed in the presence of cycloheximide to inhibit protein synthesis. The experiment was performed once. **(D)** Quantification of fluorescence intensity at the brightest region near the flagellar tip. Receiver versus donor (R/D) intensity ratio at the flagellar tip was  $0.62 \pm 0.19$  (n=13, from 15-60 min time points) for restoring RSs (RSP3-GFP),  $0.24 \pm 0.08$  (n=8, from 120-min time points) for restoring HSP40 (GFP-HSP40), and  $0.72 \pm 0.3$  (n=9, from 60-min time points) for *de novo* assembly of GFP-HSP40 and flagellar assembly. Only flagella from the same dikaryons and in focus were used for comparison. HSP40 repairing is significantly lower than RSP3 repairing ( $p < 0.001$ ) and lower than the *de novo* assembly of GFP-HSP40 into RSs in growing flagella ( $p < 0.001$ ).

#### **4.2.4 Low Affinity of Recombinant HSP40 and NDK5**

We took an *in vitro* approach to elucidate how HSP40 might associate with RSs. Structural and morphological deficiencies of the RS mutants strongly suggest that RSP2, NDK5 and HSP40s are located at the spokeneck of mature RSs (Table 4-1) (Huang *et al.*, 1981; Patel-King *et al.*, 2004; Yang *et al.*, 2005; Pigino *et al.*, 2011). Flagella of the RSP2 mutant lack the spoke head-neck structure and are deficient in these three proteins and all head proteins, whereas the neck proteins are present in mutant flagella missing the spokehead. Notably, flagella of the *ndk5* mutant are only deficient in NDK5, HSP40 and one spokehead protein, RSP1 (Figure 3-3). Conversely, no RSPs are missing in HSP40-null flagella (Yang *et al.*, 2005). Thus, NDK5 is directly responsible for HSP40 assembly. So we hypothesize that HSP40 binds to NDK5 to associate with the RS. If this is correct, these two proteins will be co-purified as the other interactors in the RS (Kohno *et al.*, 2011; Sivadas *et al.*, 2012).



Since recombinant NDK5 precipitated (Munier *et al.*, 1998), we expressed separately in bacteria His-tagged HSP40 and Maltose-binding protein (MBP)-His-tagged NDK5<sub>1-201</sub> that contains the conserved region lacking the excessive C-terminal tail unique to green algae. Electroporation of His-tagged HSP40 restores motility to paralyzed HSP40 RNAi cells (Yang *et al.*, 2008), whereas His-NDK5<sub>1-201</sub>, following the cleavage of MBP, displays the NDK activity (Figure 3-1). These two fusion proteins were Ni-NTA purified, and mixed together, along with His-tagged TEV protease that could cleave off the His tag only from His-NDK5 that contains a TEV proteolytic site. After overnight incubation, the mixture was subjected to the 2<sup>nd</sup> round Ni-NTA affinity purification. Coomassie blue-stained gel (Figure 4-7) showed that TEV indeed excised the His tag from most His-NDK5 (compared the first lane in the left panel and middle panel), resulting in fast migrating untagged NDK5 in the flow through (Post in the middle panel), while His-TEV and residual His-NDK5 were pulled out by Ni-NTA and present in the elute. In the presence of His-HSP40, the TEV-digested, untagged NDK5 was still in the flow through (Post in the right panel), not co-purified with His-HSP40 (Elute in the right panel). Therefore, the hypothesis was not supported. Although the assembly of HSP40 requires NDK5, they exhibit low affinity toward each other.



**Figure 4-7.** Low co-purification of recombinant His-HSP40 and His-NDK5 *in vitro* despite the requirement of NDK5 for the assembly of HSP40 *in vivo*. His-HSP40, His-NDK5 (dot) and His-tagged protease that could cleave off the His tag only from His-NDK5 were expressed individually in bacteria and affinity purified with Ni-NTA (left panel). His-NDK5 was incubated overnight without or with HSP40 in the presence of His-TEV. The mixture (Pre) was then subjected to Ni-NTA purification again. Untagged NDK5 (asterisk) was in the flow through (Post) regardless of the absence (middle panel) or presence (right panel) of His-HSP40 that could be pull down by Ni-NTA (in the Elute). Only the conserved first 201 a.a. residues of NDK5 that were conserved in all NDK5 orthologues were expressed. Samples were resolved in SDS-PAGE and proteins were revealed by Coomassie blue stain.

#### 4.2.5 Structural Modeling of HSP40 and the RS Neck

To contemplate how HSP40 may associate with the RS with low affinity to the nearby protein required for its assembly (Figure 4-7) and without influencing RS morphology (Figure 4-4), we performed structural modeling, taking advantage of existing structures of homologous molecular domains and the surface rendering of intact human and algal RSs from previous cryo-ET studies (Lin *et al.*, 2014; Pigino *et al.*, 2011). Overlay shows remarkable similarities (grey and green in Figure 4-8A, left panel), especially around the neck region, although algal orthologues of RSPs that contribute to the neck region contain additional sequences (Gopal *et al.*, 2012). Viewed from the tip

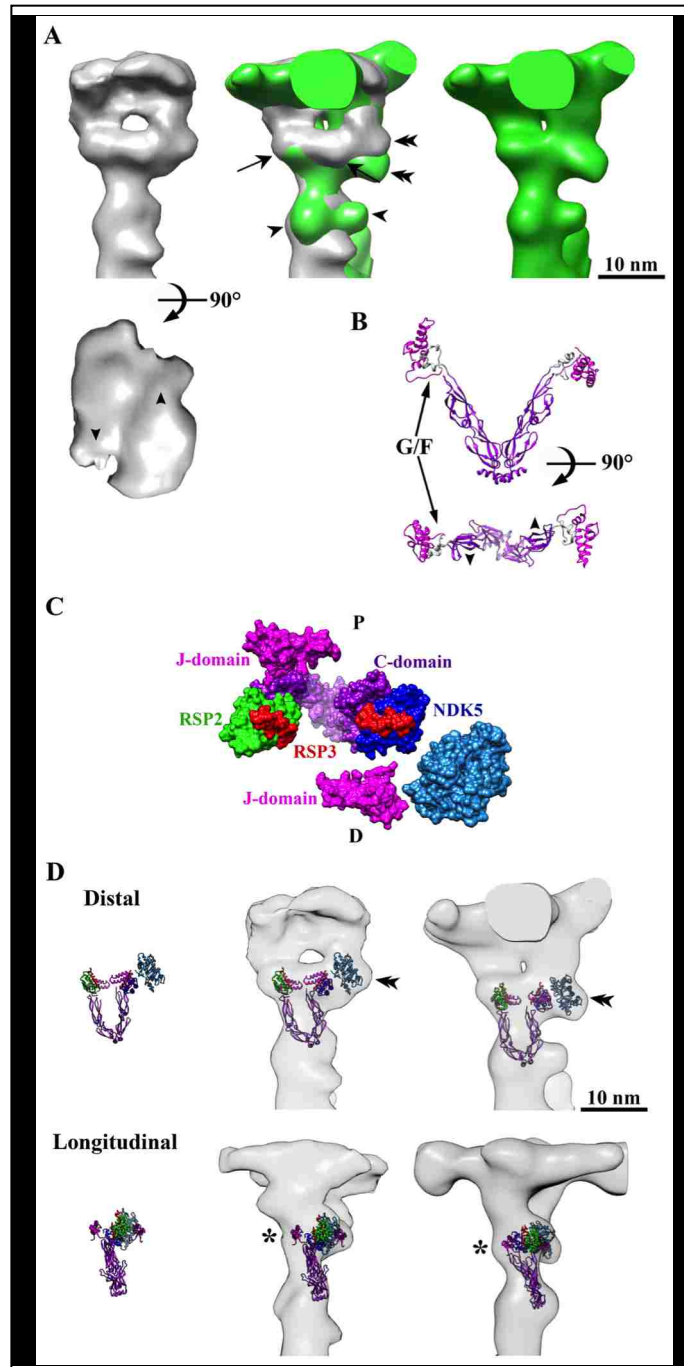
(distal view), the neck has two nodules (arrows), consistent with the two lobules in the cryo-ET (Figure 4-4). It is worth mentioning that while this region and the spokehead above are absent in the neck-less RS mutant, *pf24*, the affected area actually extends toward the pair of stalk nodules in algal RSs (arrowheads) (Pigino *et al.*, 2011). We reason that HSP40 should be located within this swath of area that is abnormal in *pf24* RSs. The top view (bottom panel) shows the spokehead with two modules arranged in rotational symmetry (arrowheads). Consistent with this, while the first recently solved HSP40 structure appears like a V as expected (Figure 4-8B, top panel) (Barends *et al.*, 2013), a 90-degree rotation reveal rotational symmetry of the C-domain dimer (Figure 4-8B, bottom panel, arrowheads). Therefore, HSP40 has a basic platform to fit the contour of the RS core.

Using the Chimera program we first modeled the core, placing into the neck region the Dpy30/AH complex from the Set1-like histone methyltransferase complex (PDB accession number, 4RIQ, Tremblay *et al.*, 2014) to represent the Dpy30 domain homodimers from RSP2 (green) and NDK5 (blue), and the AH from RSP3 (red) (Figure 4-8C. Top view) as proposed (Gopal *et al.*, 2012; Sivadas *et al.*, 2012). Space-filled models alone are shown for clarity. However, surface renderings with a ribbon model (distal views and side views in Figure 4-8D) show that these structures are insufficient to fill up the entire space.

We reasoned that the excess space at the neck and an area below were occupied by HSP40 dimer. Since the G/F rich region is presumed disorder and diverged substantially (Yan *et al.*, 1999; Lopez *et al.*, 2003), only J domain and C domain are modeled. As the angle and shape of C-domain dimers also vary substantially (e.g. Sa *et*

*al.*, 2000; Suzuki *et al.*, 2010), the crystal structure is selected from the most similar HSP40 homologue, positioned below the neck modules (purple, PDB accession number, 3AGZ, Suzuki *et al.*, 2010). Two J domains (magenta, PDB accession number, 2CTP) are placed juxtaposed but at the opposite side of the two Dpy30/AH complexes (Figure 4-8C). We envisage that J and C domains are connected by the disordered G/F region, which is nearly as long as the J domain, wrapping around the Dpy30/AH complex. Next to the NDK5's Dpy30 domain (blue) is its NDK domain dimer (cyan, PDB accession number, 4ENO, Kim *et al.*, 2013) nudged into the asymmetric protrusion (Figure 4-8A, double arrowheads).

This steric arrangement using domains from non-RS proteins largely fits the space in RSs from humans (Figure 4-8D, middle panels) and *Chlamydomonas* (right panels). The dimeric spoke HSP40 resembles two malleable front claws of a crab, bracing together the two Dpy30/AH modules in the core of the RS. It is conceivable that when the claws are absent, the two arm/head units could split and/or tilt as shown in EM sections (Figure 4-1B, arrowheads). However, we cannot rule out the possibilities that the V-shaped HSP40 is part of the bifurcated arms above the neck to hold the two head modules together, or is inverted directing toward the RS base. The precise model will have to wait for high resolution structural studies of the *bona fide* RS complex.



**Figure 4-8.** Structural modeling of the RS neck region. (A) The 2<sup>nd</sup> RS (RS2) in each 96-nm axonemal repeat from human (left panel; EMDB accession number 5950, Li *et al.*, 2014) and *Chlamydomonas* (right panel; EMDB accession number 1941, Pigino *et al.*, 2011), viewed from the flagellar tip. The middle panel shows the overlay. Arrows and arrowheads point to a pair of nodules at the neck and the stalk respectively. Double arrowheads point to an asymmetric protrusion. The top view shows two head modules

positioned in rotational symmetry (bottom panel). **(B)** The structure of a dimeric bacterial HSP40 (PDB accession number 4J80). The presumptive disordered G/F region between J-domains to the V-shaped C-domain dimer becomes ordered in crystals. A 90° rotation shows rotational symmetry of the C-domain dimer (arrowheads in opposite directions). **(C)** Top view of a space-filled model illustrating the key structural components in the region below the bifurcated arms. P, proximal; D, distal. **(D)** Distal view (top panel) and longitudinal view (bottom panel) of ribbon models alone (left panels), and overlay with human RS2 (middle panels) and with *Chlamydomonas* RS2 (right panels). Each of the neck nodules (arrows) harbors a unit of an amphipathic helix from RSP3 (red) that anchors a Dpy30 domain homodimer from RSP2 (green) or NDK5 (blue) (an equivalent structure from a Set1-like histone methyltransferase complex, PDB accession number 4RIQ). Each unit is further surrounded by a J domain (magenta, PDB accession number 2CTP) and the invisible G/F-rich region that connects to the top of a V-shaped C domain dimer (purple, PDB accession number 3AGX) near a tubercle (asterisk) visible from the longitudinal view. The G/F region is not shown because of sequence divergence and structural flexibility. The NDK domain dimer of NDK5 (cyan, represented by NDK1, PDB accession number 4ENO) is placed in the asymmetric protrusion evident from the distal view (double arrowheads).

### 4.3 Discussion

While HSP40s are the presumptive partners of HSP70s in the chaperone system, they could also operate in critical yet disparate processes without the involvement of HSP70s. However, how HSP40s operate in either condition remains elusive, partly due to the malleable structures of HSP40. By taking advantage of the well-defined RS complex that exists in two states and the available tools for *Chlamydomonas*, this study sheds light on flagellar biology and the versatility of HSP40s.

#### 4.3.1 HSP40 is Needed for RS Structural Stability

The different deformation degrees of HSP40-minus RSs reflect the role of spoke HSP40 and the strengths and limitations of each EM method (Nicastro, 2009). The images in cryo-electron subtomogram averaging (Figure 4-4) that preserve bona fide axonemal ultrastructure indicate that most HSP40-RSs retain the typical morphology *in*

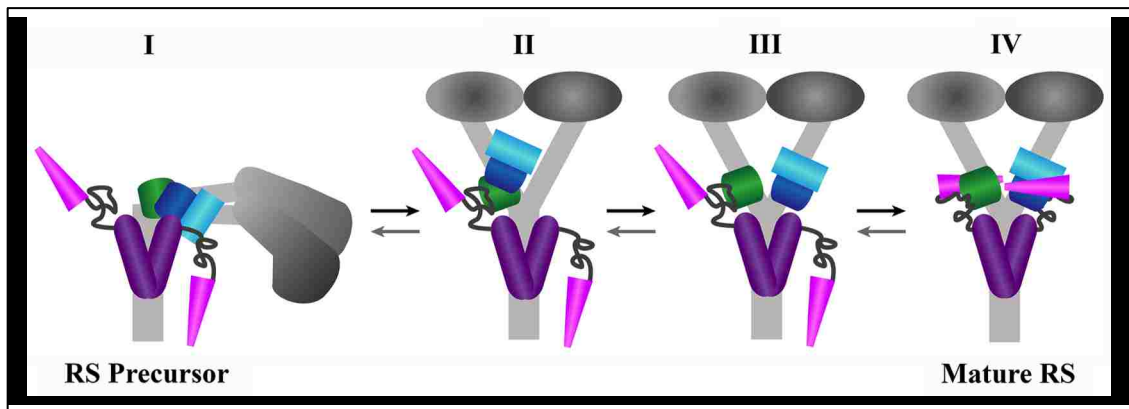
*vivo*, although deformed subpopulations are lost in averaging. On the other hand, the mostly deformed RSs in axonemes (Figure 4-1B) are exacerbated by the traditional EM procedures and the absence of the flagellar membrane. And yet this harsh procedure unequivocally reveals the propensity of HSP40-minus RS to deform. Thus, HSP40 confers structural stability to RSs to support the mechanical feedback as predicted (Yang *et al.*, 2008).

#### ***4.3.2 Delayed Repair of Existing HSP40-minus RSs Sheds Light on HSP40 and Dikaryon Rescue***

The identical polarity for the repair of missing HSP40 and missing whole RSs (Figure 4-6B, 6A) strongly suggests that HSP40, like RS precursors, also reaches the tip first in order to be restored to the existing flagella in dikaryons. However, the limited repair of missing HSP40 even after 2 hours is far slower than the evident repair of whole RSs (Figure 4-6A) and other axonemal complexes (e.g. Piperno *et al.*, 1996) within 30 mins; and *de novo* assembly of GFP-HSP40 with RSs during flagellar regeneration within 1 hour (Figure 4-6C). Previous studies also used dikaryon rescue to investigate partial RS defects (Luck *et al.*, 1977; Huang *et al.*, 1981). Although the biochemical readouts were not designed to reveal quantitative information, flagella were harvested 2.5 hours after mixing cells perhaps to increase rescue.

The inefficiency of restoring HSP40 to HSP40 minus RS cannot be attributed to presumed slow diffusion of free HSP40 particles, since diffusion of large and small particles in flagella could be as fast as IFT, if not faster (Ye *et al.*, 2013; Harris *et al.*, 2016); and the presumed IFT-independent repair of dynein arms occurs within 30 mins (Piperno *et al.*, 1996). Nor can this be explained by poor accessibility of soluble GFP-

HSP40 to RSs within the 9 outer doublets, since electroporation of RNAi cells in HSP40-containing solutions rescued motility within a minute (Yang *et al.*, 2008). The simplest explanation is that trafficking and assembly of HSP40 and RSs are tightly coupled. Free HSP40 are not readily available for the repair of defective RSs existing in the flagella. We propose that HSP40 rides with the RS precursor during IFT, like escorting client polypeptides. The typical hydrophobic HSP40-client interactions may be disrupted during flagellar extraction or fractionation, causing separation of HSP40 and RS precursor particles (Yang *et al.*, 2005) (Figure 4-9, panel I). Only when microtubules turnover at the tip (Wallace and Rosenbaum, 2001), whole RSs with GFP-HSP40 could be incorporated into axonemes. Or only the GFP-HSP40 that falls off RS precursors could repair HSP40-minus RSs.



**Figure 4-9.** A schematic picture depicting coupled trafficking and refolding of HSP40 and its RS client. HSP40 dimer primarily uses its V-shaped C domain (purple) to tether to the stalk region of the  $\Gamma$ -shape RS precursor in which only RSP2's Dpy30 domain dimer (green) binds to the base of one arm (panel I). Upon their arrival at the flagellar tip, the precursor converts into a Y-shaped complex with bifurcated arms and two head modules arranged in rotational symmetry (II). Subsequently the newly available 2<sup>nd</sup> arm anchors NDK5's Dpy30 domain dimer (blue) (III). The transformation induces the disordered G/F domains (wiggly lines) and J domains (pink) of HSP40 to refold around



the properly anchored Dpy30 domains to form the mature RS (IV). The confinement by the crab arm-like dimeric HSP40 prevents the singular spokehead from splitting when it is pulled by the central pair apparatus during the beat cycle or *in vitro*. This model also predicts unfolding in the reverse order (grey arrows) when the RS is recycled back to the cell body.

This interpretation is relevant to the evolving concepts of IFT mechanisms. Since it is presumed that IFT trains are equipped with various adaptors for carrying individual axonemal complexes and tubulins (e.g. Qin *et al.*, 2004; Hou *et al.*, 2007; Ahmed *et al.*, 2008; Bhogaraju *et al.*, 2013), it should be faster to grow new flagella or to restore full particles (Figure 4-6C and 6A; Johnson and Rosenbaum, 1992) that could attach to adaptors than to restore parts to partial complexes in existing flagella. The repair of parts would become more efficient if cargo-adaptor relationship is not strict (reviewed by Pedersen, 2016), if there are alternative trafficking modalities for parts of axonemal complexes, or if axoneme turnover could be promoted. Further studies of the repair of partial defects in various axonemal complexes (Piperno *et al.*, 1996; Lechtreck *et al.*, 2013) will shed new light on flagellar trafficking and assembly (Dutcher, 2014); and may guide emerging gene therapy for ciliopathies (McIntyre *et al.*, 2013).

#### ***4.3.3 Modeling Predicts the Actions of HSP40***

The structural model (Figure 4-8) explains a number of observations. It predicts that HSP40 dimer interacts with a swath of surfaces contributed by multiple proteins. This comports with the multivalent transient interactions of HSP40 with HSP70 and substrate proteins (Ahmad *et al.*, 2011), and with the low affinity of HSP40 for NDK5 (Figure 4-7) that is required for HSP40 assembly. Embrace of the crab arm-like dimeric

HSP40 stabilizes the RS so it could properly transduce mechanical feedback that ensures the rhythmicity of flagellar beating (Yang *et al.*, 2008); and to prevent RSs from deformation *in vitro* (Figure 4-1B). It also explains why recombinant HSP40 lacking the conserved J domain could rescue the motility of the RNAi cells but with a slower velocity than that of cells receiving intact HSP40 (Yang *et al.*, 2008). RSs partially enclosed by the C-domain and the G/F domain could be less durable during mechanical feedback, leading to intermittent asynchronous flagella, zig-zag trajectory and a slower velocity (Wei *et al.*, 2010) and steering deficiencies (Gopal *et al.*, 2012). Hence the J domain in the spoke HSP40 is conserved for the structural purpose rather than for activation of HSP70's ATPase activity, thus the activation HPD-tripeptide motif has diverged in vertebrate orthologues.

This model also predicts the transition of HSP40 and RS during assembly (Figure 4-9). We propose that, for all the proteins in the spoke head-neck region, only RSP2 binds to RSP3 in  $\Gamma$ -shaped RS precursors, which lack the signature bifurcated arms although containing all subunits in this area except HSP40 (Yang *et al.*, 2008; Diener *et al.*, 2011) (panel I). This prediction is based on RSP2 is required for the assembly of the whole spoke head-neck area (Huang *et al.*, 1981; Patel-King *et al.*, 2004; Yang *et al.*, 2004) (Table 4-1) and human RSP2 also interacts with NDK5 directly in yeast two-hybrid system (Rual *et al.*, 2005; Wang *et al.*, 2009). Therefore, RSP2 could be sufficient to tether all subunits in the head-neck directly or indirectly in the precursor. This is consistent with the phenotypes of the RSP2 mutant and NDK5 mutant (Table 4-1; Figure 3-3). HSP40 uses its V-shaped C domain to associate with the stalk region in the precursor during trafficking (Figure 4-9), analogous to client shuttling. Upon exiting IFT

at the flagellar tip, the precursor refolds into the Y-shaped complex with two head modules oriented in rotational symmetry (panel II), followed by docking of NDK5's Dpy30 domain to the AH in the RSP3 molecule for the second arm (panel III). Since HSP40-minus RS are Y-shaped mostly (Figure 4-4), these steps do not require HSP40. However, the new conformation induces refolding of the flexible G/F region and J domain of the nearby poised HSP40 dimer around the two Dpy30 domain dimers (panel IV) to strengthen the neck-stalk connection. This assembly process may be reversible (grey arrows), as Y-shaped RSs unfold back to  $\Gamma$ -shaped precursors when being recycled back to the cell body (Qin *et al.*, 2004).

In summary, this study proposes that spoke HSP40 uses co-chaperone features meant for transient interactions with many clients to travel with a specific client and to associate with the client constitutively after refolding. This role is essential for flagellar motility and thus species fitness. With remarkably malleable structures but slightly different sequences, the numerous HSP40 paralogues may help various client polypeptides or molecular complexes in a similar fashion, with or without HSP70s.

## CHAPTER 5: DISCUSSION

This dissertation centering on the two *Chlamydomonas* mutant strains, *ndk5* and *pf33*, reveals why eukaryotes allocate the members of two primordial protein families, NDK and HSP40, to the axonemal complex, RS, which likely exists in the common ancestral eukaryotic cells. The findings support a model predicting the intimate interactions of these two molecules to establish the signature Y-shaped molecular complex for a force-generating machine. These insights in turn shed new light on the fundamental mechanisms of these two protein families and the diverse cellular processes that involve them.

### *5.1 New Spokeneck Model*

RSs were once depicted as drumstick-like complexes as observed using traditional EM, which is prone to cause deformation and has limited resolution (Nicastro, 2009). Only after much improvement of cryo-ET and sub-tomogram averaging, the bona fide morphology of the Y-shaped complex with a hole in the enlarged head-neck region emerged (Pigino *et al.*, 2011; Nicastro lab). This morphology is interesting, since bifurcated arms that shape the hole also exist in the H3K4 histone methyltransferase complex that contains a Dpy30 domain containing protein; and are part of its atypical enzymatic catalytic site (Takahashi *et al.*, 2011). Thus it is proposed that the Dpy30 domain is used to build molecular complexes with bifurcated arms (Gopal *et al.*, 2012).

In the RS, the bifurcated arms are crucial for the function and divergence of RSs. Each arm connects to one of the two head modules, which in turn contact a CP projection

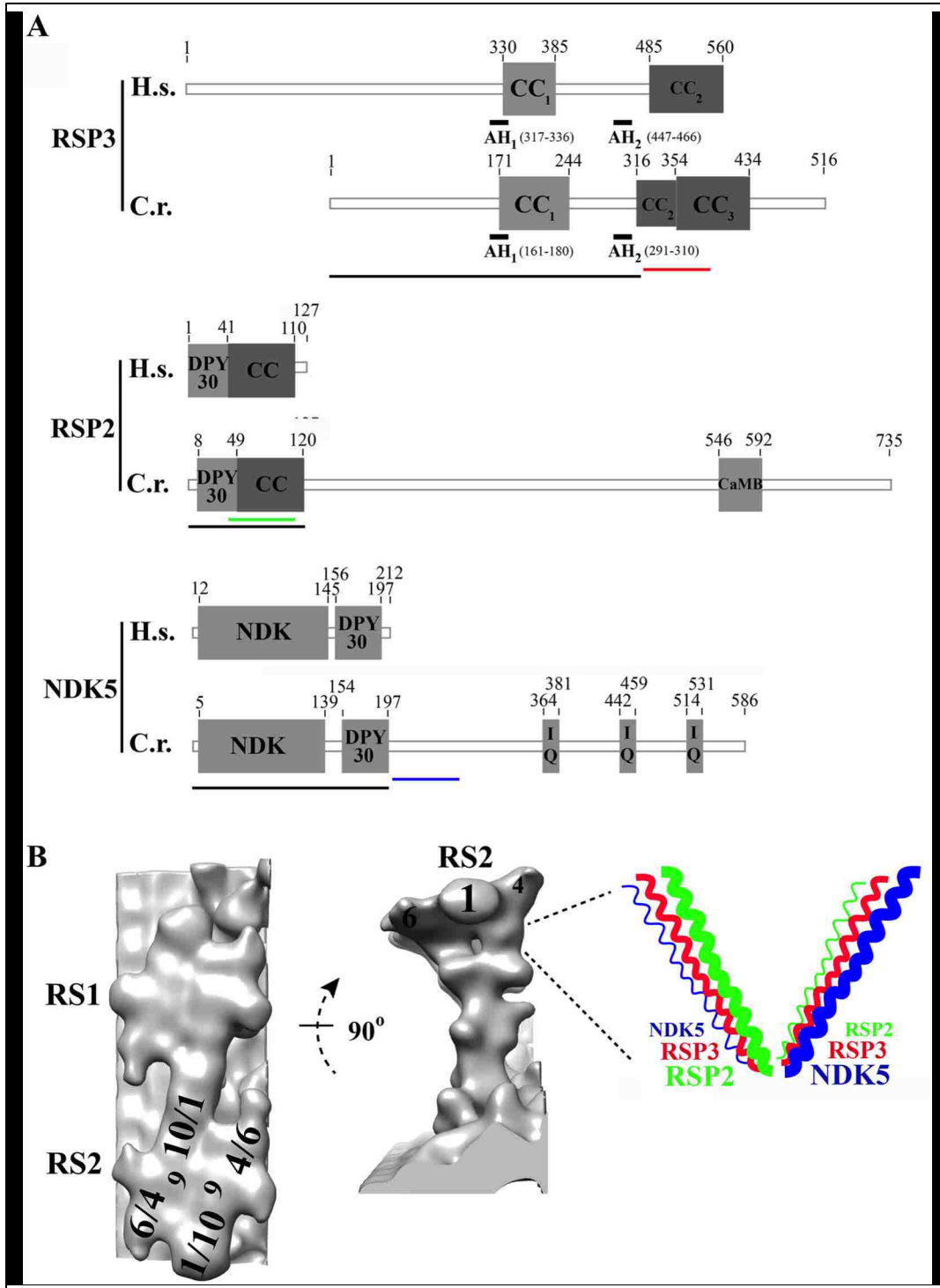
transiently during flagella rhythmic beating. Thus, the angle and length of the arms must be precise. In addition, as the Y-shaped complexes at the bend tilt and then recover to get ready for the next beat cycle, the physical property of the arms must be able to support the repeated tilt-and-recover actions at a 60 beat/second frequency. Interestingly, the bifurcated arms are not evident in the  $\Gamma$ -shaped RS precursors. Thus molecules at the neck must undergo drastic remodeling during assembly and disassembly. This dissertation shows that the two spoke subunits from the primordial NDK and HSP40 protein family are instrumental for the formation and stability of this critical region, along with the other two subunits, RSP2 and RSP3. It also explains the divergences of these molecules (Figure 5-1A).

Systematic investigation of truncated RSP3 transgenic strains predicts that RSP2 and NDK5 are tethered to the spokeneck through interactions between the conserved DPY30 domain in RSP2 and NDK5, and the second amphipathic helix (AH<sub>2</sub>) of RSP3 (Figure 5-1A) (Sivadas *et al.*, 2012). Fitting of the two Dpy30/AH modules to the base underneath the bifurcated arm (Figure 4-8) is consistent with the previous prediction that C-terminal alpha helices adjacent to the Dpy30 domain and AH in RSP2 and RSP3 respectively fold into coiled coils that constitute the essential element of bifurcated arms (Gopal *et al.*, 2012; Sivadas *et al.*, 2012). Based on the fitting of N-terminal NDK domain of NDK5 into the asymmetric neck nodules, we further postulate that the extensive C-terminal region unique to *Chlamydomonas* NDK5 and its close kin is also directed toward the spokehead.

Taken together, we predict that the C-termini of *Chlamydomonas* RSP2, NDK5 and RSP3 dimers fold into two identical tri-thread coiled coils which form the bifurcated

arms and part of the spokehead (Figure 5-1B) (Zhu *et al.*, 2016). In particular, the proximal ~ 70-aa region contributes to the arms. Since NDK5 orthologs from most organisms do not possess a C-terminal extension, the coiled coils may only consist of the two short helices from RSP2 and RSP3. This interpretation suggests that the hole in cryo-ET based surface rendition of human RSs should be bigger (Figure 4-8A); and is consistent with fewer tendrils in their spokeheads (Lin *et al.*, 2014); and the localization to the head of a tag at the RSP3's C terminus (Oda *et al.*, 2014). The excessive C-terminal extension of *Chlamydomonas* RSP2, RSP3 and NDK5 may enhance structural stability and force transduction of the head-neck region that transiently contacts the CP projection (Warner and Satir, 1974; Lindemann, 2004). The NDK5 assembly model can be tested at near-atomic resolution using advanced single particle analysis of cryo-ET of flagella from transgenic strain expressing NDK5 with a C-terminal tag for positioning or lacking the C-terminal extension.

As the two modules in each spokehead are arranged in rotational symmetry, this model predicts that the two coiled coils are positioned in opposite orientations, with NDK5's calmodulin-binding C-terminal extension directing toward RSP1. This means that the NDK5/RSP1 extension forms the bridge connecting RS1 and RS2 (Figure 5-1B, left panel) that is absent in the RSs of human. This is consistent with the fact that human NDK5 and RSP1 lack these extensions. It is possible that the bridge in *Chlamydomonas* flagella strengthens the mechanical feedback, whereas most organisms that lack this bridge instead generate the third RS, RS3, for a similar purpose.



**Figure 5-1.** New spokeneck model. (A) Divergence of spokeneck proteins in *Chlamydomonas* and human. Conserved regions are underlined with black bars. CaMB and IQ are calmodulin binding motifs. C.r., *Chlamydomonas reinhardtii*; H.s., Homo

sapiens; CC, Coiled coil; AH, Amphipathic helix. **(B)** A model of the bifurcated arms at the spokeneck. Left and middle panels, top and side view of the surface rendering of *Chlamydomonas* flagella highlighting RSs (Lin et al., 2014). 1, 4, 6, 9 and 10, depict the predicted position of respective spoke head subunits. Right panel, a model depicting that each arm is a coiled coil folded from three ~ 70 a.a. helices from RSP3 (red), RSP2 (green) and NDK5 (blue). The model predicts that the NDK5 orthologs that only have the conserve NDK domain and Dpy30 domain do not contribute to the arms, whereas algal NDK5 stabilizes RSP1 with its additional extension that binds calmodulin. Different thicknesses of the helices reflect the rotational symmetry arrangement of the bifurcated arms. Thick helices toward the head indicate the proximity to the viewer. NDK5's C-terminal extension (blue) may project toward RSP1, forming a bridge connecting RS1 and RS2 in each axonemal repeat.

This model also explains how calcium/calmodulin may modulate motility.

Calcium is a universal second messenger for the regulations of ciliary and flagellar beating (reviewed by Smith and Yang, 2004). While cilia and flagella harbor numerous calmodulin molecules and calmodulin inhibitors perturb flagellar movement, whether and how calmodulin modulates motility remains elusive. Given the presence of calmodulin in isolated RS particles (Yang *et al.*, 2001), and multiple calmodulin-binding proteins in RS and RS associated complex (Yang *et al.*, 2004; Patel-king *et al.*, 2004; Dymek and Smith, 2007), and perhaps others in the CP (Wargo *et al.*, 2005; Dipetrillo and Smith, 2010), calmodulin likely acts on multiple axonemal sites simultaneously and differentially when intraflagellar calcium concentration rises, triggered by flagella touching physical objects (Fujiu *et al.*, 2011) or by flagella depolarization following light-induced opening of channelrhodopsin in the eye spot (Berthold *et al.*, 2008).

We envisage that when *Chlamydomonas* experiences stimuli, rising concentrations allow calcium and calmodulin to act on calmodulin binding sites in RSP2 and NDK5 C-terminal extensions. This could modulate the RS-CP transient juncture to alter the mechanical feedback and thus to alter the waveform or beat frequency. This



prediction is supported by the steering anomalies of *Chlamydomonas* mutant cells lacking RSP2's C-terminal extension under bright light (Gopal *et al.*, 2012). It will be interesting to test how mutations of the C-terminal region in NDK5 alone or with RSP2 will affect flagellar motility.

## **5.2 Refined Structural Roles of NDK5**

Although the roles of RSP2 and NDK5 appear similar since both contain the Dpy30 domain that binds an AH in RSP3 and have similar calmodulin-binding C-terminal extension, the disparate RS assembly defects in RSP2 and NDK5 mutant flagella reveal their hierarchical relationship in assembly (Table 4-1). All RSPs in the neck and head region are diminished in RSP2 mutant flagella (Huang *et al.*, 1981; Yang *et al.*, 2004), whereas only HSP40 and RSP1 are diminished in NDK5 mutant flagella (Figure 3-3). We postulate that RSP2 is central to the assembly of all subunits in this region, whereas NDK5 specifically interacts with HSP40 and RSP1. The selective loss of RSP1 seems contrary to the presumptive co-assembly of all 5 spokehead subunits (Huang *et al.*, 1981; Diener *et al.*, 2011). The question is when NDK5 becomes tethered to RSP1 and when RSP1 is lost in *ndk5* mutant flagella. If NDK5 tethers RSP1 to the RS precursors, RSP1 will be absent in the RS precursors from *ndk5* mutant. Conversely, if RSP1 is present in the precursor, likely RSP1 is lost during or after the reconfiguration of precursors. Either result will shed light on RS folding in the cell body and at the flagella tip. Notably assembly of HSP40 and RSP1 doesn't require NDK activity or the inter-subunit crosstalk since they are normal in the RS in NDK5<sub>H121A</sub> flagella that lack the NDK activity and DN flagella in which inter-subunit crosstalk likely impairs (Figure 3-5

and Figure 3-7). Thus their assembly seems to merely require the presence of NDK5 polypeptides.

Importantly, the structural role of NDK5 is not restricted to the assembly of these two proteins. Despite the disparate compositional deficiencies in the RSP2 mutant (*pf24*) and NDK5 mutant (*ndk5*), the residual RSs in cryo-ET appear similar (Pigino *et al.*, 2011; Figure 4-4). This suggests that the other RSPs in the head/neck region in the *ndk5* mutant flagella cannot fold into a uniform stable structure. This leads to the model that, after anterograde IFT, NDK5 permits the conversion of the  $\Gamma$ -shaped precursor to the Y-shaped final structure (Figure 4-9). If the model is correct, isolated RSs from *ndk5* flagella may resemble the  $\Gamma$ -shaped precursors revealed by negative stain EM (Diener *et al.*, 2011). Testing this is important, since NDK is not known to promote protein folding except in one study that shows a fish NDK by itself regulates the dissociation of polypeptide from HSP70 (Leung and Hightower, 1997).

### ***5.3 Inter-subunit Crosstalk of NDK***

The most intriguing finding in this dissertation is that, although both NDK5 and NDK5<sub>H121A</sub> rescued all the *ndk5* phenotypes, co-expression of these two different forms caused a number of DN effects, including inhibition of RS assembly, flagella generation, and phosphorylation of RSP3 and NDK5. Since this is not due to degradation and overexpression of mutant molecules (Figure 3-8), a possible explanation is that the action of NDK5 involves inter-subunit crosstalk, which is perturbed if NDK5 dimer is comprised of two incompatible isoforms. As discussed in Chapter 3, a number of studies support this notion.

### ***5.3.1 Inter-subunit Crosstalk for the Canonical Mechanism of NDK***

The direct evidence came from the inter-subunit phosphotransfer of NDK activity of the recombinant NDKs from *Salmonella typhimurium* (Dar and Chakraborti, 2010). It is possible but cumbersome to test if the NDK activity of NDK5/NDK5<sub>H121A</sub> heterodimer is also disrupted. Since NDK abundance is reduced in the DN flagella, reduced NDK activity could be attributed to reduced abundance of NDK5 polypeptides (Figure 3-7) instead of impaired inter-subunit crosstalk. One way to resolve this is to purify RSs from WT and DN flagella, and measure the NDK activity of the same amounts of proteins. The other is to compare the NDK activity of purified recombinant homo- or hetero-oligomers. To purify heteromeric NDK5 will require engineering a new construct with a distinct tag that could address the precipitation propensity of NDK5 and allow purification of heteromers. However, the inherent propensity of DPY30 domains to form tetramers may lead to oligomers of higher orders (Tremblay *et al.*, 2014). It could be easier to express and purify soluble heteromeric hexamers of group I NDKs. However, it will be still challenging to control the ratio of two variants in one hexamer. Thus NDK5 in RS presents a unique opportunity for investigation of inter-subunit crosstalk in NDK.

### ***5.3.2 Implications of Inter-subunit Crosstalk***

As mentioned in Chapter 3, NDKs can carry out a number of actions aside from the conversion of triphosphate and diphosphate nucleosides. Furthermore, inter-subunit crosstalk is not limited to the NDK activity either, since NDK5's NDK activity is dispensable for RS assembly and flagella generation. We propose that the molecular motions for different reactions are different, but require inter-subunit crosstalk

nonetheless. Two functional protomers that adopt different actions will impair the function of a dimer.

This explanation may be applicable to H121-independent phosphorylation. Aside from H121, NDK isoforms typically have additional phosphorylated residues (Parks and Agarwal, 1973). It has been assumed that the latter is due to non-specific phosphotransfer from the unstable phosphohistidine. Although this is possible, autophosphorylation of purified NDK without the conserved His (MacDonald *et al.*, 1993) strongly suggest that NDK has an alternative H121-independent phosphotransferring mechanism. This is contrary to the requirement of the conserved His for the NDK activity. As NDK paralogues diverge substantially (Desvignes *et al.*, 2009), it is possible that each NDK may differ in His-independent protein kinase activity. We are partial to the notion that both NDK5 and NDK5<sub>H121A</sub> can autophosphorylate albeit using distinct H121-dependent and independent mechanisms and thus both migrate identically in western blots (Figure 3-5). However, probably when most, if not all, of the variant and WT protomer assemble into heteromers, the disconcerted inter-subunit crosstalk hinder either reactions, leading to poor assembled RSs with hypophosphorylated NDK5 in the DN flagella (Figure 3-7).

The inter-subunit crosstalk – either His-dependent or –independent - is supported by the findings of 2-4 moles of phosphate per mole of human and yeast hexameric NDKs (Parks and Agarwal, 1973). This suggests that only subsets of monomers within one oligomer could operate at one time. In the same vein, NDK5 polypeptides are resolved into two bands of similar intensity (Figure 3-5; 3-7). One possibility is that only one NDK5 protomer in a dimer became phosphorylated, or one protomer is the substrate of the other. Identifying phosphoresidues in NDK5 and RSP3 could be informative in

revealing the differential phosphorylation mechanisms, how phosphorylation promotes RS assembly, and whether this activity is impaired in the DN flagella.

Exactly what triggers DN phenotypes remains unclear. The fluctuated rates of DN transgenic strains from each transformation suggest that simply expressing NDK5<sub>H121A</sub> in WT cells is insufficient to cause DN phenotypes. We reason that translation of mutant and WT NDK5 mRNA and subsequent dimerization somehow have to be coupled to defy automatic dimerization of two adjacent identical polypeptides translated from the same mRNA. Creation of DN diploid cells by mating (Dutcher, 1995) could test if a 1:1 ratio of NDK5 and NDK5<sub>H121A</sub> is sufficient to trigger DN effects.

#### ***5.4 Structural Role of Spoke HSP40***

Although HSP40s and HSP70s constitute a powerful chaperone system for folding diverse polypeptides, independent lines of evidence indicate this canonical mechanism is not applicable to spoke HSP40 (Yang *et al.*, 2008). Instead, it is specific for stabilizing - rather than active refolding - the structure of the RS complex without the participation of HSP70 (Figure 4-4). Nonetheless, modeling suggests that spoke HSP40 adopts the mechanism for HSP40-client interactions for assembly and perhaps disassembly of RS complex.

This interpretation is founded on the normal morphology of most RSs from HSP40 mutants revealed by either cryo-ET (Figure 4-4) or thin section EM of intact flagella (Yang *et al.*, 2008). The procedure of thin section EM partly account for the small fraction of deformed RSs in flagella and the increased number of deformed RS when the flagellar membrane was removed. Some of the deformed RSs may be caused by

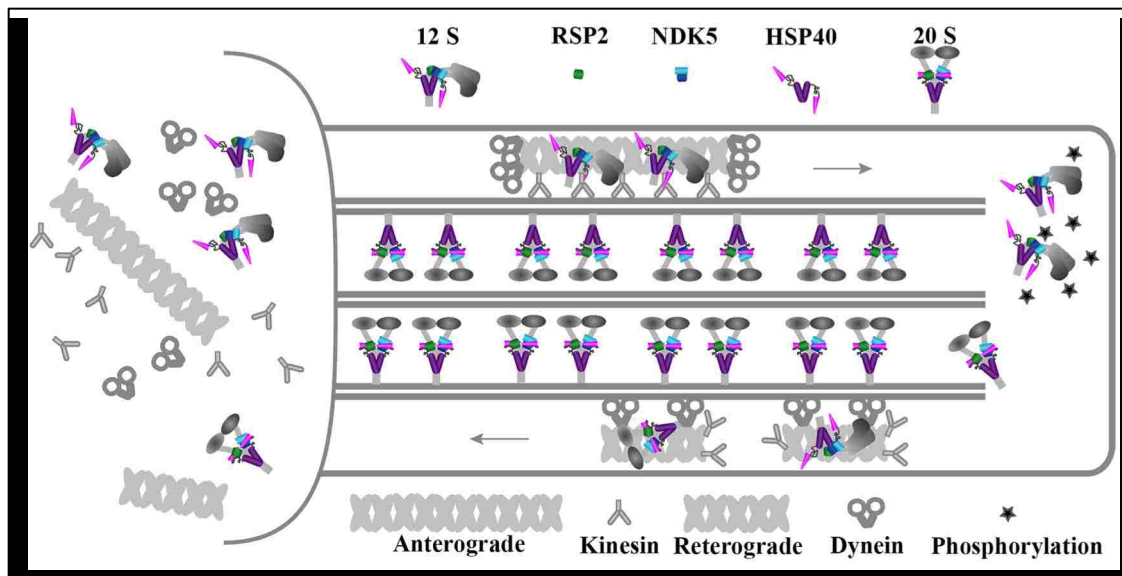
the mechanical feedback of the RS/CP system (Lindemann, 2004), whereas impaired force-bearing capacity of HSP40-minus RSs cause jerky flagella (Yang *et al.*, 2008). Cryo-ET of HSP40 mutant flagella fixed during active jerking might reveal where deformed HSP40-minus RSs are. Clustering of deformed RSs will indicate that mechanical forces distort HSP40-minus RSs, which prevents the progression of the beat cycle and results in jerky flagella. Randomly distributed deformed RSs will indicate their inherent structural instability without HSP40.

The normal morphology of most HSP40-minus RSs suggests that HSP40 confers structural stability by forming a sprawling HSP40 dimer rather than a single module. High resolution single molecule analysis or crystallography will be needed to test this. Modeling predicts that HSP40 dimer operates like crabs' claws bracing two sets of dimeric Dpy30 domain into one functional unit (Figure 4-8). This action may strengthen the neck-stalk juncture for force bearing, preventing the split of these two structural units during force transmission, or excessive tilt of RSs at the bent. The latter deformations are evident in the cross section of fixed HSP40-minus flagella (Yang *et al.*, 2008). The assembly model predicts that bracing with HSP40 dimer occurs after the refolding of the  $\Gamma$ -shaped precursor to Y-shaped mature complex, which may require NDK5 (Figure 4-9). Presumably only after the conformational switch, the claw-like N-termini of the standby HSP40 dimer could fold around the two modules of dimeric Dpy30 domain at the neck.

### ***5.5 Trafficking and Assembly of Spoke HSP40***

The minimal repair of missing HSP40 in dikaryons after 2 hours (Figure 4-6) suggests that HSP40 travels with the RS precursor during anterograde IFT (Figure 5-2),

analogous to the paradigm that HSP40s shuttle clients to HSP70s. Because of the co-trafficking and co-assembly, in theory, the repair of HSP40 to HSP40-minus RSs will not occur unless an entire outer doublet segment with defective RSs reassembles during the stochastic turn over at the tip, which is in fact far slower than flagellar generation (Marshall and Rosenbaum, 2001). This interpretation is consistent with 1% per hour RS turnover rate in fully-grown flagella (Song and Dentler, 2001). In the same line, in previous study to reveal the repair of the missing spokehead, flagella were harvested from dikaryons after 2.5 hours under dim light (Luck *et al.*, 1977). It will be interesting to investigate whether dim light treatment heightens microtubule turnover and thus hastens the replacement of partially defective RSs in dikaryons. This also could be tested with Cytochalasin D that is known to increase axoneme turnover rate (Dentler and Adams, 1992). Presumably, HSP40 repair in dikaryons will increase in the presence of Cytochalasin D. The strategies – physical or chemical treatment- for improving the repair of paralyzed *Chlamydomonas* flagella missing part of an axonemal complex such as RSs, N-DRC (Huang *et al.*, 1982) and the CP (Adams *et al.*, 1981) could guide gene therapy of PCD patients with similar minor axonemal defects in the future.



**Figure 5-2.** RS assembly model. Dimeric HSP40 is part of the RS precursor that is delivered from the cell body to the flagellar tip by kinesin-powered anterograde IFT. Once exiting IFT, RS precursors undergo a series of changes along with phosphorylation (star) to promote the conversion of 12S  $\Gamma$ -shaped precursor into 20S Y-shaped RSs in the axoneme. NDK5 is central to these changes, including refolding of the neck region that is followed by the refolding of HSP40's N-terminal region around RSP2 and NDK5 nodules at neck. The reconfigured retrograde trains loaded with disassembled RSs will be driven by dynein motors to the cell body. For clarity, IFT trains and motors are not shown at the tip. NDK5 also promotes RSP3 phosphorylation that may accelerate RS docking.

The proposed interactions between HSP40 and RS precursor might be applicable to various HSP40-client associations. Despite extensive studies of HSP40s in diverse experimental systems, exactly how HSP40 interacts with client remains speculative. It is assumed that polypeptides associate with the region outside the J domain. As a type II HSP40, the diverged sequence in the G/F domain and C domain of spoke HSP40 may account for its mono-specificity. The typical hydrophobic interaction between clients and HSP40s (Li *et al.*, 2003) could be disrupted during flagellar extracts preparation, causing the dissociation of HSP40 from the RS precursor (Yang *et al.*, 2005).



The proposed sequential refolding of spoke HSP40 and RS precursor resembles the presumptive interplays among HSP40, clients and HSP70. It is proposed that after recruiting a client to HSP70, HSP40 binds and stimulates the ATPase activity of HSP70 (Figure 1-5). ATP hydrolysis increases the affinity of HSP70 for clients, causing the transfer of client peptides to HSP70 and the release of HSP40. The apparent difference here is spoke HSP40 becomes stably associated with mature RS, perhaps through high affinity binding after refolding with the crab arm-like N-terminal regions.

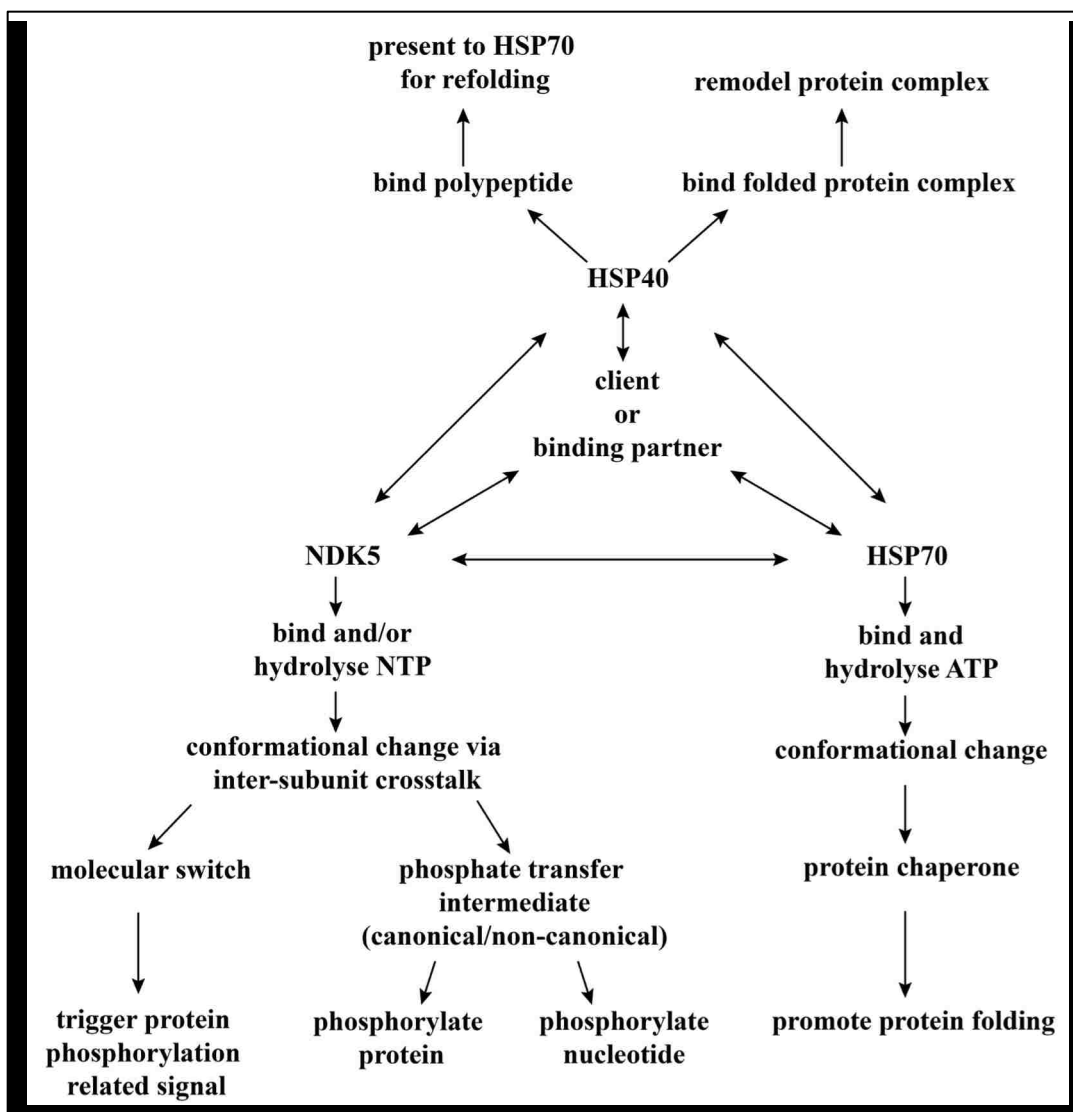
Although mammalian spoke HSP40 lacks the ATPase activating motif in the signature J domain, and the J domain is not required for the action of spoke HSP40 in *Chlamydomonas* (Yang *et al.*, 2008), we cannot rule out the possibility that HSP70 is involved in the upstream RS assembly processes. For example, HSP70s may be involved in folding RS precursors in cell body and the release of RS precursors from IFT trains at the flagella tip. Given spoke HSP40 is the only HSP40 present in *Chlamydomonas* flagella, HSP70 in flagella must operate in a non-canonical way. For example, other flagellar proteins may assist HSP70. Previous studies have shown that non-HSP40 proteins can activate the ATPase activity of HSP70 (Hainzl *et al.*, 2004; Wegele *et al.*, 2003), or the weak basal ATPase activity is sufficient for HSP70 molecules to carry out some of the chaperone functions in vitro (Mayer and Bukau, 2005). Alternatively, other HSP40 isoforms may be delivered into flagella to assist HSP70s only during assembly or disassembly, however, are not detected in proteomes of full-length flagella at the steady state.

The involvement of HSP40s in the refolding of multimeric complexes for diverse cellular processes is more common than previously appreciated. Interestingly, no matter

whether HSP70 is involved, HSP40 triggers disassembly of multimeric complexes, such as clathrin coat (Xiao *et al.*, 2006) and spliceosome (Sahi *et al.*, 2010), and the release of biogenesis factors from ribosome (Hageman *et al.*, 2010; Gillis *et al.*, 2013). In light of this, it is possible that HSP40 might be involved in the conversion of Y-shaped RSs into  $\Gamma$ -shaped precursors for recycling.

Interestingly, two independent studies reported the interactions of HSP70 and NDKs. A NDK in fish cells modulated the function of HSP70 by maintaining the monomeric state of HSP70 and releasing polypeptide from HSP70 (Leung and Hightower, 1997). *Escherichia coli* NDK can interact, albeit weakly, with HSP70 and might phosphorylate HSP70-bound ADP (Barthel and Walker, 1999). Since HSP70 continuously consumes ATP, closely associated NDKs potentially can promptly provide ATP to HSP70, a scenario similar to the physical coupling of NDK with dynamic GTPase for the perpetual membrane fusion and fission (Boissan *et al.*, 2014). The mutual interactions and the major functions of NDKs, HSP40 and HSP70 are summarized in Figure 5-3.

Under certain conditions, NDKs - like HSP70s - could continuously consume NTPs. Perhaps HSP40 directly associated with NDK modulate the NTP binding or hydrolysis activity of NDK through its malleable structures. This could be tested by comparing the NDK activity in HSP40-minus flagella and WT flagella. We speculate that this triangle relationship may evolve into the dual partnership between NDK and HSP40 in the RS, whereas HSP70 adopts a new partner or simply become dispensable.



**Figure 5-3.** Summary of putative interactions (double headed arrow) and functions of HSP40, NDK and HSP70. Both NDK and HSP70 consume NTP to trigger conformational changes but for different reactions in diverse cellular processes.

### ***5.6 Potential Mechanisms of DN Phenotypes***

The fact that RSs are assembled into the short flagella of DN cells but become less abundant and hypophosphorylated suggests that NDK5 has broader roles beyond the assembly of the spokeneck region. In fact, a number of mutant strains also have paralyzed flagella with hypophosphorylated RSP3 (Gupta *et al.*, 2012; Alford *et al.*, 2013). Thus the assembly and trafficking of RSs complex are not all-or-none reactions.

One way to elucidate this broader assembly role of NDK5 revealed by the DN phenotypes is to reveal the distribution of RSs in DN flagella. By using fluorescence imaging, our preliminary data shows that RS deficiency in DN flagella is more severe at the distal ends, as in the flagella of the *pf27* mutant (Alford *et al.*, 2013). One explanation is impaired anterograde trafficking of RS precursors. It was shown that cargoes could dissociate from IFT trains (Wren *et al.*, 2013). If, without functional NDK5, RS precursors prematurely dissociate from IFT trains, the problem would exacerbate as the flagella length increases, leading to distal assembly defects.

We propose an affinity theory to explain the premature dissociation. The affinity between IFT trains and RS precursors is low. They will not bind unless they are concentrated at the loading area near the flagellar entrance (Qin *et al.*, 2004); they are modified by phosphorylation to increase affinity; or there are “seat belt” factors, such as PF27, that stabilize the weak interaction at the low concentration zones, such as the flagella compartment. These possibilities are not mutually exclusive. NDK5 may work as a non-canonical kinase or a recruiter of kinase that phosphorylates RS or IFT particles to increase the intermolecular affinity during anterograde trafficking. This action is perturbed in DN strains due to disconcerted inter-subunit crosstalk. Failure to reach the

tip explains why the distal RS deficiencies in DN flagella cannot be repaired despite IFT trains continuously deliver cargoes in full-grown flagella (Qin *et al.*, 2004). In the dikaryons, the distal RS deficiency in *pf27* (Alford *et al.*, 2013) and DN flagella may be repairable once the tip-ward trafficking is secured by cytoplasmic complementation in dikaryons.

Alternatively, RSs in DN flagella are evenly distributed throughout the flagella albeit with a reduced abundance. This will suggest a reduced rate in RS loading or in assembly relative to other axonemal complexes. Similar phenotype was observed in the *oda16* mutant flagella in which outer dynein arm abundance is evenly reduced (Ahmed *et al.*, 2008). It is proposed that ODA16 is the adaptor specifically aiding outer dynein arm to associate with a subunit in the IFT particles (Hou *et al.*, 2007). Analogous to this, heterodimeric NDK5 may hinder the action of the RS adaptor, such as PF27, causing fewer RSs to enter flagella, but those that get on IFT trains could go on to assemble properly. Or the adaptor acts in the same way as ODA16 but the deficiency of ODA that is located outside the 9 outer doublets, the same side as IFT, can be repaired, whereas RSs that are located within 9 outer doublets cannot be repaired by diffusion of disassociated RS precursors.

The last scenario is that RSs with heterodimeric NDK5 are enriched at the flagella tip. This scenario will suggest that RSs in DN flagella cannot disassociate from IFT trains or assemble into axoneme, and thus stuck at the unloading zone. In this case, the role of NDK5 is to promote RS unloading or docking. Therefore, determining the distribution of RSs in the DN flagella will reveal the roles of NDK5 in addition to the structure role.

We are partial to the notion that NDK5-mediated phosphorylation also promotes

flagella generation (Figure 3-5 and 3-7) and could be partially replaced by other flagella NDKs (Pazour *et al.*, 2005) or protein kinases implicated in flagellar assembly or length control (reviewed by Wilson *et al.*, 2008). In the absence of NDK5, the redundant enzymes may assist RS assembly but not the assembly of the entire flagella; therefore *ndk5* flagella have normal abundance of defective RSs but are short. Whereas, in the presence of non-functional heterodimeric NDK5, the redundant enzymes may not be able to compliment any deficiency, therefore, DN flagella have reduced RS and also are short.

Taken together, the two projects in this dissertation provide new explanations to the long-standing questions in the fields of flagella biology, NDKs and the chaperone machinery. It also rediscovered old data that demand reassessment. The well-defined RSs and the versatile model organism *Chlamydomonas* will provide an opportunity to further resolve these fundamental questions in the future.

## BIBLIOGRAPHY

- Admiraal, S. J., B. Schneider, P. Meyer, J. Janin, M. Veron, D. Deville-Bonne, and D. Herschlag. 1999. "Nucleophilic Activation by Positioning in Phosphoryl Transfer Catalyzed by Nucleoside Diphosphate Kinase." *Biochemistry* 38 (15): 4701-4711.
- Ahmad, A., A. Bhattacharya, R. A. McDonald, M. Cordes, B. Ellington, E. B. Bertelsen, and E. R. Zuiderweg. 2011. "Heat Shock Protein 70 kDa Chaperone/DnaJ Cochaperone Complex Employs an Unusual Dynamic Interface." *Proceedings of the National Academy of Sciences of the United States of America* 108 (47): 18966-18971.
- Ahmed, N. T., C. Gao, B. F. Lucker, D. G. Cole, and D. R. Mitchell. 2008. "ODA16 Aids Axonemal Outer Row Dynein Assembly through an Interaction with the Intraflagellar Transport Machinery." *The Journal of Cell Biology* 183 (2): 313-322.
- Ajit Tamadaddi, C. and C. Sahi. 2016. "J Domain Independent Functions of J Proteins." *Cell Stress & Chaperones* 21 (4): 563-570.
- Alford, L. M., A. L. Mattheyses, E. L. Hunter, H. Lin, S. K. Dutcher, and W. S. Sale. 2013. "The *Chlamydomonas* Mutant pf27 Reveals Novel Features of Ciliary Radial Spoke Assembly." *Cytoskeleton (Hoboken, N.J.)* 70 (12): 804-818.
- Attwood, P. V. and T. Wieland. 2015. "Nucleoside Diphosphate Kinase as Protein Histidine Kinase." *Naunyn-Schmiedeberg's Archives of Pharmacology* 388 (2): 153-160.
- Barbar, E. and A. Nyarko. 2015. "Polybivalency and Disordered Proteins in Ordering Macromolecular Assemblies." *Seminars in Cell & Developmental Biology* 37: 20-25.
- Barends, T. R., R. W. Brosi, A. Steinmetz, A. Scherer, E. Hartmann, J. Eschenbach, T. Lorenz, et al. 2013. "Combining Crystallography and EPR: Crystal and Solution Structures of the Multidomain Cochaperone DnaJ." *Acta Crystallographica. Section D, Biological Crystallography* 69 (Pt 8): 1540-1552.
- Barthel, T. K. and G. C. Walker. 1999. "Inferences Concerning the ATPase Properties of DnaK and Other HSP70s are Affected by the ADP Kinase Activity of Copurifying Nucleoside-Diphosphate Kinase." *The Journal of Biological Chemistry* 274 (51): 36670-36678.
- BERG, P. and W. K. JOKLIK. 1953. "Transphosphorylation between Nucleoside Polyphosphates." *Nature* 172 (4387): 1008-1009.
- Berthold, P., R. Schmitt, and W. Mages. 2002. "An Engineered *Streptomyces Hygroscopicus* Aph 7" Gene Mediates Dominant Resistance Against Hygromycin B in *Chlamydomonas Reinhardtii*." *Protist* 153 (4): 401-412.
- Berthold, P., S. P. Tsunoda, O. P. Ernst, W. Mages, D. Gradmann, and P. Hegemann. 2008. "Channelrhodopsin-1 Initiates Phototaxis and Photophobic Responses in

- Chlamydomonas* by Immediate Light-Induced Depolarization." *The Plant Cell* 20 (6): 1665-1677.
- Bhogaraju, S., L. Cajanek, C. Fort, T. Blisnick, K. Weber, M. Taschner, N. Mizuno, et al. 2013. "Molecular Basis of Tubulin Transport within the Cilium by IFT74 and IFT81." *Science (New York, N.Y.)* 341 (6149): 1009-1012.
- Biggs, J., N. Tripoulas, E. Hersperger, C. Dearolf, and A. Shearn. 1988. "Analysis of the Lethal Interaction between the Prune and Killer of Prune Mutations of *Drosophila*." *Genes & Development* 2 (10): 1333-1343.
- Bloch, M. A. and K. A. Johnson. 1995. "Identification of a Molecular Chaperone in the Eukaryotic Flagellum and its Localization to the Site of Microtubule Assembly." *Journal of Cell Science* 108 ( Pt 11) (Pt 11): 3541-3545.
- Boissan, M., G. Montagnac, Q. Shen, L. Griparic, J. Guitton, M. Romao, N. Sauvonnet, et al. 2014. "Membrane Trafficking. Nucleoside Diphosphate Kinases Fuel Dynamin Superfamily Proteins with GTP for Membrane Remodeling." *Science (New York, N.Y.)* 344 (6191): 1510-1515.
- Burton, P. R. 1973. "Some Structural and Cytochemical Observations on the Axial Filament Complex of Lung-Fluke Spermatozoa." *Journal of Morphology* 140 (2): 185-195.
- Cai, X., S. Srivastava, S. Surindran, Z. Li, and E. Y. Skolnik. 2014. "Regulation of the Epithelial Ca(2)(+) Channel TRPV5 by Reversible Histidine Phosphorylation Mediated by NDPK-B and PHPT1." *Molecular Biology of the Cell* 25 (8): 1244-1250.
- Cao, M., G. Li, and J. Pan. 2009. "Regulation of Cilia Assembly, Disassembly, and Length by Protein Phosphorylation." *Methods in Cell Biology* 94: 333-346.
- Carotenuto, M., E. Pedone, D. Diana, P. de Antonellis, S. Dzeroski, N. Marino, L. Navas, et al. 2013. "Neuroblastoma Tumorigenesis is Regulated through the Nm23-H1/H-Prune C-Terminal Interaction." *Scientific Reports* 3: 1351.
- Chang, C. L., J. R. Strahler, D. H. Thoraval, M. G. Qian, R. Hinderer, and S. M. Hanash. 1996. "A Nucleoside Diphosphate Kinase A (nm23-H1) Serine 120-->Glycine Substitution in Advanced Stage Neuroblastoma Affects Enzyme Stability and Alters Protein-Protein Interaction." *Oncogene* 12 (3): 659-667.
- Chang, C. L., X. X. Zhu, D. H. Thoraval, D. Ungar, J. Rawwas, N. Hora, J. R. Strahler, S. M. Hanash, and E. Radany. 1994. "Nm23-H1 Mutation in Neuroblastoma." *Nature* 370 (6488): 335-336.
- Chen, X. G., X. Jiang, J. Gu, M. Xu, Y. Wu, Y. Deng, C. Zhang, et al. 2015. "Genome Sequence of the Asian Tiger Mosquito, *Aedes Albopictus*, Reveals Insights into its Biology, Genetics, and Evolution." *Proceedings of the National Academy of Sciences of the United States of America* 112 (44): 5907.



- Cheng, Y. C., B. Robison, and R. E. Parks. 1973. "Demonstration of the Heterogeneity of Nucleoside Diphosphokinase in Rat Tissues." *Biochemistry* 12 (1): 5-10.
- Cole, D. G., D. R. Diener, A. L. Himelblau, P. L. Beech, J. C. Fuster, and J. L. Rosenbaum. 1998. "*Chlamydomonas* Kinesin-II-Dependent Intraflagellar Transport (IFT): IFT Particles Contain Proteins Required for Ciliary Assembly in *Caenorhabditis Elegans* Sensory Neurons." *The Journal of Cell Biology* 141 (4): 993-1008.
- Craft, J. M., J. A. Harris, S. Hyman, P. Kner, and K. F. Lehtreck. 2015. "Tubulin Transport by IFT is Upregulated during Ciliary Growth by a Cilium-Autonomous Mechanism." *The Journal of Cell Biology* 208 (2): 223-237.
- Cuello, F., R. A. Schulze, F. Heemeyer, H. E. Meyer, S. Lutz, K. H. Jakobs, F. Niroomand, and T. Wieland. 2003. "Activation of Heterotrimeric G Proteins by a High Energy Phosphate Transfer Via Nucleoside Diphosphate Kinase (NDPK) B and Gbeta Subunits. Complex Formation of NDPK B with Gbeta Gamma Dimers and Phosphorylation of His-266 IN Gbeta." *The Journal of Biological Chemistry* 278 (9): 7220-7226.
- Curry, A. M., B. D. Williams, and J. L. Rosenbaum. 1992. "Sequence Analysis Reveals Homology between Two Proteins of the Flagellar Radial Spoke." *Molecular and Cellular Biology* 12 (9): 3967-3977.
- D'Angelo, A., L. Garzia, A. Andre, P. Carotenuto, V. Aglio, O. Guardiola, G. Arrigoni, et al. 2004. "Prune cAMP Phosphodiesterase Binds nm23-H1 and Promotes Cancer Metastasis." *Cancer Cell* 5 (2): 137-149.
- Dar, H. H. and P. K. Chakraborti. 2010. "Intermolecular Phosphotransfer is Crucial for Efficient Catalytic Activity of Nucleoside Diphosphate Kinase." *The Biochemical Journal* 430 (3): 539-549.
- Deane, J. A., D. G. Cole, E. S. Seeley, D. R. Diener, and J. L. Rosenbaum. 2001. "Localization of Intraflagellar Transport Protein IFT52 Identifies Basal Body Transitional Fibers as the Docking Site for IFT Particles." *Current Biology : CB* 11 (20): 1586-1590.
- Dentler, W. L. and C. Adams. 1992. "Flagellar Microtubule Dynamics in *Chlamydomonas*: Cytochalasin D Induces Periods of Microtubule Shortening and Elongation; and Colchicine Induces Disassembly of the Distal, but Not Proximal, Half of the Flagellum." *The Journal of Cell Biology* 117 (6): 1289-1298.
- Desvignes, T., P. Pontarotti, C. Fauvel, and J. Bobe. 2009. "Nme Protein Family Evolutionary History, a Vertebrate Perspective." *BMC Evolutionary Biology* 9: 256.
- Di, L., S. Srivastava, O. Zhdanova, Y. Sun, Z. Li, and E. Y. Skolnik. 2010. "Nucleoside Diphosphate Kinase B Knock-Out Mice have Impaired Activation of the K<sup>+</sup> Channel KCa3.1, Resulting in Defective T Cell Activation." *The Journal of Biological Chemistry* 285 (50): 38765-38771.

- Diener, D. R., L. H. Ang, and J. L. Rosenbaum. 1993. "Assembly of Flagellar Radial Spoke Proteins in *Chlamydomonas*: Identification of the Axoneme Binding Domain of Radial Spoke Protein 3." *The Journal of Cell Biology* 123 (1): 183-190.
- Diener, D. R., P. Yang, S. Geimer, D. G. Cole, W. S. Sale, and J. L. Rosenbaum. 2011. "Sequential Assembly of Flagellar Radial Spokes." *Cytoskeleton (Hoboken, N.J.)* 68 (7): 389-400.
- Dong, X., Y. Peng, Y. Peng, F. Xu, X. He, F. Wang, X. Peng, B. Qiang, J. Yuan, and Z. Rao. 2005. "Characterization and Crystallization of Human DPY-30-Like Protein, an Essential Component of Dosage Compensation Complex." *Biochimica Et Biophysica Acta* 1753 (2): 257-262.
- Donnelly, M. I., M. Zhou, C. S. Millard, S. Clancy, L. Stols, W. H. Eschenfeldt, F. R. Collart, and A. Joachimiak. 2006. "An Expression Vector Tailored for Large-Scale, High-Throughput Purification of Recombinant Proteins." *Protein Expression and Purification* 47 (2): 446-454.
- Duriez, B., P. Duquesnoy, E. Escudier, A. M. Bridoux, D. Escalier, I. Rayet, E. Marcos, A. M. Vojtek, J. F. Bercher, and S. Amselem. 2007. "A Common Variant in Combination with a Nonsense Mutation in a Member of the Thioredoxin Family Causes Primary Ciliary Dyskinesia." *Proceedings of the National Academy of Sciences of the United States of America* 104 (9): 3336-3341.
- Dutcher, S. K. 2014. "The Awesome Power of Dikaryons for Studying Flagella and Basal Bodies in *Chlamydomonas Reinhardtii*." *Cytoskeleton (Hoboken, N.J.)* 71 (2): 79-94.
- Dymek, E. E. and E. F. Smith. 2007. "A Conserved CaM- and Radial Spoke Associated Complex Mediates Regulation of Flagellar Dynein Activity." *The Journal of Cell Biology* 179 (3): 515-526.
- Fernandez-Gonzalez, A., S. Kourembanas, T. A. Wyatt, and S. A. Mitsialis. 2009. "Mutation of Murine Adenylate Kinase 7 Underlies a Primary Ciliary Dyskinesia Phenotype." *American Journal of Respiratory Cell and Molecular Biology* 40 (3): 305-313.
- Fowkes, M. E. and D. R. Mitchell. 1998. "The Role of Preassembled Cytoplasmic Complexes in Assembly of Flagellar Dynein Subunits." *Molecular Biology of the Cell* 9 (9): 2337-2347.
- Fujiu, K., I. Manabe, and R. Nagai. 2011. "Renal Collecting Duct Epithelial Cells Regulate Inflammation in Tubulointerstitial Damage in Mice." *The Journal of Clinical Investigation* 121 (9): 3425-3441.
- Fujiu, K., Y. Nakayama, H. Iida, M. Sokabe, and K. Yoshimura. 2011. "Mechanoreception in Motile Flagella of *Chlamydomonas*." *Nature Cell Biology* 13 (5): 630-632.
- Gallaher, S. D., S. T. Fitz-Gibbon, A. G. Glaesener, M. Pellegrini, and S. S. Merchant. 2015. "*Chlamydomonas* Genome Resource for Laboratory Strains Reveals a Mosaic

- of Sequence Variation, Identifies True Strain Histories, and Enables Strain-Specific Studies." *The Plant Cell* 27 (9): 2335-2352.
- Gillis, J., S. Schipper-Krom, K. Juenemann, A. Gruber, S. Coolen, R. van den Nieuwendijk, H. van Veen, et al. 2013. "The DNAJB6 and DNAJB8 Protein Chaperones Prevent Intracellular Aggregation of Polyglutamine Peptides." *The Journal of Biological Chemistry* 288 (24): 17225-17237.
- Gopal, R., K. W. Foster, and P. Yang. 2012. "The DPY-30 Domain and its Flanking Sequence Mediate the Assembly and Modulation of Flagellar Radial Spoke Complexes." *Molecular and Cellular Biology* 32 (19): 4012-4024.
- Gupta, A., D. R. Diener, P. Sivadas, J. L. Rosenbaum, and P. Yang. 2012. "The Versatile Molecular Complex Component LC8 Promotes several Distinct Steps of Flagellar Assembly." *The Journal of Cell Biology* 198 (1): 115-126.
- Hageman, J., M. A. Rujano, M. A. van Waarde, V. Kakkar, R. P. Dirks, N. Govorukhina, H. M. Oosterveld-Hut, N. H. Lubsen, and H. H. Kampinga. 2010. "A DNAJB Chaperone Subfamily with HDAC-Dependent Activities Suppresses Toxic Protein Aggregation." *Molecular Cell* 37 (3): 355-369.
- Hainzl, O., H. Wegele, K. Richter, and J. Buchner. 2004. "Cns1 is an Activator of the Ssa1 ATPase Activity." *The Journal of Biological Chemistry* 279 (22): 23267-23273.
- Harris, J. A., Y. Liu, P. Yang, P. Kner, and K. F. Lehtreck. 2016. "Single-Particle Imaging Reveals Intraflagellar Transport-Independent Transport and Accumulation of EB1 in *Chlamydomonas* Flagella." *Molecular Biology of the Cell* 27 (2): 295-307.
- Horani, A., T. W. Ferkol, S. K. Dutcher, and S. L. Brody. 2016. "Genetics and Biology of Primary Ciliary Dyskinesia." *Paediatric Respiratory Reviews* 18: 18-24.
- Hou, Y., H. Qin, J. A. Follit, G. J. Pazour, J. L. Rosenbaum, and G. B. Witman. 2007. "Functional Analysis of an Individual IFT Protein: IFT46 is Required for Transport of Outer Dynein Arms into Flagella." *The Journal of Cell Biology* 176 (5): 653-665.
- Hsu, D. R., P. T. Chuang, and B. J. Meyer. 1995. "DPY-30, a Nuclear Protein Essential Early in Embryogenesis for *Caenorhabditis Elegans* Dosage Compensation." *Development (Cambridge, England)* 121 (10): 3323-3334.
- Huang, B., G. Piperno, Z. Ramanis, and D. J. Luck. 1981. "Radial Spokes of *Chlamydomonas* Flagella: Genetic Analysis of Assembly and Function." *The Journal of Cell Biology* 88 (1): 80-88.
- Huang, B., Z. Ramanis, and D. J. Luck. 1982. "Suppressor Mutations in *Chlamydomonas* Reveal a Regulatory Mechanism for Flagellar Function." *Cell* 28 (1): 115-124.
- Ikeda, T. 2010. "NDP Kinase 7 is a Conserved Microtubule-Binding Protein Preferentially Expressed in Ciliated Cells." *Cell Structure and Function* 35 (1): 23-30.

- Ito, N., K. Kamiguchi, K. Nakanishi, A. Sokolovskya, Y. Hirohashi, Y. Tamura, A. Murai, et al. 2016. "A Novel Nuclear DnaJ Protein, DNAJC8, can Suppress the Formation of Spinocerebellar Ataxia 3 Polyglutamine Aggregation in a J-Domain Independent Manner." *Biochemical and Biophysical Research Communications* 474 (4): 626-633.
- Jaffrey, S. R. and S. H. Snyder. 1996. "PIN: An Associated Protein Inhibitor of Neuronal Nitric Oxide Synthase." *Science (New York, N.Y.)* 274 (5288): 774-777.
- Jiang, H., A. Shukla, X. Wang, W. Y. Chen, B. E. Bernstein, and R. G. Roeder. 2011. "Role for Dpy-30 in ES Cell-Fate Specification by Regulation of H3K4 Methylation within Bivalent Domains." *Cell* 144 (4): 513-525.
- Jiang, X. and D. Stern. 2009. "Mating and Tetrad Separation of *Chlamydomonas Reinhardtii* for Genetic Analysis." *Journal of Visualized Experiments : JoVE* (30). pii: 1274. doi (30): 10.3791/1274.
- Jivan, A., S. Earnest, Y. C. Juang, and M. H. Cobb. 2009. "Radial Spoke Protein 3 is a Mammalian Protein Kinase A-Anchoring Protein that Binds ERK1/2." *The Journal of Biological Chemistry* 284 (43): 29437-29445.
- Johnson, K. A. and J. L. Rosenbaum. 1992. "Polarity of Flagellar Assembly in *Chlamydomonas*." *The Journal of Cell Biology* 119 (6): 1605-1611.
- Kamiya, R. 1988. "Mutations at Twelve Independent Loci Result in Absence of Outer Dynein Arms in *Chlamydomonas Reinhardtii*." *The Journal of Cell Biology* 107 (6 Pt 1): 2253-2258.
- Kampinga, H. H. and E. A. Craig. 2010. "The HSP70 Chaperone Machinery: J Proteins as Drivers of Functional Specificity." *Nature Reviews. Molecular Cell Biology* 11 (8): 579-592.
- Karamohamed, S., T. Nordstrom, and P. Nyren. 1999. "Real-Time Bioluminometric Method for Detection of Nucleoside Diphosphate Kinase Activity." *BioTechniques* 26 (4): 728-734.
- Karlsson, A., S. Mesnildrey, Y. Xu, S. Morera, J. Janin, and M. Veron. 1996. "Nucleoside Diphosphate Kinase. Investigation of the Intersubunit Contacts by Site-Directed Mutagenesis and Crystallography." *The Journal of Biological Chemistry* 271 (33): 19928-19934.
- Kim, K. S., S. Kustu, and W. Inwood. 2006. "Natural History of Transposition in the Green Alga *Chlamydomonas Reinhardtii*: Use of the AMT4 Locus as an Experimental System." *Genetics* 173 (4): 2005-2019.
- Kim, M. S., J. Jeong, J. Jeong, D. H. Shin, and K. J. Lee. 2013. "Structure of Nm23-H1 Under Oxidative Conditions." *Acta Crystallographica. Section D, Biological Crystallography* 69 (Pt 4): 669-680.
- King, S. M. 2016. "Axonemal Dynein Arms." *Cold Spring Harbor Perspectives in Biology* 8 (11): 10.1101/cshperspect.a028100.

- King, S. M., C. G. Wilkerson, and G. B. Witman. 1991. "The Mr 78,000 Intermediate Chain of *Chlamydomonas* Outer Arm Dynein Interacts with Alpha-Tubulin in Situ." *The Journal of Biological Chemistry* 266 (13): 8401-8407.
- Kohno, T., K. Wakabayashi, D. R. Diener, J. L. Rosenbaum, and R. Kamiya. 2011. "Subunit Interactions within the *Chlamydomonas* Flagellar Spokehead." *Cytoskeleton (Hoboken, N.J.)* 68 (4): 237-246.
- Kozminski, K. G., K. A. Johnson, P. Forscher, and J. L. Rosenbaum. 1993. "A Motility in the Eukaryotic Flagellum Unrelated to Flagellar Beating." *Proceedings of the National Academy of Sciences of the United States of America* 90 (12): 5519-5523.
- Kubo, T., M. Hirono, T. Aikawa, R. Kamiya, and G. B. Witman. 2015. "Reduced Tubulin Polyglutamylation Suppresses Flagellar Shortness in *Chlamydomonas*." *Molecular Biology of the Cell* 26 (15): 2810-2822.
- Lascu, I., A. Chaffotte, B. Limbourg-Bouchon, and M. Veron. 1992. "A Pro/Ser Substitution in Nucleoside Diphosphate Kinase of *Drosophila Melanogaster* (Mutation Killer of Prune) Affects Stability but Not Catalytic Efficiency of the Enzyme." *The Journal of Biological Chemistry* 267 (18): 12775-12781.
- Lascu, I. and P. Gonin. 2000. "The Catalytic Mechanism of Nucleoside Diphosphate Kinases." *Journal of Bioenergetics and Biomembranes* 32 (3): 237-246.
- Lechtreck, K. F., T. J. Gould, and G. B. Witman. 2013. "Flagellar Central Pair Assembly in *Chlamydomonas Reinhardtii*." *Cilia* 2 (1): 15.
- Lechtreck, K. F., E. C. Johnson, T. Sakai, D. Cochran, B. A. Ballif, J. Rush, G. J. Pazour, M. Ikebe, and G. B. Witman. 2009. "The *Chlamydomonas Reinhardtii* BBSome is an IFT Cargo Required for Export of Specific Signaling Proteins from Flagella." *The Journal of Cell Biology* 187 (7): 1117-1132.
- LeDizet, M. and G. Piperno. 1995. "The Light Chain p28 Associates with a Subset of Inner Dynein Arm Heavy Chains in *Chlamydomonas* Axonemes." *Molecular Biology of the Cell* 6 (6): 697-711.
- Leung, S. M. and L. E. Hightower. 1997. "A 16-kDa Protein Functions as a New Regulatory Protein for Hsc70 Molecular Chaperone and is Identified as a Member of the Nm23/Nucleoside Diphosphate Kinase Family." *The Journal of Biological Chemistry* 272 (5): 2607-2614.
- Li, J., X. Qian, and B. Sha. 2003. "The Crystal Structure of the Yeast Hsp40 Ydj1 Complexed with its Peptide Substrate." *Structure (London, England : 1993)* 11 (12): 1475-1483.
- Li, X., R. Zhang, W. Patena, S. S. Gang, S. R. Blum, N. Ivanova, R. Yue, et al. 2016. "An Indexed, Mapped Mutant Library Enables Reverse Genetics Studies of Biological Processes in *Chlamydomonas Reinhardtii*." *The Plant Cell* 28 (2): 367-387.

- Liang, J., S. R. Jaffrey, W. Guo, S. H. Snyder, and J. Clardy. 1999. "Structure of the PIN/LC8 Dimer with a Bound Peptide." *Nature Structural Biology* 6 (8): 735-740.
- Lin, J., D. Tritschler, K. Song, C. F. Barber, J. S. Cobb, M. E. Porter, and D. Nicastro. 2011. "Building Blocks of the Nexin-Dynein Regulatory Complex in *Chlamydomonas* Flagella." *The Journal of Biological Chemistry* 286 (33): 29175-29191.
- Lin, J., W. Yin, M. C. Smith, K. Song, M. W. Leigh, M. A. Zariwala, M. R. Knowles, L. E. Ostrowski, and D. Nicastro. 2014. "Cryo-Electron Tomography Reveals Ciliary Defects Underlying Human RSPH1 Primary Ciliary Dyskinesia." *Nature Communications* 5: 5727.
- Lindemann, C. B. 2004. "Testing the Geometric Clutch Hypothesis." *Biology of the Cell* 96 (9): 681-690.
- Liu, P., Y. K. Choi, and R. Z. Qi. 2014. "NME7 is a Functional Component of the Gamma-Tubulin Ring Complex." *Molecular Biology of the Cell* 25 (13): 2017-2025.
- Lu, Q. and M. Inouye. 1996. "Adenylate Kinase Complements Nucleoside Diphosphate Kinase Deficiency in Nucleotide Metabolism." *Proceedings of the National Academy of Sciences of the United States of America* 93 (12): 5720-5725.
- Luck, D., G. Piperno, Z. Ramanis, and B. Huang. 1977. "Flagellar Mutants of *Chlamydomonas*: Studies of Radial Spoke-Defective Strains by Dikaryon and Revertant Analysis." *Proceedings of the National Academy of Sciences of the United States of America* 74 (8): 3456-3460.
- MacDonald, N. J., A. De la Rosa, M. A. Benedict, J. M. Freije, H. Krutsch, and P. S. Steeg. 1993. "A Serine Phosphorylation of Nm23, and Not its Nucleoside Diphosphate Kinase Activity, Correlates with Suppression of Tumor Metastatic Potential." *The Journal of Biological Chemistry* 268 (34): 25780-25789.
- MacDonald, N. J., J. M. Freije, M. L. Stracke, R. E. Manrow, and P. S. Steeg. 1996. "Site-Directed Mutagenesis of nm23-H1. Mutation of Proline 96 Or Serine 120 Abrogates its Motility Inhibitory Activity upon Transfection into Human Breast Carcinoma Cells." *The Journal of Biological Chemistry* 271 (41): 25107-25116.
- Marshall, W. F. and J. L. Rosenbaum. 2001. "Intraflagellar Transport Balances Continuous Turnover of Outer Doublet Microtubules: Implications for Flagellar Length Control." *The Journal of Cell Biology* 155 (3): 405-414.
- Martin, N. C. and U. W. Goodenough. 1975. "Gametic Differentiation in *Chlamydomonas Reinhardtii*. I. Production of Gametes and their Fine Structure." *The Journal of Cell Biology* 67 (3): 587-605.
- Mayer, M. P. and B. Bukau. 2005. "Hsp70 Chaperones: Cellular Functions and Molecular Mechanism." *Cellular and Molecular Life Sciences : CMLS* 62 (6): 670-684.

- Mayfield, S. P., P. Bennoun, and J. D. Rochaix. 1987. "Expression of the Nuclear Encoded OEE1 Protein is Required for Oxygen Evolution and Stability of Photosystem II Particles in *Chlamydomonas Reinhardtii*." *The EMBO Journal* 6 (2): 313-318.
- McIntyre, J. C., C. L. Williams, and J. R. Martens. 2013. "Smelling the Roses and Seeing the Light: Gene Therapy for Ciliopathies." *Trends in Biotechnology* 31 (6): 355-363.
- McVittie, A. 1972. "Flagellum Mutants of *Chlamydomonas Reinhardtii*." *Journal of General Microbiology* 71 (3): 525-540.
- Merchant, S. S., S. E. Prochnik, O. Vallon, E. H. Harris, S. J. Karpowicz, G. B. Witman, A. Terry, et al. 2007. "The *Chlamydomonas* Genome Reveals the Evolution of Key Animal and Plant Functions." *Science (New York, N.Y.)* 318 (5848): 245-250.
- Mitchell, B. F., L. B. Pedersen, M. Feely, J. L. Rosenbaum, and D. R. Mitchell. 2005. "ATP Production in *Chlamydomonas Reinhardtii* Flagella by Glycolytic Enzymes." *Molecular Biology of the Cell* 16 (10): 4509-4518.
- Mitchell, D. R. 2007. "The Evolution of Eukaryotic Cilia and Flagella as Motile and Sensory Organelles." *Advances in Experimental Medicine and Biology* 607: 130-140.
- . 2003. "Orientation of the Central Pair Complex during Flagellar Bend Formation in *Chlamydomonas*." *Cell Motility and the Cytoskeleton* 56 (2): 120-129.
- Mitchell, D. R. and M. Nakatsugawa. 2004. "Bend Propagation Drives Central Pair Rotation in *Chlamydomonas Reinhardtii* Flagella." *The Journal of Cell Biology* 166 (5): 709-715.
- Mitchell, D. R. and W. S. Sale. 1999. "Characterization of a *Chlamydomonas* Insertional Mutant that Disrupts Flagellar Central Pair Microtubule-Associated Structures." *The Journal of Cell Biology* 144 (2): 293-304.
- Muimo, R., Z. Hornickova, C. E. Riemen, V. Gerke, H. Matthews, and A. Mehta. 2000. "Histidine Phosphorylation of Annexin I in Airway Epithelia." *The Journal of Biological Chemistry* 275 (47): 36632-36636.
- Munier, A., C. Feral, L. Milon, V. P. Pinon, G. Gyapay, J. Capeau, G. Guellaen, and M. L. Lacombe. 1998. "A New Human nm23 Homologue (nm23-H5) Specifically Expressed in Testis Germinal Cells." *FEBS Letters* 434 (3): 289-294.
- Munier, A., C. Serres, M. L. Kann, M. Boissan, C. Lesaffre, J. Capeau, J. P. Fouquet, and M. L. Lacombe. 2003. "Nm23/NDP Kinases in Human Male Germ Cells: Role in Spermiogenesis and Sperm Motility?" *Experimental Cell Research* 289 (2): 295-306.
- Nicastro, D. 2009. "Cryo-Electron Microscope Tomography to Study Axonemal Organization." *Methods in Cell Biology* 91: 1-39.

- Nyarko, A., Y. Song, J. Novacek, L. Zidek, and E. Barbar. 2013. "Multiple Recognition Motifs in Nucleoporin Nup159 Provide a Stable and Rigid Nup159-Dyn2 Assembly." *The Journal of Biological Chemistry* 288 (4): 2614-2622.
- Oda, T., H. Yanagisawa, T. Yagi, and M. Kikkawa. 2014. "Mechanotransduction between Central Apparatus and Radial Spokes Controls Axonemal Dynein Activity." *The Journal of Cell Biology* 204 (5): 807-819.
- Ogawa, K. and I. R. Gibbons. 1976. "Dynein 2. A New Adenosine Triphosphatase from Sea Urchin Sperm Flagella." *The Journal of Biological Chemistry* 251 (18): 5793-5801.
- Ogawa, K., H. Takai, A. Ogiwara, E. Yokota, T. Shimizu, K. Inaba, and H. Mohri. 1996. "Is Outer Arm Dynein Intermediate Chain 1 Multifunctional?" *Molecular Biology of the Cell* 7 (12): 1895-1907.
- Omoto, C. K., I. R. Gibbons, R. Kamiya, C. Shingyoji, K. Takahashi, and G. B. Witman. 1999. "Rotation of the Central Pair Microtubules in Eukaryotic Flagella." *Molecular Biology of the Cell* 10 (1): 1-4.
- Omoto, C. K. and C. Kung. 1979. "The Pair of Central Tubules Rotates during Ciliary Beat in Paramecium." *Nature* 279 (5713): 532-534.
- Padma, P., A. Hozumi, K. Ogawa, and K. Inaba. 2001. "Molecular Cloning and Characterization of a Thioredoxin/Nucleoside Diphosphate Kinase Related Dynein Intermediate Chain from the Ascidian, *Ciona intestinalis*." *Gene* 275 (1): 177-183.
- Pan, J. and W. Snell. 2007. "The Primary Cilium: Keeper of the Key to Cell Division." *Cell* 129 (7): 1255-1257.
- Pandit, S., S. Paul, L. Zhang, M. Chen, N. Durbin, S. M. Harrison, and B. C. Rymond. 2009. "Spp382p Interacts with Multiple Yeast Splicing Factors, Including Possible Regulators of Prp43 DExD/H-Box Protein Function." *Genetics* 183 (1): 195-206.
- Parks, R.E.J. and Agarwal, R.P. 1973. Nucleoside diphosphokinases. *Enzymes* 8: 307-334.
- Pazour, G. J., N. Agrin, J. Leszyk, and G. B. Witman. 2005. "Proteomic Analysis of a Eukaryotic Cilium." *The Journal of Cell Biology* 170 (1): 103-113.
- Pazour, G. J., C. G. Wilkerson, and G. B. Witman. 1998. "A Dynein Light Chain is Essential for the Retrograde Particle Movement of Intraflagellar Transport (IFT)." *The Journal of Cell Biology* 141 (4): 979-992.
- Pedersen, L. B. 2017. "Tubulin Transport in Cilia: How Many Tubulin Cargo-Binding Sites Per IFT Particle? (Retrospective on DOI 10.1002/Bies.201400007)." *BioEssays: News and Reviews in Molecular, Cellular and Developmental Biology* 39 (1): 1.
- Perales-Calvo, J., A. Muga, and F. Moro. 2010. "Role of DnaJ G/F-Rich Domain in Conformational Recognition and Binding of Protein Substrates." *The Journal of Biological Chemistry* 285 (44): 34231-34239.



- Pettersen, E. F., T. D. Goddard, C. C. Huang, G. S. Couch, D. M. Greenblatt, E. C. Meng, and T. E. Ferrin. 2004. "UCSF Chimera--a Visualization System for Exploratory Research and Analysis." *Journal of Computational Chemistry* 25 (13): 1605-1612.
- Pigino, G., K. H. Bui, A. Maheshwari, P. Lupetti, D. Diener, and T. Ishikawa. 2011. "Cryoelectron Tomography of Radial Spokes in Cilia and Flagella." *The Journal of Cell Biology* 195 (4): 673-687.
- Pigino, G., A. Maheshwari, K. H. Bui, C. Shingyoji, S. Kamimura, and T. Ishikawa. 2012. "Comparative Structural Analysis of Eukaryotic Flagella and Cilia from *Chlamydomonas*, Tetrahymena, and Sea Urchins." *Journal of Structural Biology* 178 (2): 199-206.
- Piperno, G., K. Mead, and S. Henderson. 1996. "Inner Dynein Arms but Not Outer Dynein Arms Require the Activity of Kinesin Homologue Protein KHP1(FLA10) to Reach the Distal Part of Flagella in *Chlamydomonas*." *The Journal of Cell Biology* 133 (2): 371-379.
- Postel, E. H., S. J. Berberich, S. J. Flint, and C. A. Ferrone. 1993. "Human C-Myc Transcription Factor PuF Identified as nm23-H2 Nucleoside Diphosphate Kinase, a Candidate Suppressor of Tumor Metastasis." *Science (New York, N.Y.)* 261 (5120): 478-480.
- Qin, H., D. R. Diener, S. Geimer, D. G. Cole, and J. L. Rosenbaum. 2004. "Intraflagellar Transport (IFT) Cargo: IFT Transports Flagellar Precursors to the Tip and Turnover Products to the Cell Body." *The Journal of Cell Biology* 164 (2): 255-266.
- Rasala, B. A., D. J. Barrera, J. Ng, T. M. Plucinak, J. N. Rosenberg, D. P. Weeks, G. A. Oyler, T. C. Peterson, F. Haerizadeh, and S. P. Mayfield. 2013. "Expanding the Spectral Palette of Fluorescent Proteins for the Green Microalga *Chlamydomonas Reinhardtii*." *The Plant Journal : For Cell and Molecular Biology* 74 (4): 545-556.
- Rosenbaum, J. L. and F. M. Child. 1967. "Flagellar Regeneration in Protozoan Flagellates." *The Journal of Cell Biology* 34 (1): 345-364.
- Rosenbaum, J. L. and G. B. Witman. 2002. "Intraflagellar Transport." *Nature Reviews.Molecular Cell Biology* 3 (11): 813-825.
- Rosengard, A. M., H. C. Krutzsch, A. Shearn, J. R. Biggs, E. Barker, I. M. Margulies, C. R. King, L. A. Liotta, and P. S. Steeg. 1989. "Reduced Nm23/Awd Protein in Tumour Metastasis and Aberrant Drosophila Development." *Nature* 342 (6246): 177-180.
- Rual, J. F., K. Venkatesan, T. Hao, T. Hirozane-Kishikawa, A. Dricot, N. Li, G. F. Berriz, et al. 2005. "Towards a Proteome-Scale Map of the Human Protein-Protein Interaction Network." *Nature* 437 (7062): 1173-1178.
- Sadek, C. M., A. Jimenez, A. E. Damdimopoulos, T. Kieselbach, M. Nord, J. A. Gustafsson, G. Spyrou, et al. 2003. "Characterization of Human Thioredoxin-Like 2. A Novel Microtubule-Binding Thioredoxin Expressed Predominantly in the Cilia of

- Lung Airway Epithelium and Spermatid Manchette and Axoneme." *The Journal of Biological Chemistry* 278 (15): 13133-13142.
- Sahi, C., T. Lee, M. Inada, J. A. Pleiss, and E. A. Craig. 2010. "Cwc23, an Essential J Protein Critical for Pre-mRNA Splicing with a Dispensable J Domain." *Molecular and Cellular Biology* 30 (1): 33-42.
- Sale, W. S. and P. Satir. 1977. "Direction of Active Sliding of Microtubules in Tetrahymena Cilia." *Proceedings of the National Academy of Sciences of the United States of America* 74 (5): 2045-2049.
- Satouh, Y. and K. Inaba. 2009. "Proteomic Characterization of Sperm Radial Spokes Identifies a Novel Spoke Protein with an Ubiquitin Domain." *FEBS Letters* 583 (13): 2201-2207.
- Satouh, Y., P. Padma, T. Toda, N. Satoh, H. Ide, and K. Inaba. 2005. "Molecular Characterization of Radial Spoke Subcomplex Containing Radial Spoke Protein 3 and Heat Shock Protein 40 in Sperm Flagella of the Ascidian *Ciona intestinalis*." *Molecular Biology of the Cell* 16 (2): 626-636.
- Sha, B., S. Lee, and D. M. Cyr. 2000. "The Crystal Structure of the Peptide-Binding Fragment from the Yeast Hsp40 Protein Sis1." *Structure (London, England : 1993)* 8 (8): 799-807.
- Shaner, N. C., G. G. Lambert, A. Chammas, Y. Ni, P. J. Cranfill, M. A. Baird, B. R. Sell, et al. 2013. "A Bright Monomeric Green Fluorescent Protein Derived from Branchiostoma Lanceolatum." *Nature Methods* 10 (5): 407-409.
- Silflow, C. D., X. Sun, N. A. Haas, J. W. Foley, and P. A. Lefebvre. 2011. "The Hsp70 and Hsp40 Chaperones Influence Microtubule Stability in *Chlamydomonas*." *Genetics* 189 (4): 1249-1260.
- Sivadas, P., J. M. Dienes, M. St Maurice, W. D. Meek, and P. Yang. 2012. "A Flagellar A-Kinase Anchoring Protein with Two Amphipathic Helices Forms a Structural Scaffold in the Radial Spoke Complex." *The Journal of Cell Biology* 199 (4): 639-651.
- Smith, E. F. and P. Yang. 2004. "The Radial Spokes and Central Apparatus: Mechano-Chemical Transducers that Regulate Flagellar Motility." *Cell Motility and the Cytoskeleton* 57 (1): 8-17.
- Snell, W. J. 1976. "Mating in *Chlamydomonas*: A System for the Study of Specific Cell Adhesion. I. Ultrastructural and Electrophoretic Analyses of Flagellar Surface Components Involved in Adhesion." *The Journal of Cell Biology* 68 (1): 48-69.
- Song, L. and W. L. Dentler. 2001. "Flagellar Protein Dynamics in *Chlamydomonas*." *The Journal of Biological Chemistry* 276 (32): 29754-29763.
- South, P. F., I. M. Fingerman, D. P. Mersman, H. N. Du, and S. D. Briggs. 2010. "A Conserved Interaction between the SDI Domain of Bre2 and the Dpy-30 Domain of

- Sdc1 is Required for Histone Methylation and Gene Expression." *The Journal of Biological Chemistry* 285 (1): 595-607.
- Srivastava, S., Z. Li, K. Ko, P. Choudhury, M. Albaqumi, A. K. Johnson, Y. Yan, et al. 2006. "Histidine Phosphorylation of the Potassium Channel KCa3.1 by Nucleoside Diphosphate Kinase B is Required for Activation of KCa3.1 and CD4 T Cells." *Molecular Cell* 24 (5): 665-675.
- Srivastava, S., O. Zhdanova, L. Di, Z. Li, M. Albaqumi, H. Wulff, and E. Y. Skolnik. 2008. "Protein Histidine Phosphatase 1 Negatively Regulates CD4 T Cells by Inhibiting the K<sup>+</sup> Channel KCa3.1." *Proceedings of the National Academy of Sciences of the United States of America* 105 (38): 14442-14446.
- Steeg, P. S., G. Bevilacqua, L. Kopper, U. P. Thorgerirsson, J. E. Talmadge, L. A. Liotta, and M. E. Sobel. 1988. "Evidence for a Novel Gene Associated with Low Tumor Metastatic Potential." *Journal of the National Cancer Institute* 80 (3): 200-204.
- Steeg, P. S., M. Zollo, and T. Wieland. 2011. "A Critical Evaluation of Biochemical Activities Reported for the Nucleoside Diphosphate Kinase/Nm23/Awd Family Proteins: Opportunities and Missteps in Understanding their Biological Functions." *Naunyn-Schmiedeberg's Archives of Pharmacology* 384 (4-5): 331-339.
- Stelter, P., R. Kunze, D. Flemming, D. Hopfner, M. Diepholz, P. Philippsen, B. Bottcher, and E. Hurt. 2007. "Molecular Basis for the Functional Interaction of Dynein Light Chain with the Nuclear-Pore Complex." *Nature Cell Biology* 9 (7): 788-796.
- Sturtevant, A. H. 1956. "A Highly Specific Complementary Lethal System in *Drosophila melanogaster*." *Genetics* 41 (1): 118-123.
- Susan K. Dutcher. 1995. Mating and Tetrad Analysis in *Chlamydomonas reinhardtii*. *Cilia and Flagella* 47: 531-540.
- Suzuki, H., S. Noguchi, H. Arakawa, T. Tokida, M. Hashimoto, and Y. Satow. 2010. "Peptide-Binding Sites as Revealed by the Crystal Structures of the Human Hsp40 Hdj1 C-Terminal Domain in Complex with the Octapeptide from Human Hsp70." *Biochemistry* 49 (39): 8577-8584.
- Takacs-Vellai, K., T. Vellai, Z. Farkas, and A. Mehta. 2015. "Nucleoside Diphosphate Kinases (NDPKs) in Animal Development." *Cellular and Molecular Life Sciences : CMLS* 72 (8): 1447-1462.
- Takahashi, Y. H., G. H. Westfield, A. N. Oleskie, R. C. Trievel, A. Shilatifard, and G. Skiniotis. 2011. "Structural Analysis of the Core COMPASS Family of Histone H3K4 Methylases from Yeast to Human." *Proceedings of the National Academy of Sciences of the United States of America* 108 (51): 20526-20531.
- Takei, G. L., D. Miyashiro, C. Mukai, and M. Okuno. 2014. "Glycolysis Plays an Important Role in Energy Transfer from the Base to the Distal End of the Flagellum in Mouse Sperm." *The Journal of Experimental Biology* 217 (Pt 11): 1876-1886.

- Tam, L. W., P. T. Ranum, and P. A. Lefebvre. 2013. "CDKL5 Regulates Flagellar Length and Localizes to the Base of the Flagella in *Chlamydomonas*." *Molecular Biology of the Cell* 24 (5): 588-600.
- Tepper, A. D., H. Dammann, A. A. Bominaar, and M. Veron. 1994. "Investigation of the Active Site and the Conformational Stability of Nucleoside Diphosphate Kinase by Site-Directed Mutagenesis." *The Journal of Biological Chemistry* 269 (51): 32175-32180.
- Thakur, R. K., P. Kumar, K. Halder, A. Verma, A. Kar, J. L. Parent, R. Basundra, A. Kumar, and S. Chowdhury. 2009. "Metastases Suppressor NM23-H2 Interaction with G-Quadruplex DNA within C-MYC Promoter Nuclease Hypersensitive Element Induces C-MYC Expression." *Nucleic Acids Research* 37 (1): 172-183.
- Tiwari, S., K. V. Kishan, T. Chakrabarti, and P. K. Chakraborti. 2004. "Amino Acid Residues Involved in Autophosphorylation and Phosphotransfer Activities are Distinct in Nucleoside Diphosphate Kinase from Mycobacterium Tuberculosis." *The Journal of Biological Chemistry* 279 (42): 43595-43603.
- Tremblay, V., P. Zhang, C. P. Chaturvedi, J. Thornton, J. S. Brunzelle, G. Skiniotis, A. Shilatifard, M. Brand, and J. F. Couture. 2014. "Molecular Basis for DPY-30 Association to COMPASS-Like and NURF Complexes." *Structure (London, England : 1993)* 22 (12): 1821-1830.
- Vogel, P., R. W. Read, G. M. Hansen, B. J. Payne, D. Small, A. T. Sands, and B. P. Zambrowicz. 2012. "Congenital Hydrocephalus in Genetically Engineered Mice." *Veterinary Pathology* 49 (1): 166-181.
- Wagner, P. D., P. S. Steeg, and N. D. Vu. 1997. "Two-Component Kinase-Like Activity of nm23 Correlates with its Motility-Suppressing Activity." *Proceedings of the National Academy of Sciences of the United States of America* 94 (17): 9000-9005.
- Wagner, P. D. and N. D. Vu. 1995. "Phosphorylation of ATP-Citrate Lyase by Nucleoside Diphosphate Kinase." *The Journal of Biological Chemistry* 270 (37): 21758-21764.
- Wang, X., Z. Lou, X. Dong, W. Yang, Y. Peng, B. Yin, Y. Gong, et al. 2009. "Crystal Structure of the C-Terminal Domain of Human DPY-30-Like Protein: A Component of the Histone Methyltransferase Complex." *Journal of Molecular Biology* 390 (3): 530-537.
- Warner, F. D. and P. Satir. 1974. "The Structural Basis of Ciliary Bend Formation. Radial Spoke Positional Changes Accompanying Microtubule Sliding." *The Journal of Cell Biology* 63 (1): 35-63.
- Wegele, H., M. Haslbeck, J. Reinstein, and J. Buchner. 2003. "Sti1 is a Novel Activator of the Ssa Proteins." *The Journal of Biological Chemistry* 278 (28): 25970-25976.
- Wei, M., P. Sivadas, H. A. Owen, D. R. Mitchell, and P. Yang. 2010. "*Chlamydomonas* Mutants Display Reversible Deficiencies in Flagellar Beating and Axonemal Assembly." *Cytoskeleton (Hoboken, N.J.)* 67 (2): 71-80.

- Wilkie, A. O. 1994. "The Molecular Basis of Genetic Dominance." *Journal of Medical Genetics* 31 (2): 89-98.
- Williams, B. D., M. A. Velleca, A. M. Curry, and J. L. Rosenbaum. 1989. "Molecular Cloning and Sequence Analysis of the *Chlamydomonas* Gene Coding for Radial Spoke Protein 3: Flagellar Mutation Pf-14 is an Ochre Allele." *The Journal of Cell Biology* 109 (1): 235-245.
- Williams, J. C., P. L. Roulhac, A. G. Roy, R. B. Vallee, M. C. Fitzgerald, and W. A. Hendrickson. 2007. "Structural and Thermodynamic Characterization of a Cytoplasmic Dynein Light Chain-Intermediate Chain Complex." *Proceedings of the National Academy of Sciences of the United States of America* 104 (24): 10028-10033.
- Wilson, N. F., J. K. Iyer, J. A. Buchheim, and W. Meek. 2008. "Regulation of Flagellar Length in *Chlamydomonas*." *Seminars in Cell & Developmental Biology* 19 (6): 494-501.
- Wirschell, M., F. Zhao, C. Yang, P. Yang, D. Diener, A. Gaillard, J. L. Rosenbaum, and W. S. Sale. 2008. "Building a Radial Spoke: Flagellar Radial Spoke Protein 3 (RSP3) is a Dimer." *Cell Motility and the Cytoskeleton* 65 (3): 238-248.
- Xiao, J., L. S. Kim, and T. R. Graham. 2006. "Dissection of Swa2p/Auxilin Domain Requirements for Cochaperoning Hsp70 Clathrin-Uncoating Activity in Vivo." *Molecular Biology of the Cell* 17 (7): 3281-3290.
- Xin, X., J. F. Rual, T. Hirozane-Kishikawa, D. E. Hill, M. Vidal, C. Boone, and N. Thierry-Mieg. 2009. "Shifted Transversal Design Smart-Pooling for High Coverage Interactome Mapping." *Genome Research* 19 (7): 1262-1269.
- Yang, P., D. R. Diener, J. L. Rosenbaum, and W. S. Sale. 2001. "Localization of Calmodulin and Dynein Light Chain LC8 in Flagellar Radial Spokes." *The Journal of Cell Biology* 153 (6): 1315-1326.
- Yang, P., D. R. Diener, C. Yang, T. Kohno, G. J. Pazour, J. M. Dienes, N. S. Agrin, et al. 2006. "Radial Spoke Proteins of *Chlamydomonas* Flagella." *Journal of Cell Science* 119 (Pt 6): 1165-1174.
- Yang, P. and W. S. Sale. 1998. "The Mr 140,000 Intermediate Chain of *Chlamydomonas* Flagellar Inner Arm Dynein is a WD-Repeat Protein Implicated in Dynein Arm Anchoring." *Molecular Biology of the Cell* 9 (12): 3335-3349.
- Yang, P., C. Yang, and W. S. Sale. 2004. "Flagellar Radial Spoke Protein 2 is a Calmodulin Binding Protein Required for Motility in *Chlamydomonas Reinhardtii*." *Eukaryotic Cell* 3 (1): 72-81.
- Yang, P., C. Yang, M. Wirschell, and S. Davis. 2009. "Novel LC8 Mutations have Disparate Effects on the Assembly and Stability of Flagellar Complexes." *The Journal of Biological Chemistry* 284 (45): 31412-31421.

- Ye, F., D. K. Breslow, E. F. Koslover, A. J. Spakowitz, W. J. Nelson, and M. V. Nachury. 2013. "Single Molecule Imaging Reveals a Major Role for Diffusion in the Exploration of Ciliary Space by Signaling Receptors." *eLife* 2: e00654.
- Zhang, F., Y. Qi, K. Zhou, G. Zhang, K. Linask, and H. Xu. 2015. "The cAMP Phosphodiesterase Prune Localizes to the Mitochondrial Matrix and Promotes mtDNA Replication by Stabilizing TFAM." *EMBO Reports* 16 (4): 520-527.
- Zhu, X., Y. Liu, P. Sivadas, A. Gupta, and P. Yang. 2013. "Molecular Tools for Studying the Radial Spoke." *Methods in Enzymology* 524: 19-36.
- Zhu, X., Liu, Y., and Yang, P. 2016. Radial Spokes-A Snapshot of the Motility Regulation, Assembly, and Evolution of Cilia and Flagella. In: Cilia, ed. W.F. Marshall and R. Basto. Cold Spring Harb Perspect Bio. 57-69.
- Zhu, X., Poghosyan, E., Gopal, R., Liu, Y, Ciruelas, K.S., Maizy, Y., Diener, D.R., King, S.M. Ishikawa, T., and Yang, P. **General and specific promotions of flagellar assembly by a flagellar nucleoside diphosphate kinase.** Submitted.